Simulation of fluid flow and heat transfer to study hot water production potential from naturally-fractured geothermal reservoirs

Author:
Shaik, Abdul Ravoof

Publication Date:
2012

DOI:
https://doi.org/10.26190/unsworks/15844

Simulation of Fluid Flow and Heat Transfer to Study Hot Water Production Potential from Naturally-Fractured Geothermal Reservoirs

By

Abdul Ravoof Shaik

Supervisor: Prof. Sheik S Rahman

Dissertation Submitted to The University of New South Wales in partial fulfillment of the requirements for the Degree of Doctor of Philosophy
In
Petroleum Engineering

School of Petroleum Engineering
The University of New South Wales
Sydney, NSW, AUSTRALIA

December 2011

ORIGINALITY STATEMENT

„I hereby declare that this submission is my own work and to the best of my knowledge it contains no materials previously published or written by another person, or substantial proportions of material which have been accepted for the award of any other degree or diploma at UNSW or any other educational institution, except where due acknowledgement is made in the thesis. Any contribution made to the research by others, with whom I have worked at UNSW or elsewhere, is explicitly acknowledged in the thesis. I also declare that the intellectual content of this thesis is the product of my own work, except to the extent that assistance from others in the project's design and conception or in style, presentation and linguistic expression is acknowledged.‟

Signed …………………………………………….............

Date …………………………………………….............

ACKNOWLEDGEMENTS

I want to express my deepest gratitude to my adviser Prof. Sheik S Rahman for his consistent support and guidance throughout my PhD studies. The lessons learned from him will be an invaluable asset in my career. It would have been impossible to complete this work without his helpful supervision. I would like to extend my sincere appreciation to my all colleagues for their continuous support. I also would like to express my gratefulness for financial support from the Faculty of Engineering of The University of New South Wales.

I would like to thank Nino Zajaczkowski for paying immediate attention to my computer and software related needs. His helpful attitude is deeply appreciated. I also want to thank my fellow graduate students in the petroleum engineering department, who have accompanied me in this long but exciting journey.

I would like to thank the cheerful faces of the members of the Coles@Rhodes team both past and present and, the respect they accorded to me, made my functioning at Coles, easier. A special thanks goes to Ms Katherine Nweiser, as ex-service manager, Coles@rhodes. For me, Katherine has always been the person I could ask for favors to give me extra shifts (or give me day off) whenever I needed them. I would like to thank her from the bottom of my heart. I would also like to thank Ben Muller and Steve Allen for improving my management skills which will be a valuable asset in every step of my life.

Most importantly, I am grateful to my parents, Mr. Subhani Shaik and Mrs. Shakeera Shaik for enduring numerous difficulties in their efforts to provide me with a good education and childhood.

DEDICATION

I dedicate this thesis to my family

Abstract

Typically naturally fractured geothermal reservoirs has low matrix permeability, and fluid flow is primarily controlled by complicated fracture patterns. The major hurdles for estimating recoverable energy in such reservoirs are generation of a discrete fracture map and handling the vast amount of data on fracture geometry (aperture, length, and orientation) for simulation of fluid flow and heat transfer. To add complexity to the matter, dynamic heat transfer between fractured rock and circulating fluid must be investigated for better prediction of total heat recovered from naturally fractured geothermal reservoirs.

To overcome some of these difficulties, a number of methods were proposed according to the representation of fractured medium, the type of fracture network, and the size of domain of interest. Most of the previous works in this area assumed either fractured geothermal system as cubic blocks separated by fractures or/and an instantaneous local thermal equilibrium while simulating heat extraction from the fractured geothermal systems.

In the present work a 3D numerical model is developed to evaluate potential for heat recovery from naturally fractured geothermal reservoirs. For this purpose a numerical procedure is developed to address three major issues: characterization of naturally fractured reservoirs, simulation of fluid flow through interconnected fracture system, and heat transfer between matrix and circulating fluid. Field data is statistically analyzed (stochastic analysis) to develop discrete fracture network. A finite element based fluid flow model,

which includes a permeability tensor model, is developed to simulate fluid flow through interconnected fracture system. Heat transfer model is based on rock fluid temperature approach to study thermal drawdown of a geothermal reservoir during its productive life.

The proposed methodology has been validated against previously published results. Several numerical experiments are carried out to illustrate how the methodology could be used to evaluate geothermal potential of a reservoir and how different reservoir and operating conditions affect reservoir performance including fracture connectivity, production rate etc. From the results of this study it can be seen that characteristic properties of fractures, such as fracture interconnectivity, contact area between fluid and matrix and fracture density as well as flow rates affect heat recovery from naturally fractured geothermal reservoirs.

Publications

The following publications are co-authored by the author of this thesis. They are based on the concepts introduced in this study.

Published:

1. **Shaik**, A. R. and S. S. Rahman.2011 "Numerical Simulation of Fluid-Rock Coupling Heat Transfer in Naturally Fractured Geothermal System". Applied Thermal Engineering In Press, Accepted Manuscript, doi:10.1016/j.applthermaleng.2011.01.038.

2. Koh, J., **Shaik**, A.R. and Rahman, S.S.2011: “An innovative 3D thermo-poroelastic model for studying the long term behavior of geothermal systems”, Geothermal Researach Council Transactions, Vol. 35,

3. **Shaik**, A., N. Tran, Rahman,S.S. and T. Tran 2010. "Estimating Pressure Losses in Interconnected Fracture Systems: An Integrated Tensor Approach" International Journal of Geomechanics. accepted October 17, 2010; posted ahead of print October 22, 2010. doi:10.1061/(ASCE)GM.1943-5622.0000099

4. Koh, J., Gholizadeh-Doonechaly, N.,**Shaik**, A.R., Rahman, S.S., and Mortimer, L., “Reservoir Characterisation and Numerical Modelling to Reduce Project Risk and Maximise the Chance of Success An example of how to design a stimulation program and assess fluid production from the Soultz EGS, France”, Proceedings of Australian Geothermal Energy Conference, 2010, 16-18 November, Adelaide, 2010

5. **Shaik**, A.R., Koh, J., Rahman, S.S., Aghighi, M.A. and Tran, N.H., 2009. "Design and Evaluation of Well Placement and Hydraulic Stimulation for Economical Heat Recovery from Enhanced Geothermal Systems". Geothermal Research Council Transactions, Vol. 33: 251-256

6. **Shaik**, A.R., Tran, N.H., Aghighi M.A, Rahman.S.S. 2008: “An innovative reservoir simulator can help evaluate hot water production for economic development of Australian geothermal reservoirs” Geothermal Research Council Transactions, Vol 32.

Table of contents

List of tables

List of figures

Chapter 1

Introduction

1.1 Background knowledge

Naturally fractured geothermal reservoirs represent a significant portion of the world‟s geothermal energy reserves (Ghassemi et al. 2007; Jafari and Babadagli 2011). In most of these reservoirs, fractures serve as the main conduit for fluid flow. Because of their variable spatial distribution, orientation and geometry fractured reservoirs are highly heterogeneous. This makes simulation of fluid flow and heat transfer a difficult task. Simulation of fluid flow and heat transfer forms an essential part of a feasibility study which includes: potential hot water production, heat extraction rate and heat recovery factor. Moreover, achieving the economic flow rate of the commercial viability of a enhanced geothermal system is very much a function of flow rate which is should to be 70-80 l/s as reported by (Tester et al. 2006). In the literature a number of fluid flow and heat transfer simulation models exist. In some, extensively high computational resources are used to simulate fluid flow in few fractures (reservoir with very low fracture density). In others, fluid flow and heat transfer are simulated for reservoirs with uniform fracture pattern. None of these techniques can adequately address the issue of simulating fluid flow and heat transfer in arbitrarily oriented naturally fractured geothermal reservoirs (Rahman et al. 2002; Tester et al. 2006).

Characteristic properties of natural fractures play significant role in fluid flow and heat transfer in geothermal reservoirs. For geological reasons, most of the fractures possess very low matrix permeability and thus, fractures serve as the main fluid flow path. In order to effectively simulate fluid flow and heat transfer in a fractured system it is essential to incorporate a fracture network model that takes into account of fracture spatial distribution and detailed individual fracture properties such as aperture, length and orientation (Anzelius 1926; Holman 1976; Pruess and Narasimhan 1985; Hossain et al. 2002; Teimoori et al. 2005; Rees et al. 2008).

In literature three major approaches are proposed to simulate fracture network with discrete fracture properties (spatial distribution, fracture dip, and azimuth as well as fracture length and aperture). They include deterministic, stochastic and hybrid of the two. Data such as in-situ stress conditions, reservoir structure and tectonic history constitute essential part of deterministic fracture network modeling (Koh et al. 2010). Stochastic simulation of fracture network requires explicit information of fracture properties that can be obtained from well data. The hybrid approach complements both the deterministic and the stochastic approaches and offers a more realistic representation of fracture properties of a fractured reservoir (Watanabe and Takahashi 1995b; Watanabe and Takahashi 1995a; Tran 2007; Koh et al. 2010). However, all these approaches require information related to rock, fracture and stress properties to simulate fracture network. In this thesis the stochastic simulation technique is used to model the natural fracture system due to the lack of sufficient field data available in public domain.

Simulation of fluid flow in naturally fractured geothermal reservoirs have long been carried out by the continuum approach: single and dual (Pruess and Narasimhan 1985; Pruess 1991). In this approach the fractured reservoir is represented by two interacting continua whose matrix provides storage capacity and fracture provides the permeability. Thus the continuum approach fails to represent complex structure of the fractured medium adequately. With recent advancements in reservoir characterization techniques it is now possible to model discrete fractures . Direct use of discrete fractures in the continuum approach is, however, too exhaustive to simulate fluid flow (Auradou et al. 2006; Gong et al. 2006; Deo et al. 2008; Hoteit and Firoozabadi 2008). In order to overcome the limitation of the discrete fracture approach a hybrid of continuum and discrete fracture approaches is proposed in the literature (Lee et al. 2001; Castaing et al. 2002; Teimoori et al. 2005). In this approach the fractured reservoir is divided into a number of blocks and directional effective permeability tensor for each block is estimated based on the fluid flow simulation through fractures. Production is then estimated based on effective permeability tensors.

In this thesis the hybrid approach (a combination of both continuum and discrete approaches) is used to simulate fluid flow in naturally fractured geothermal reservoirs. On the other hand, simulation of the heat transfer is carried out by using three different approaches: the equivalent temperature approach, matrix-fracture temperature approach and rock-fluid temperature approach (Rees et al. 2005; Ghassemi et al. 2008; Geiger-Boschung et al. 2009). Both equivalent temperature approach and matrix-fracture temperature approach assume that the fractured medium reaches its local thermal equilibrium with circulating fluid instantaneously. Instantaneous local thermal equilibrium between matrix and fluid, however, does not adequately simulate heat transfer in reservoirs where fracture spacing is more than 2-3 meters (Sanyal et al. 2005). In order to overcome the limitations of previous methods the rock-fluid temperature approach, proposed by Anzelius (1926) to estimate heat transfer between the phases at the pore level, is further extended and used to investigate the thermal energy removed from the naturally fractured geothermal reservoirs. In the rock-fluid temperature approach the matrix and fluid temperatures are treated separately (Rees et al. 2005; Rees et al. 2008; He and Jin 2010).

1.2 Aims and significance

The thesis aims to do:

- Construct a comprehensive fracture network based on the available geological data.
- Apply a systematic permeability estimation procedure for the generated fracture network.
- Investigate the fluid flow between injector and producer through fluid induced hydraulic fracture and naturally fractured reservoirs.
- Investigate pressure losses between injector and producer in naturally fractured geothermal reservoirs with various fracture densities (low, medium and high).

- Investigate the effect of fracture network inter-connectivity on well placement.
- Investigate the rock matrix cooling due to heat transfer between hot rock matrix and cold circulating fluid.
- Investigate the effect of fracture density on the total recovery factor.
- Investigate the effect of injection schedule on heat extraction and subsequent recovery factor.
- Investigate active fracture volume (contract area) on heat recovery.
- Apply the concepts to study fluid flow through arbitrary oriented fractured network and identifying the optimum flow rate range to maximize heat extraction.

In this thesis a comprehensive methodology for simulation of fluid flow and heat transfer in naturally fractured reservoirs is presented. Significance of this approach lies in modeling fluid flow fractured media with in arbitrary oriented fractures and dynamic heat transfer between fluid and surrounding rock matrix. Because natural fracture systems are highly complex heat transfer between rock matrix and fluid remains a hugely difficult task (Tester et al. 2006).

The developed numerical model can be applied to predict heat extraction, the thermal breakthrough and the economic reservoir life. It is also possible to select optimum placement of injection and production wells in order to maximize heat transfer between fractured matrix and the circulating fluid.

1.3 Structure of the thesis

In view of the above objectives the thesis is organized as follows:

In *chapter 2*, a discrete fracture network model developed by Rahman et al (2002) is used to generate fracture network. In *chapter 3* a numerical model is developed which can simulate the fluid flow from the wellbore to natural fracture system through fluid induced hydraulic fracture is presented. In this chapter, firstly reviews different numerical techniques- which have been employed to model fluid flow through an arbitrarily oriented fractured network, is presented. Next, the governing equations to simulate fluid flow are derived. Then finite element method is used to solve numerically the system of equations. Finally, numerical results are verified against the analytical solutions and several numerical experiments are performed to study the effects of fracture density and fracture interconnectivity on the fluid production.

Modeling of heat transfer in fractured rocks is described in *Chapter 4*. First a literature survey of the existing heat recovery models is presented. This is followed by dynamic modeling of heat transfer in naturally fractured reservoirs. A parametric study on factors affecting the heat transfer and consequent heat recovery in naturally fractured geothermal reservoirs are presented.

In *Chapter 5* a summary of the major findings from this study is presented and recommendations for future work are made.

Chapter 2

Generation of Discrete Fracture Network

In this thesis a geothermal reservoir model containing arbitrarily oriented natural fractures is constructed using the methodology developed by Rahman et al. (2002). Typically three major approaches used in literature to generate discrete fracture network include: deterministic modelling, stochastic modelling and the hybrid of deterministic and stochastic modelling.

In the deterministic approach, the fracture distribution and orientation are simulated based on in-situ stress conditions, reservoir structure and tectonic history (Jensen et al. 1998). Typically the dominant fracture orientation is related to the field stress. However, estimating the characteristic properties of existing fracture network on such relationships is not valid. This is due to the fact that the initiation of fractures and their growth are a result of complicated geologic, tectonic and thermal processes over a long period, which make the quantification of characteristic properties of fractures almost impossible. Also the effect of digenesis and mineralisation, which can alter fracture characteristics after they have formed, need to be considered in the simulation (Nelson 2001; Koh et al. 2010).

In the stochastic approach, discrete fractures are simulated by analyzing explicit fracture information (e.g., fracture orientation, aperture and density from different well locations) statistically so that distributions of fracture properties away from the wells could be predicted. Then, fractures are generated by stationary Poisson processes (i.e., random processes) according to the characterised distributions of individual properties. The stochastic generation is carried out until the total number of fractures or fracture intensity is satisfied (Rahman et al. 2002; Koh et al. 2011). However, it ignores the stress condition, tectonic history and geological structure data and, therefore the prediction of fracture properties away from the well bore is may not represent the actual fracture system on the field. In order to overcome the limitations of both approaches recently a hybrid technique to simulate discrete fracture network has been proposed by Golozadeh et al, (2011). In this technique fracture density, generated by the deterministic approach, is used as one of the input to the stochastic simulation.

In this thesis, the stochastic simulation technique is used to in this thesis to generate the natural fracture networks due to the lack of sufficient field data available in public domain.

2.1 Mathematical formulation for fracture network generation

In this study fracture networks are simulated based on the explicit fracture data such as: fracture dip, fracture azimuth, fractal dimension and fracture density (Rahman et al. 2002)

Fracture density is defined as the total fracture length per unit area (in 2D) or total fracture area per unit volume (in 3D). This definition represents the total number of fracture counts and their relative sizes (Rahman et al. 2002; Tran 2007; Tran et al. 2007). Visual image of fractures crossing the wellbore can be obtained from well log data such as: borehole televewer (BHTV), formation multiscan log (FMS), formation micrometer log (FML), video imaging, borehole camera and image logs (Warren and

Root 1963). Thus the fracture density is calculated as the total fracture intersected area with wellbore per unit volume using wellbore images (in conjunction with core description).

Fractal dimension (D) quantifies the degree to which curves or surfaces fill space over a range of scales. Thus, the fracture patterns can be described to a considerable aspect of practical fracture geometry by using D and proportionality constant (C). The box-counting method is often used for determining the fractal dimension of a fracture trace on a map. In the box-counting method, a square region with a side length of L_0 encloses a number of fractures as shown in **Fig. 2.1**. The square region is then divided into L^2_0 /l_2 square boxes of a side length of l. If N(I) is the number of boxes that intersect or contain the fractures and the fracture systems are assumed as a self-similar structure, then N(I) can be expressed as (Hirata 1989; Rahman et al. 2002):

$$N\ I\ = \frac{C}{l^D} \tag{2.1}$$

The value of D, can be estimated from the slope of the line of double logarithmic plot of N(I), against L_0/l plotted based on sample data (see **Fig. 2.2**).

For depicting the natural fracture network by the fractal concept, a cubic block with an edge length of L is considered as shown in **Fig. 2.3(a)**. Within this volume, fractures are distributed following the relationship between the number of fractures and their radius as in **Eqn.2.1**. All fracture shapes are considered as penny-shape (circular). In order to simplify and generalize the problem, both the volume of the block and the fracture positions are normalized by the side length as in **Fig. 2.3(b)**. In the normalized model the total number of fractures is expressed by the symbol n and the i^{th} (i =1, 2, 3, . . . n) fracture is defined by three parameters: the position of fractures centre, $O_i(x, y, z)$; the angle of fracture plane, θ_i, which passes through the fracture centre line with the horizontal plane of the block and the fracture radius, r_i. In order to define the fracture centre $O_i(x, y, z)$, it is assumed that fractures do not intersect to form the clusters and the x, y and z co-ordinates of fracture centre are defined by generating random numbers lying between 0 and 1 in three directions. The angle of fracture orientation, θ_i is also generated randomly. The natural fracture systems are commonly orientated in the direction which can be determined from the data observed in samples. The present model has considered fracture orientations in specified ranges of azimuth and dip for a number of fracture sets observed in the field. The generated fracture orientations from the discrete fracture model, which do not fall within any of these ranges, are removed from the generated fracture data.

By manipulating **Eqn. 2.1**, a relationship can be derived to define fracture radii in terms of fractal dimension. The number of characteristic fractures, n_r whose radii are equal to or greater than r can be expressed using Eqn. 2.1 as:

$$n_r = Cr^{-D} \tag{2.2}$$

If n_{rmax} and n_{rmin} are the numbers of fractures having their radii within the maximum fracture radius r_{max} and the minimum radius r_{min}, respectively, the number of fractures, $n_{r\min}^{r\max}$ between the specified upper and lower radii can be estimated as:

$$n_{r\min}^{r\max} = C(r_{\min}^{-D} - r_{\max}^{-D}) \quad (2.3)$$

Considering a factor α which represents the fraction of the total number of fractures counting from r_{min} upward and the radius of the largest fracture in that fraction, r_α the relationship for this fraction can be written using **Eqn. 2.3** as:

$$n_{r\min}^{r\alpha} = \alpha n_{r\min}^{r\max} = \alpha C(r_{\min}^{-D} - r_{\max}^{-D}) = C(r_{\min}^{-D} - r_{\alpha}^{-D}) \quad (2.4)$$

Rearranging the last two items of **Eqn. 2.4** and eliminating C, r_α can be derived as:

$$r_\alpha = \left[(1-\alpha) r_{\min}^{-D} + \alpha r_{\max}^{-D}\right]^{-1/D} \quad (2.5)$$

Eqn. 2.5 is executed repeatedly with different values of α which is varied as a random deviate between 0 and 1. A fracture radius, r_α is defined each time within r_{min} and r_{max} and assigned to fracture whose centre and orientation are define. The whole process is repeated until the desired fracture density is achieved by the generated fractures.

2.2 Discrete fracture generation for Patchawarra Formation of the Cooper Basin

To study heat transfer between matrix and circulating fluid in naturally fractured geothermal reservoir the Patchawarra Formation of the Cooper Basin is considered (Mildren et al. 2005). Field location map and partial stratigraphic volume for the Coooper-Eromanga Basin is shown in **Figs 2.4** and **2.5**. Field A is located proximally to the main Cooper Basin depecentres and reservoir thickness across the field varies significantly (up to 87%). The in-situ stress field is determined to be strike-slip with σ_{Hmax} oriented approximately 117^0N.

In Cooper Basin Patchwarra formation is located at a depth of 2660m. The Patchawarra Formation is the thickest formation of the Gidgealpa Group, exceeding 300 m in the deepest part of the basin. The base of the formation is marked in part by a 25m thick suite of distributary beds, named the Moorari Beds (Kapel 1972). This unit is made up of grey-black carbonaceous shale, with minor coal. The middle section of the Patchawarra Formation is made up of thick coals and thick, clean sandstones. These sandstones are characterized by porosities averaging 10.7% and more than 75% of the sandstones have a permeability of less than 5 mD. The upper Patchawarra Formation is dominantly a shale sequence. Two simultaneous acoustic and resistivity (STAR) image logs from Well A and Well B have shown that the natural fracture density of Field A is more enhanced at the crest of the structure than at the flanks (Hirata 1989). It has also been identified that the dip of the dominant natural fracture trend varies from 30^0 - 60^0. The strike of 065^0N is predicted to have greater hydraulic conductivity with respect to the in-situ stress field (see **Figs. 2.6 - 2.9**). The reservoir properties of Patchwarra Formation at well A are shown in Table 2.1. The STAR resistivity images logs from Well A have shown that the fracture network have a fracture density of 0.32 m^{-1}. This value along with strike and dip data is used in this study to generate the discrete fracture network. In **Fig 2.10** the generated fracture network with penny shaped geometry is presented. Also two horizontal cross sections of fracture network at 3000m and 3300m in **Figs 2.11** and **2.12**. The virgin reservoir temperature is reported to be in the range of 140^0C -200^0C. In this study to maintain the consistency the initial reservoir temperature is assumed to be 200^0C. In order to investigate the effect of the fracture density on pressure losses between injector and producer three additional fracture densities: 0.007m^{-1}, 0.026 m^{-1}, 0.14 m^{-1} representing a deeper portion of Patwarra formation are considered. The fracture network corresponds to the fracture densities 0.007m^{-1}, 0.026 m^{-1} and 0.14 m^{-1} are presented in **Figs. 2.13- 2.15**.

2.3 Closure

In this chapter the geological data presented in Figs 2.3-2.9 are used to identify the dominant natural fracture trend such as fracture dip, fracture azumath, fractal dimension and fracture density. The natural fracture trends are used as the objective functions and fractures are generated by the stationary Poisson processes (i.e., random processes). Using Rahman et al. (2002)"s approach stochastic fracture generation is carried out until total number of fractures or fracture intensity is satisfied. The generated fracture network expected to represent the existing fracture system of Patchwarra formation.

Table 2.1: Reservoir properties observed using STAR resistivity image logs from Well A.

Top edge (m)	2660.9
Bottom edge (m)	2879.33
Thickness (m)	218.4
Number of Fractures	69
Fracture density (fractures/m)	0.32
Fractures dip	30^0-60^0
Fractures strike	065^0N

Table 2.2: Reservoir properties observed using STAR resistivity image logs from Well B.

Top edge (m)	2660.9
Bottom edge (m)	2879.33
Thickness (m)	218.4
Number of Fractures	14
Fracture density (fractures/m)	0.07
Fractures dip	30^0-60^0
Fractures strike	065^0N

2.4 Figures

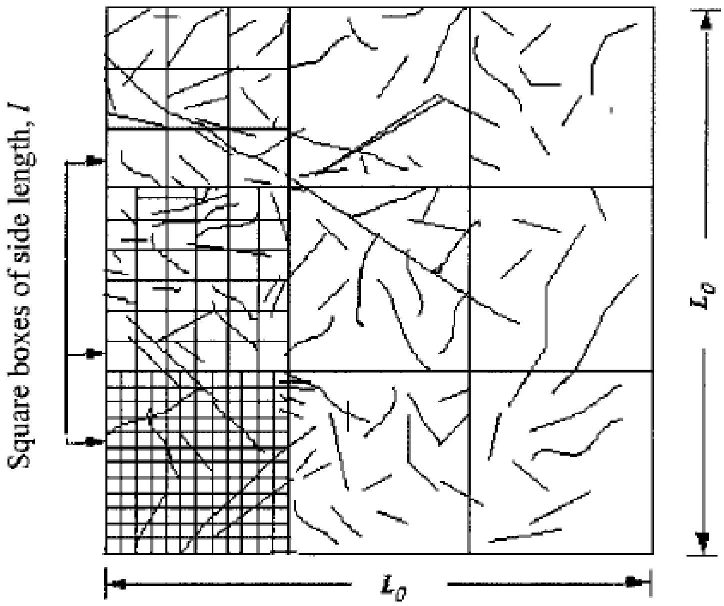

Fig 2.1: Illustration of natural fractures described by the box-counting method (Rahman et al. 2002).

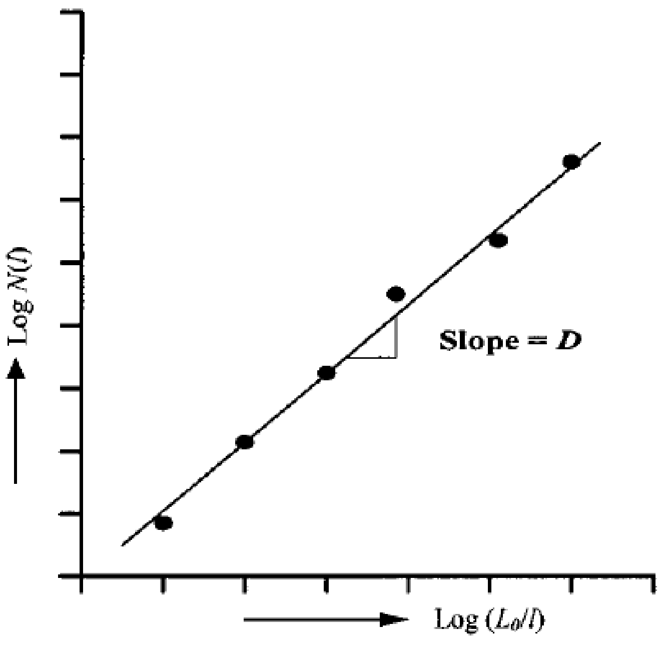

Fig. 2.2: Typical logarithmic plot for estimation of fractal dimension, D using the box-counting method.

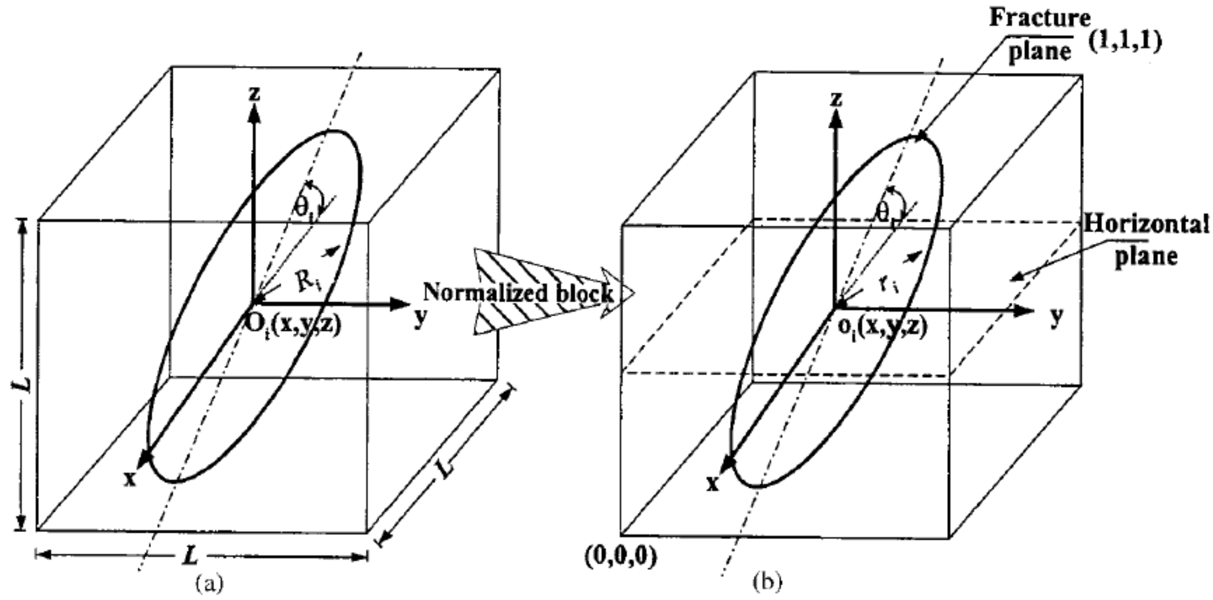

Fig 2.3: Three-dimensional fracture network modelling: (a) a cubic block of side length L, (b) normalized block of unit length in (|x,y,z) co-ordinate system.

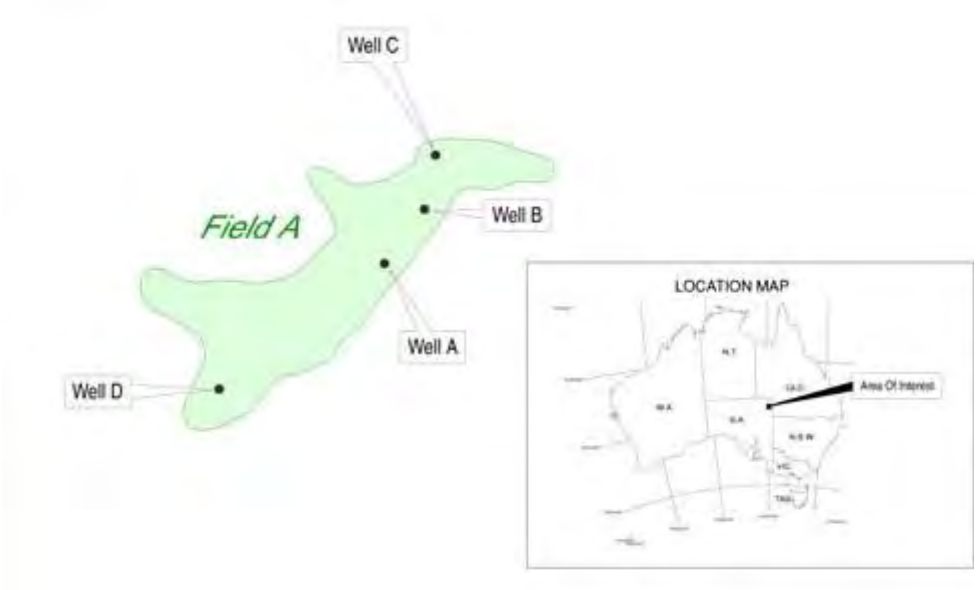

Fig 2.4: Field A location map within the Cooper basin, Australia illustration the locations of Wells A and B (Mildren et al. 2005).

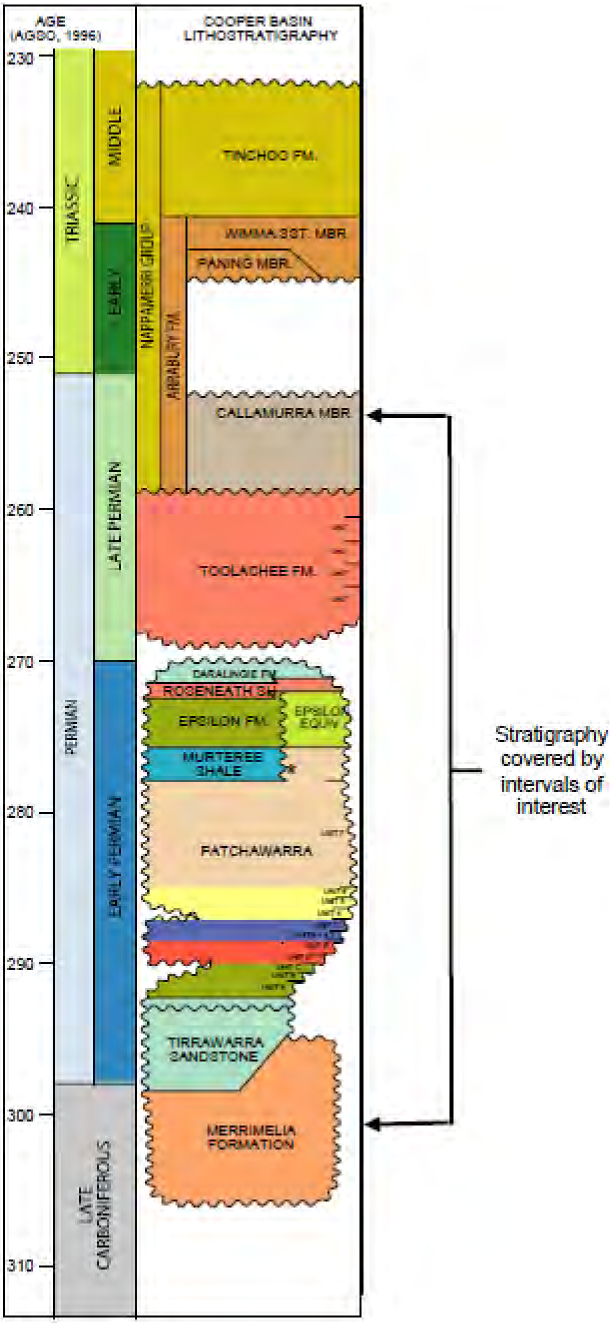

Fig 2.5: Partial stratigraphic column for the Cooper- Eromanga Basin (Mildren et al. 2005).

.

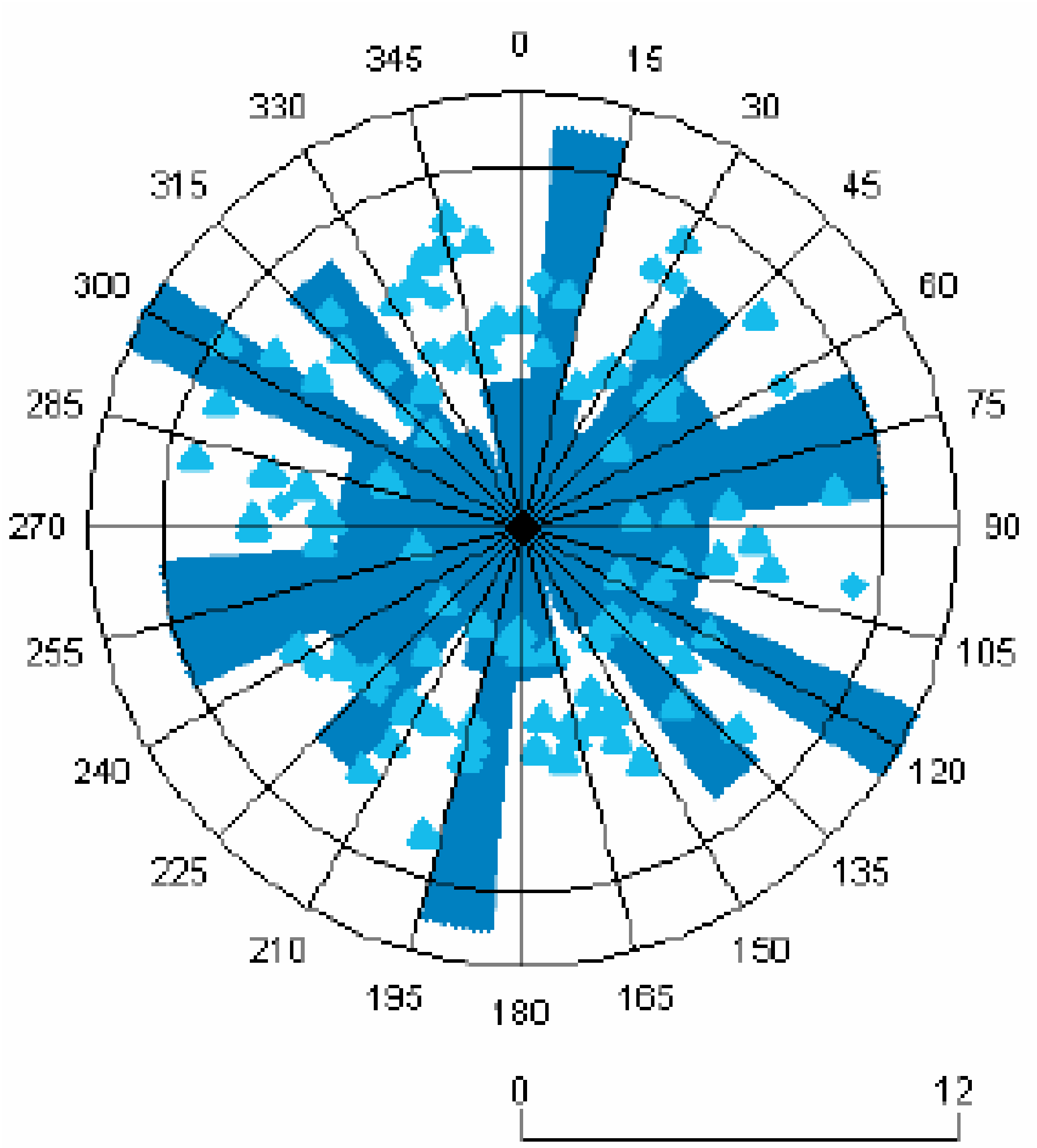

Fig 2.6: Summary of the fracture orientation within Well A identified from STAR resistivity images. Rose plots superimposed on the steronet with faults plots as poles to planes (Mildren et al. 2005).

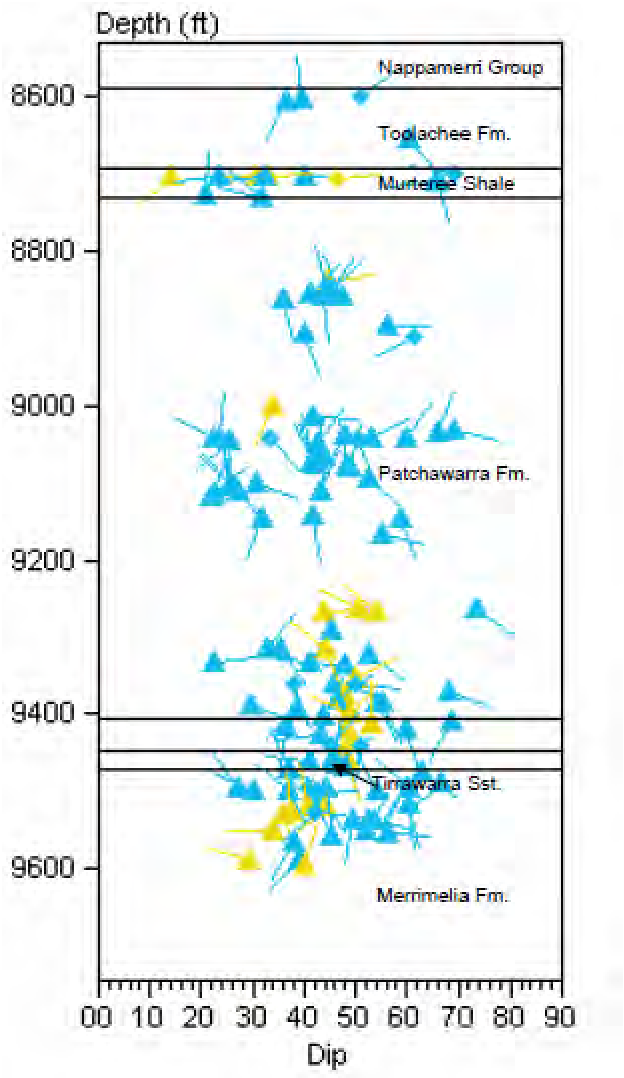

Fig 2.7: Summary of the fracture distribution within Well A identified from STAR resistivity images. Rose plots superimposed on the steronet with faults plots as poles to planes (Mildren et al. 2005).

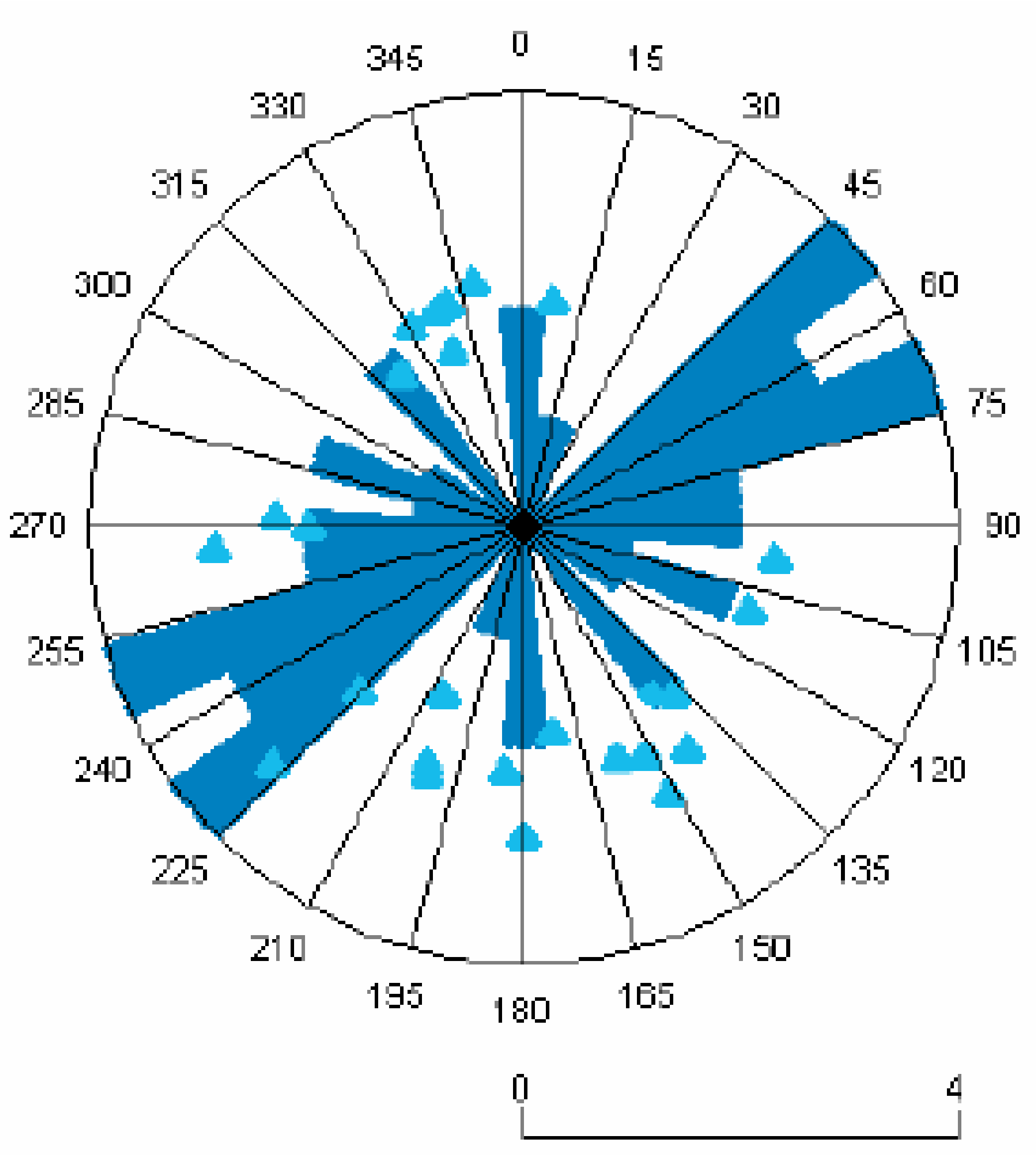

Fig 2.8: Summary of the fracture orientation within Well B identified from STAR resistivity images. Rose plots superimposed on the steronet with faults plots as poles to planes (Mildren et al. 2005).

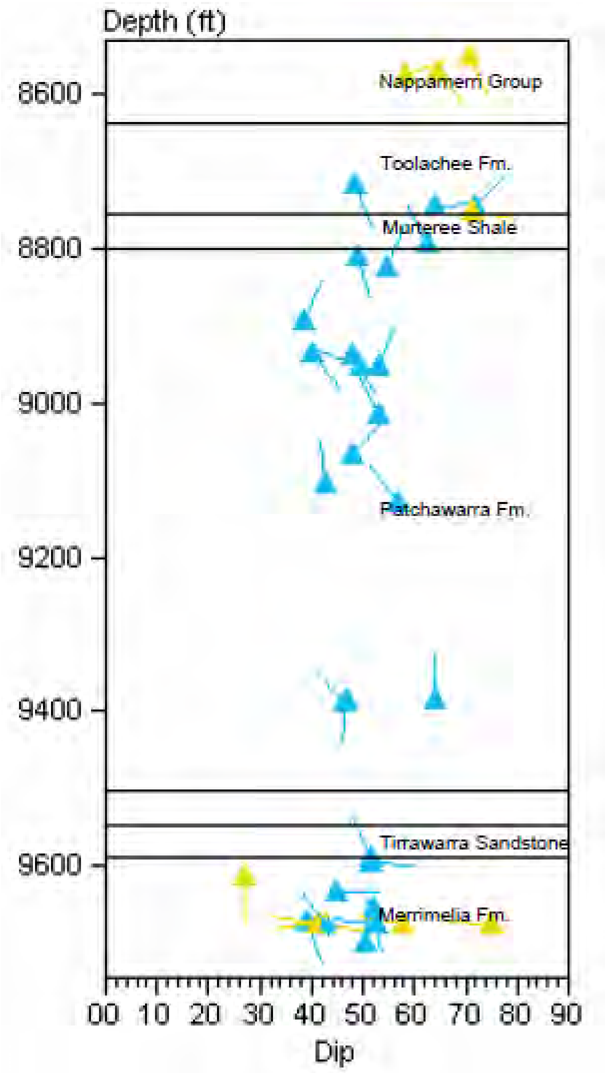

Fig 2.9: Summary of the fracture distribution within Well B identified from STAR resistivity images. Rose plots superimposed on the steronet with faults plots as poles to planes (Mildren et al. 2005).

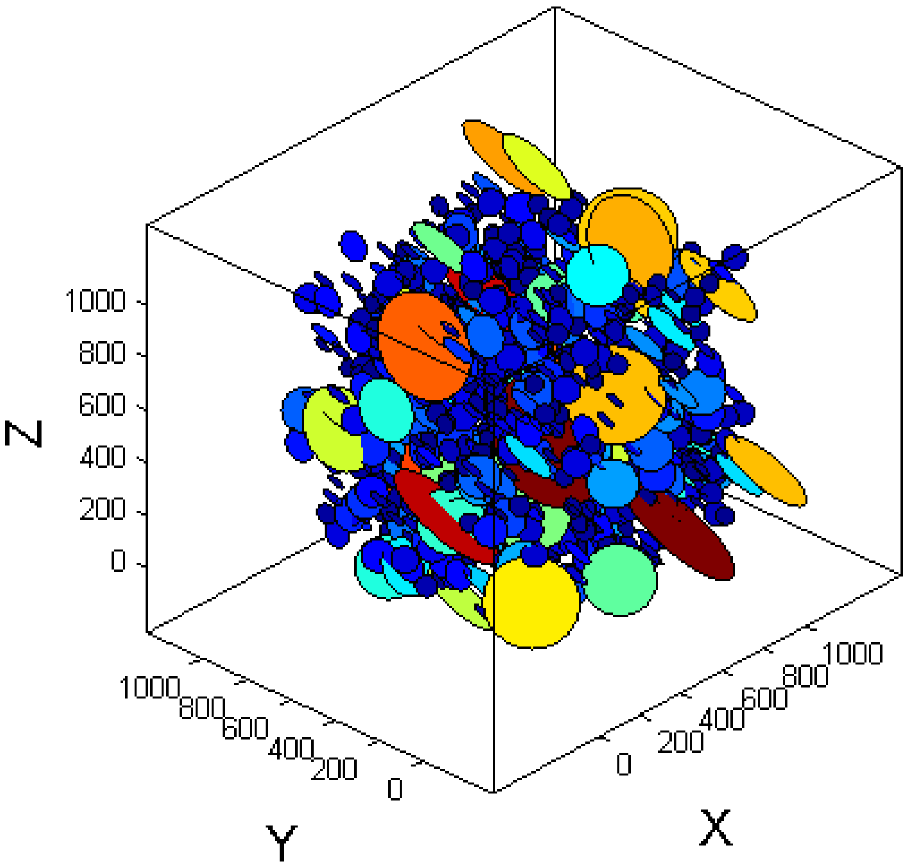

Fig 2.10: Generated discrete fracture map with a fracture density of 0.32 m^{-1}.

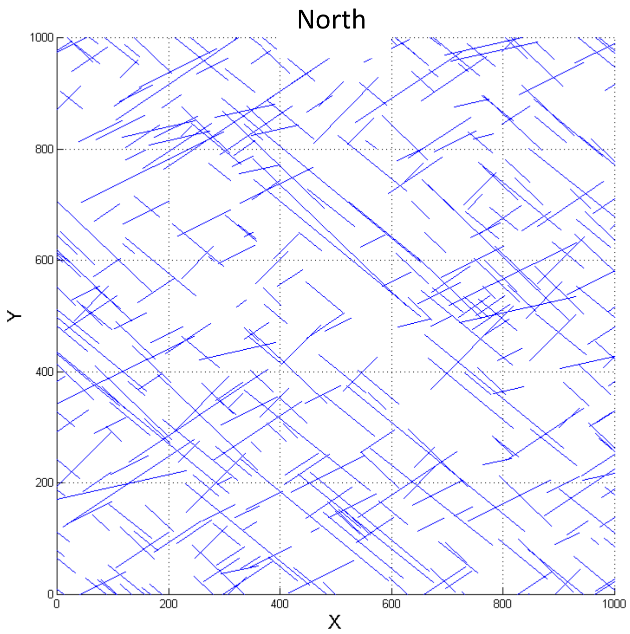

Fig 2.11: Horizontal section at 3000m below surface of discrete fracture map with a fracture density of 0.32 m^{-1}.

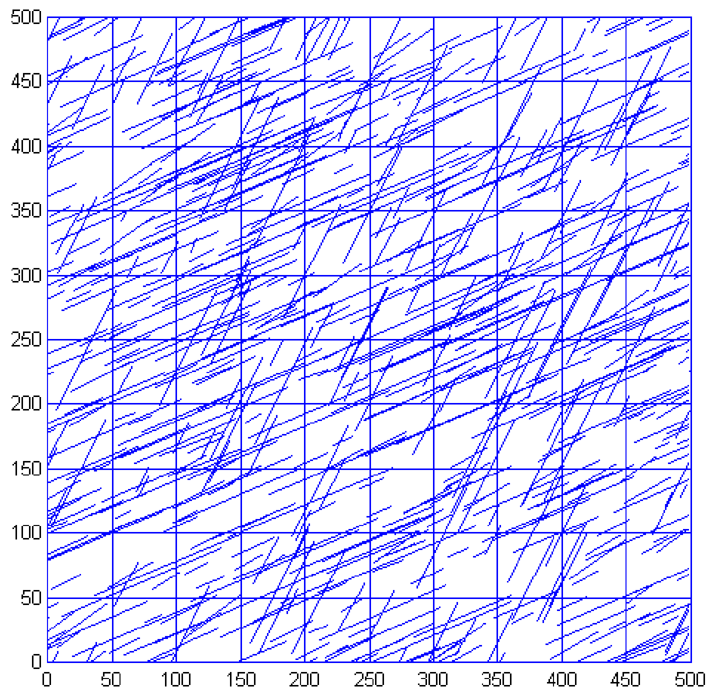

Fig 2.12: Horizontal section at 3150m below surface of discrete fracture map with a fracture density of 0.32 m^{-1}.

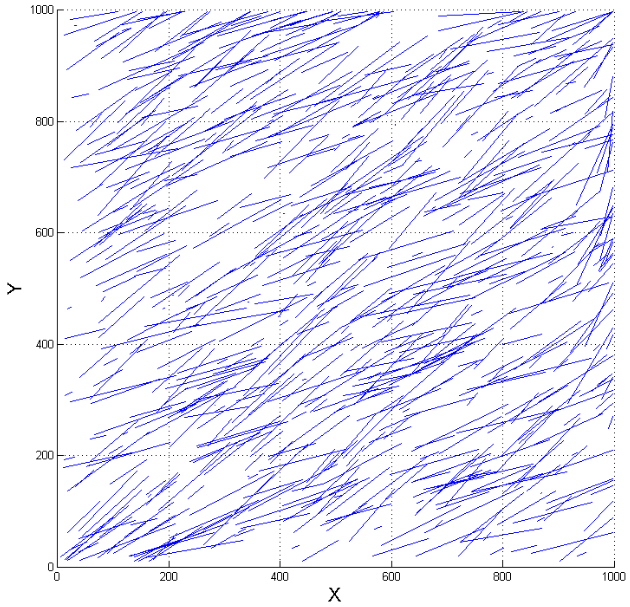

Fig 2.13: Horizontal section at 3000m below surface of discrete fracture map with a fracture density of 0.14 m^{-1}.

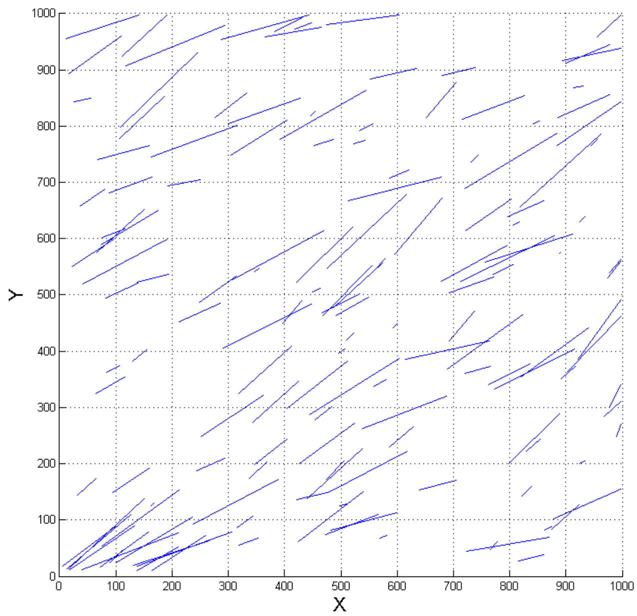

Fig 2.14: Horizontal section at 3000m below surface of discrete fracture map with a fracture density of 0.026 m^{-1}.

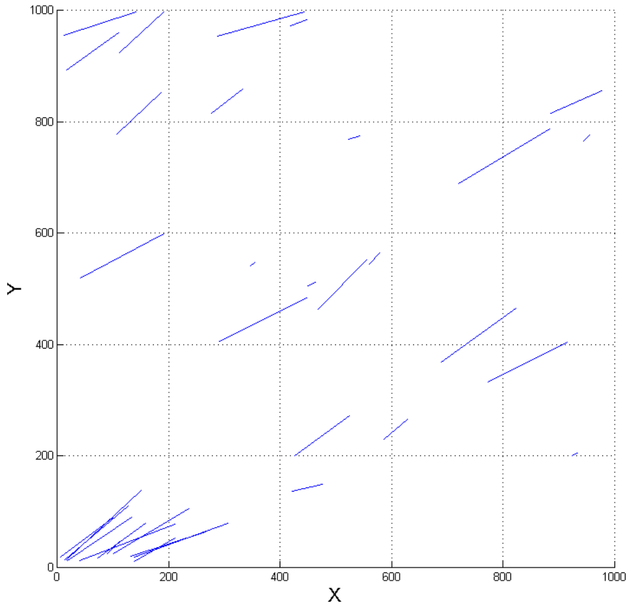

Fig 2.15: Horizontal section at 3000m below surface of discrete fracture map with a fracture density of 0.007 m^{-1}.

Chapter 3

Simulation of Fluid Flow and Estimation of Production from Naturally Fractured Geothermal Reservoirs

In this chapter a numerical model is developed based on the finite element method to simulate fluid flow and prediction of hot water production from naturally fractured geothermal reservoirs. The numerical model is extension to previously developed numerical model by Teimoori et al. (2005) which was primarily focused on investigating the steady state fluid flow in naturally fractured reservoirs. The present model is able to simulate unsteady state flow between wellbore to natural fracture system through fluid induced hydraulic fracture. The present numerical model extended three dimensional as well.

Effect of fracture density, fracture orientation and the flow rate on pressure losses between injector and producer are studied. The effect of well placement for a given fracture set on production rate is also studied.

3.1. Introduction

Typically, naturally fractured geothermal reservoirs have low matrix permeability and fluid flow is mainly controlled by fracture properties. Estimation of production rate and pressure drawdown are difficult tasks as fractures are arbitrarily oriented and fluid flow through such a complicated fracture system is a challenging task. In order to address this issue a number of methods were proposed in literature based on the representation of the fractured medium, the type of fracture network and the size of domain of interest. For instance, in a single continuum approach, the fractured medium is represented by an equivalent porous medium (Hayashi et al. 1999). Bulk macroscopic values of the fractured medium are defined by averaging point-to-point variations in the petrophysical properties over a representative volume (Chin and Nagel 2004). In the dual continuum approach, however, fractures and matrix are represented as multiple interacting continua, where the fractures provide permeability and the matrix provides storage capacity (Warren and Root 1963). Thus, typically fractured porous media are represented as two equivalent fracture and matrix media consisting of identical rectangular matrix blocks separated by an orthogonal network of fractures (Barenblatt et al. 1990) .

Although this approach has the advantage of investigating the complex process of matrix-fracture interaction, it is not able to account for fluid flow through the complex structure of fracture networks (Bai et al. 1994). Also, heterogeneity of the fractured rock is represented by fracture spacing only. Thus, the individual fractures are not treated explicitly (El-Zein et al. 2005). In another attempt, Pruess and Narasimhan (1985) extended the dual continuum model by introducing the multiple interacting continua (MINC) where the matrix block is discretized into smaller units. The well-known commercial software TOUGH2, which is used to simulate fluid flow in geothermal reservoirs, uses the MINC approach . The major problem associated with the MINC approach is the use of equivalent hydraulic properties, especially permeability, for fractured networks. Despite having many advantages both the single and dual continuum approaches do not effectively simulate fluid flow through naturally fractured geothermal reservoirs (Juliusson and Horne 2010). In a recent study Juliusson and Horne (2010) has concluded that single and dual continuum models are not suitable to estimate heat extraction from naturally fractured geothermal reservoirs. This is due to the fact that naturally fractured geothermal reservoirs have non-uniform fractures and both single and dual continuum models are primarily developed for the purpose of homogenous reservoirs and reservoirs with uniform fractures respectively.

To overcome the limitations of the continuum approaches, a discrete fracture network approach was proposed. In this approach, fracture and matrix are discretised by a mesh system. Equations for fluid flow are solved by both exact and approximated methods, e.g. the boundary element method, finite element method, finite volume method and mixed finite element method (Kazemi et al. 1976; Niessner et al. 2005; Hoteit and Firoozabadi 2008). In spite of their advantages over the continuum methods, these discrete models could not overcome their inherent disadvantage of requiring extremely high computational resources (or prolonged runtimes). Moreover simulation of fluid flow between fracture and surrounding matrix needs extensive mesh refinement around fractures. (Deo et al. 2008; Xing 2008; Geiger-Boschung et al. 2009). In a recent study Hoteit and Firozabadi (2008) was able to simulate fluid flow in a few fractures by using the mixed finite element method. Based on these results it can be concluded that the use of discrete fracture network approach is limited either to a small area within a domain or to domain of a low fracture density. An example for an exhaustive use of high computation resources is the GeoSys/RockFlow software (an open source code). This software requires high performance computational techniques to simulate fluid flow (Kemmler et al. 2005; Watanabe et al. 2010). Based on the previous attempts to address the problems associated with the fluid flow through naturally fractured geothermal reservoirs it can be concluded that the dual-porosity approach and the discrete fracture approach cannot address the issues pertinent to the simulation of fluid flow through the naturally fractured geothermal reservoirs efficiently and an alternate approach which is called hybrid scheme, has been proposed (Pruess and Narasimhan 1985; Gong et al. 2006; Juliusson and Horne 2010).

The hybrid scheme has been developed as an alternative to the discrete fracture network in which the block-based effective permeability tensor has been introduced to represent fracture networks (Castaing et al. 2002; Teimoori et al. 2005; Blum et al. 2009). In this approach each grid-block with fractures is replaced by a homogeneous grid-block having an equivalent permeability tensor, which takes into account of the geometry of the actual fractures. Several methods have been proposed in literature to calculate the effective permeability tensor. Oda (1985) introduced a statistical approach for calculating the equivalent permeability tensor of a fractured reservoir using the geometry of fracture network. This approach, however, does not account for the flow through matrix and matrix to fracture or fracture to matrix. Lough et al.(1998) extended the effective permeability tensor approach by proposing a two dimensional flow model which accounts for flow through fractures and matrix to fracture or fracture to matrix. Later Bourbiaux et al. (1998) extended the two dimensional flow model to investigate size of representative elementary volume (RPV)using specific boundary conditions. Min et al. (2004) have used a stochastic approach and REV to simulate fluid flow in fractured network and to calculate the effective permeability tensor. However, it is important to note that the characteristic properties of discrete fractures in each grid block (REV) are not used to simulate fluid flow. A comprehensive 2D model to simulate fluid flow was proposed by Teimoori et al. (2004). Short fractures are considered as part of matrix and Laplace"s equation with the interface boundary condition is used to simulate fluid flow while the Poisson"s equation is applied to medium and long fractures as well as the part of matrix that is located around these fractures. They used the boundary element method with periodic boundary conditions in each grid block.

3.2. Formulation of 3D fluid flow simulation

The methodology developed by Teimoori, Chen et al. (2005) is used to calculate the grid based effective permeability tensor. In this approach fractures are classified as long, medium or short fractures. Typically, effective permeability is described as a full tensor that relates the average pressure gradient ∇p to the average fluid velocity, V as:

$$V = -\vec{\vec{K}} \nabla p \tag{3.1}$$

where, $\vec{\vec{K}}$ is the local permeability tensor describing the directional effect of fracture or a set of fractures on fluid flow. Assuming that fluid flow in matrix and fracture obeys Darcy"s Law and Cubic Law respectively, the governing equations of fluid flow in a two-dimensional fractured rock can be expressed as:

$$\text{Fracture:} \quad k_{fs} \frac{\partial^2 p_i}{\partial L^2} + Q_f + q_{ff} = 0 \tag{3.2}$$

Matrix: $$k_{ms}\frac{\partial^2 p_m}{\partial x^2}+k_{ms}\frac{\partial^2 p_m}{\partial y^2}+Q_m=0 \qquad (3.3)$$

where, k_{fs} is the fracture permeability, L is the one-dimensional coordinate, p is the pressure and subscripts *m* and *f* represent the matrix and fracture, respectively. Terms Q_m and Q_f represent the flow rates in matrix and fractures, respectively. q_{ff} is the flow rate at the point of intersection of intersecting fractures. Matrix permeability is assumed to be constant in the horizontal and vertical directions as in a homogeneous system, and fracture permeability is calculated using the Cubic Law with the parallel plate assumption by which the mean fluid velocity in a fracture is proportional to the square of the fracture aperture (Novakowski et al. 2006). Fracture roughness has been ignored in this model. The fracture permeability can be expressed as:

$$k_{fs}=7.482x10^{12}h_s^2 \qquad (3.4)$$

where, h_s is the fracture aperture which is initially derived from a fracture characterisation model. Individual fracture properties such as the fracture length, aperture and orientation are used to calculate the effective permeability as shown in **Fig. 3.1**. The interface boundary conditions for short fractures are expressed as:

$$v(x_1,0).\overline{n}1=-v(x_1,1).\overline{n}2 \qquad (3.5)$$

$$v_{mi}=-v_{fi} \qquad (3.6)$$

where, $v_{mi}=\vec{v}_m.\vec{n}$, $v_{fi}=\vec{v}_f.\vec{n}$ and p_{mi} and p_{fi} are the matrix and fracture pressures at the interface, respectively and $\vec{v}_f$ and $\vec{v}_m$ are the fracture and matrix velocities, respectively. Boundary conditions along medium and long fracture boundaries are written as:

$$p_{fi} = p_{av} \tag{3.7}$$

$$v^{+}_{mi} - v^{-}_{mi} = Q_i \tag{3.8}$$

where, $v^{+}_{mi} = v^{+}_{m}.\overline{n}$, $v^{-}_{mi} = v^{-}_{m}.\overline{n}$ and p_{av} is the average pressure inside the fracture and p_{fi} represents the pressure along the fracture boundaries. v^{+}_{mi} and v^{-}_{mi} are the velocities on the opposite nodes on the fracture faces. Q_i depends on the source strength of the fracture and represents the flow interaction between the matrix, m and fracture, i. Pressure at the matrix-fracture interface and at the exterior boundaries of the fracture are unknown and calculated by applying the periodic boundary condition during the solution process.

The periodic boundary condition is considered for nodes along the block boundaries. This requires all fracture edges to be treated as being inside the grid block (Rijken 2005). If a fracture crosses the grid block, the fracture is treated as two different fractures which are connected at the fracture edge. Assume that Γ1 and Γ2 are two opposite faces of the grid-block in the x_2 direction and Γ3 and Γ4 are two opposite faces of the grid-block in the x_1 direction. Pressure at an arbitrary point x = (x_1, x_2) in the grid-block can be expressed as:

$$p(x) = p_o + J(x - x_o) \tag{3.9}$$

where, x_o is the centre of the region under consideration, p_o is the pressure at x_o, and J (= j1, j2) is the local pressure gradient. The periodic boundary conditions over the grid block are written as:

$$p(x_1,0)=p(x_1,1)-j_2 \qquad \text{on } \Gamma 1 \text{ and } \Gamma 3 \qquad (3.10)$$

$$v(x_1,0).\overline{n}1=-v(x_1,1).\overline{n}2 \qquad \text{on } \Gamma 1 \text{ and } \Gamma 3 \qquad (3.11)$$

$$p(0,x_2)=p(1,x_2)-j_2 \qquad \text{on } \Gamma 2 \text{ and } \Gamma 4 \qquad (3.12)$$

$$v(0,x_2).\overline{n}2=-v(1,x_2).\overline{n}4 \qquad \text{on } \Gamma 2 \text{ and } \Gamma 4 \qquad (3.13)$$

A constant pressure difference in the x_1 direction and a zero pressure difference in the x_2 direction (j1 ≠ 0 and j2 = 0) are applied to calculate the first two terms of permeability tensor k_{xx} and k_{yx} (Rijken 2005). The remaining two components of permeability tensor, k_{xy} and k_{yy} can be calculated in the same way by varying the direction of pressure gradient as j1 = 0 and j2 ≠ 0. Linear equations are solved by applying periodic boundary conditions in conjunction with boundary conditions along the fracture boundaries.

In these equations unknowns are pressure and normal velocity on the grid-block boundaries, pressure and source strength (fluid flow rate) at the fracture faces and edges, flow rate inside the fracture and flow rate at the adjoining area of intersected fractures. The source term at the fracture boundaries and flow rate inside the fracture are calculated once the pressure and velocities at fracture and block boundaries are known. By treating short and medium-long fractures differently, the calculation of permeability tensors becomes faster and more accurate than the previous models. Another advantage of the current approach is that it discretises the area which is located around the fracture, not the whole matrix inside the block (see **Fig. 3.1**). This saves computation time and reduces the numerical error during the solution process.

Once the effective permeability tensor is calculated for each grid block the fluid momentum balance equation (**Eqn. 3.14**) is used to simulate unsteady state fluid flow. The coupled form of the fluid momentum balance equation can be expressed as:

$$\phi c_t \frac{\partial p}{\partial t} = \frac{\partial}{\partial x}\left(\frac{k_{xx}}{\mu}\frac{\partial p}{\partial x}\right) + \frac{\partial}{\partial x}\left(\frac{k_{xy}}{\mu}\frac{\partial p}{\partial y}\right) + \frac{\partial}{\partial x}\left(\frac{k_{xz}}{\mu}\frac{\partial p}{\partial z}\right) + \frac{\partial}{\partial y}\left(\frac{k_{yx}}{\mu}\frac{\partial p}{\partial x}\right) + \frac{\partial}{\partial y}\left(\frac{k_{yy}}{\mu}\frac{\partial p}{\partial y}\right) + \frac{\partial}{\partial y}\left(\frac{k_{yz}}{\mu}\frac{\partial p}{\partial z}\right)$$
$$+ \frac{\partial}{\partial z}\left(\frac{k_{zx}}{\mu}\frac{\partial p}{\partial x}\right) + \frac{\partial}{\partial z}\left(\frac{k_{zy}}{\mu}\frac{\partial p}{\partial y}\right) + \frac{\partial}{\partial z}\left(\frac{k_{zz}}{\mu}\frac{\partial p}{\partial z}\right) \qquad (3.14)$$

where μ, p, c_t and ϕ represent the viscosity, pressure, total system compressibility, porosity and k represents the elements of permeability tensor. Full derivation of the Eqn. 3.14 is shown in Appendix A.

3.3 Numerical procedure

Fig. 3.2 describes the solution strategy used to simulate fluid flow through spatially distributed fractured network using the hybrid method. Initially a discrete fracture network is generated as described in chapter two. A numerical model developed as part of the thesis comprises of two modules namely tensor and flow modules to study the fluid flow through the discrete fracture network in each grid block. The model geometry includes a square reservoir block with embedded natural fractures of different size, orientation and aperture and wellbores. Spatial discretisation of such geometry is complicated due to the point to point variation in rock properties. In order to have different geometry to suit the purpose a special mesh generator is developed. Mesh generator is used to divide the whole reservoir into a number of square grid blocks. Fractures belonging to each grid block are identified and transferred to tensor module along with the mesh data. In the tensor module, governing **Eqns. 3.1** through **3.3** are discretised using the boundary element method and effective permeability tensor for each grid is calculated for the entire reservoir domain. Then the grid based effective permeability tensor map is transferred to fluid flow module to simulate fluid flow.

In fluid flow module eight nodded isoperimetric quadrilateral elements are used to discretize **Eqn. 3.14**. The main assumptions of fluid flow module are as follows:

- Fluid flow is linear throughout the reservoir.
- No chemical reaction between porous medium and injected fluid.
- Effect of hydraulic stress induced by circulating fluid on fracture aperture is ignored.
- Hydraulic fractures are treated as infinitely conductive.
- The reservoir edges are impermeable.
- Pressure losses inside the wells are negligible.
- Reservoir rock is fully saturated with fluid.
- Gravity effects are neglected.

The standard Galerkin based finite element discretization of **Eqn. 3.14** is presented in Appendix-B (Zienkiewicz and Taylor 2000). Hydraulic fractures are treated as linear elements. To minimize the memory requirement the system of linear equations are solved in band storage mode using the Linear Algebra PACKage (LAPACK) library and pressure profile and subsequent velocity profiles are evaluated at every time step inside the fractured rock.

3.4 Validation of the numerical model

Full validation of the developed numerical model is difficult due to a lack of comprehensive fluid flow model for naturally fractured geothermal reservoirs. In this study the individual modules are validated using the results of previous studies. This type of validation is widely used in the literature (Bagheri and Settari 2006; Ghassemi et al. 2008) when no other effective tool is available.

First, a fracture is rotated inside a grid block and the numerical results of diagonal and off diagonal elements of permeability tensor are verified with the mathematical solution presented by Lough et al. (1998). In this example, a fracture has a length of 0.8 units and an aperture of 1.0×10^{-4} units inside the grid-block of unit length (see **Fig. 3.3**). Matrix permeability is set to 1 mD and fracture permeability 2.0×10^{6} mD. Numerical results of effective permeability for different orientations of the fracture are presented in **Figs. 3.4 and 3.5**. The numerical results agree well with the mathematical solution presented by Lough and Lee (1998). Next, the results of effective permeability are compared with those derived numerically and experimentally by Fahad et al. (2011). For this purpose a section of the reservoir, lower part (see Fig. 9 of Fahad et al. (2011)) with a fracture density of $0.02m^{-1}$ at depth 3100m of Soultz Geothermal Reservoir in France is considered. The reservoir section is divided into 100 grid blocks. Results of effective permeability tensors in the form of ellipses along with the fracture network are presented in **Fig. 3.6**. The x and y axes of ellipse represent the magnitude of the diagonal elements of effective permeability and the direction of ellipse represents the off-diagonal terms of the effective permeability tensor. These results match very well with results of Fahad et al. (2011). Also the direction of ellipses is in line with the orientation of major fractures.

Finally the fluid flow module was validated by injecting a slightly compressible fluid into a homogeneous rock from one corner of the block and the numerical results of pressure drawdown are compared with that from an analytical solution presented by Carslaw and Jaeger (1959) and Aghighi (2007). The analytical solution is valid only for an infinite reservoir and its solution is shown in Appendix-C. In order to meet this requirement one can choose a large drainage area or small time steps or both such that the change in pore pressure is not felt at the outer boundary. Moreover the viscosity, pressure, total system compressibility, porosity and permeability are assumed to be independent of time and space in order to be consistent with the analytical solution. As shown in **Fig. 3.7**, the accuracy of the numerical results improves as the time step decreases (from hours to minutes).

3.5. Numerical experiments

In order to study the reservoir performance of naturally fractured reservoirs with four fracture densities, 0.007m^{-1}, 0.026m^{-1}, 0.14 m^{-1} and 0.32 m^{-1} as presented in Figs 2.10 -2.15 in chapter 2 are considered. A reservoir of size 1000mx1000mx300m is selected for this purpose. Four different production wells, A, B, C and D are placed at four corners and an injector at the centre of the reservoir block (see **Fig 3.8)**. The well depth is considered to be 3000m. A pair of hydraulic fractures of 22m half-length is placed at the injector. Due to the symmetry in the model geometry, only a fracture half length is placed at each production well. These fractures are used to enhance connectivity between wellbores and the fractured system. Reservoir parameters, fractured rock and fluid properties are presented in **Table 3.1**. Initially all the four reservoirs (with fracture densities, $0.007 m^{-1}$, $0.026 m^{-1}$, $0.14\ m^{-1}$ and $0.32\ m^{-1}$) are divided into different grid blocks and the permeability tensor is calculated for each grid block using permeability tensor model. **Fig 3.9** represents the permeability tensor map generated for the reservoir with a fracture density of $0.32\ m^{-1}$, at a depth of 3150m (see Fig 2.12 in chapter 2).

Fracture density on pressure loss

Results of pressure losses between the injector and the producers as a function of total production rate from production wells (A, B, C and D) are presented in **Fig.3.10**. From the results of this study it can be seen that there is a sharp increase in the pressure loss with an increase in flow rate, in particular for low fracture density reservoirs. For example, for a reservoir with a high fracture density ($0.32\ m^{-1}$) pressure loss between injector and producer reaches a value of 1500 psi for a total flow rate 138 l/s (Average reservoir impedance of $0.29\ MPa.l^{-1}\ s$). This pressure loss is very much in line with the Soutz Geothermal Field flow test data (reservoir impedance of $0.23\ MPa.l^{-1}\ s$). For the same pressure drop flow rates of 12.4 l/s, 18.8 l/s and 69 l/s can be achieved for reservoirs with fracture density of $0.007 m^{-1}$, $0.026 m^{-1}$ and $0.14\ m^{-1}$, respectively. These results indicate that the pressure loss is related to the interconnectivity of the fracture which in turn related to the fracture density. Typically a reservoir with a high fracture density has potential to produce hot water at reduced pressure losses.

Production well placement on production rate (interconnectivity)

In order to study the effect of interconnectivity between the wells on production rate two naturally-fractured reservoirs with a fracture density of 0.14 m^{-1} (medium fracture density) and 0.32 m^{-1} (high fracture density) are considered. Positions of the production wells with respect to the injection well are presented in **Fig. 3.8**. Results of pressure losses between the injector and the producers as a function of flow rate for the two fracture systems are presented in **Figs. 3.11** and **3.12**. From the results it can be seen that for both fracture densities (0.32 m^{-1} and 0.14 m^{-1}) well C provides the highest production rate while well B provides the lowest. For the reservoir with fracture density 0.14 m^{-1} a pressure loss of 500 psi experienced for the production rate of 23 l/s at well C. It has been noticed that a production rate of 55 l/s at well C has reached at pressure loss of 1500 psi between injector and producers. At this pressure loss (1500psi) production well C contributes to about 74% of total production rate for the reservoir with fracture density of 0.14 m^{-1} and 59% with fracture density of 0.32 m^{-1}. This large contribution of production at well C is due to the fact that most fractures are oriented along North-East which allowed the well C to be well connected to the induced hydraulic fracture (see Fig 2.9-2.13). Although the fracture system is oriented along the two wells A and C (North-East) well A does not contribute significantly to the production. This is because the fracture system is not well connected with the well A through the induced hydraulic fracture. It is also evident from these Figs 3.11 and 3.12 that with an increase in flow rate the pressure loss across the injector and producer increases and this increase in pressure loss is more profound for a medium fracture density reservoir than that of high fracture density reservoir.

In **Figs 3.13** and **3.14** the velocity profile for the reservoir with a fracture density of 0.14 m^{-1} and 0.32 m^{-1}, respectively are presented. From these figures it can be seen that the high fluid velocities are aligned along the fracture pattern and fluid velocity towards well C is the greatest while well B the lowest. These results suggest that well placement has significant effect on the production rate especially in naturally fractured geothermal reservoirs where fractures control major flow paths. Similar results are observed in the Beowawe Field, (50% of the total production rate) and in Dixie Vally field (35% of the total production rate) in USA where the wells are well connected to the fracture system (Tester et al. 2006). In the Hijori Geothermal Field, Japan only 25% of the injected water was recovered from the production well-OGC-2. Later, another production well was drilled which significantly decreased the water loss between injection well and production well (Tester et al. 2006)..

3.6 Closure

In this chapter, a fluid flow simulation model is developed to estimate fluid production from naturally fractured geothermal reservoirs. Fluid flowing from well to natural fracture system via fluid induced hydraulic fracture is used to study the effects of characteristic properties of fractures on pressure drawdown and consequent production rate in these geothermal reservoirs.

The numerical results have shown that the fracture pattern, which includes fracture orientation and fracture density, has a significant effect on pressure losses between the injector and producer and production rate. The numerical results also show that well placement has a significant effect on fluid production rate. With an increase in flow rate the pressure loss across the injector and producer increases and this increase in pressure loss is more profound for a low fracture density reservoir than that of the high fracture density reservoir. Block wise discretization of fractures for estimating effective permeability instead of the entire reservoir is an efficient approach to estimate fluid production efficiently at reasonable computational resources.

Table 3.1: Reservoir parameters used in this study

Parameters	Value
Reservoir porosity	0.1
Reservoir temperature (^{0}C)	200
Heat capacity of rock (J/kg ^{0}C)	1170
Density of rock (kg/m^3)	2820
Thermal conductivity of rock(W/ m ^{0}C)	2.8
Heat capacity of fluid (J/kg ^{0}C)	4200
Density of fluid (kg/m^3)	900
Thermal conductivity of fluid(W/ m ^{0}C)	0.609
Hydraulic fracture half length (m)	55
Initial water viscosity (cp)	0.3
Injected water temperature(^{0}C)	80
Fracture densities (m^{-1})	0.007,0.026,0.14 and 0.32
Well depth (m)	3000
Pressure loss between injector and producer (psi)	500,1000 and 1500
Heat transfer coefficient (mW/m^2 ^{0}C)	0.1, 1, 5 and 10

3.7 Figures

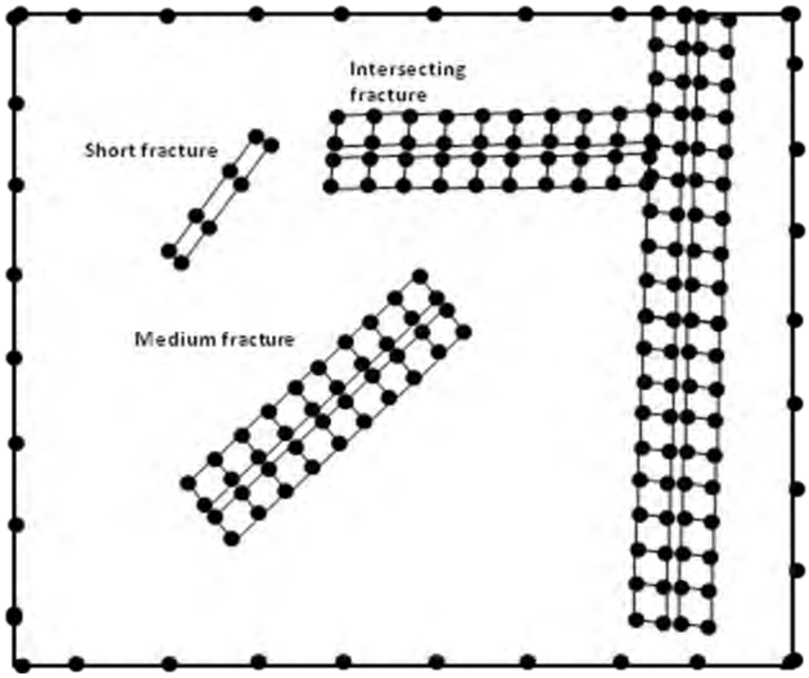

Fig. 3.1: Boundary nodes on fractures and a grid block and interior discretization in two dimensions.

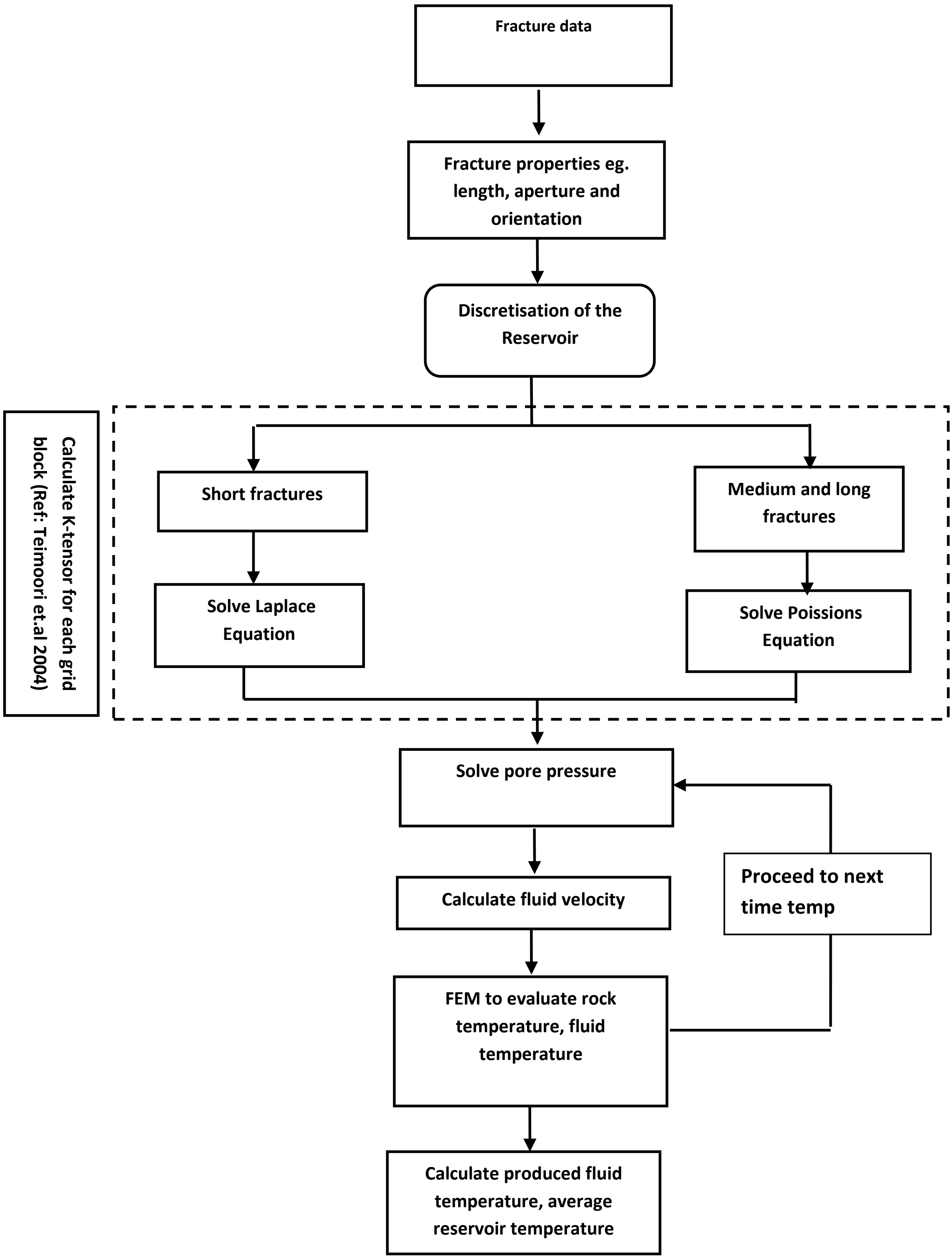

Fig. 3.2: Flow chart of the numerical procedure.

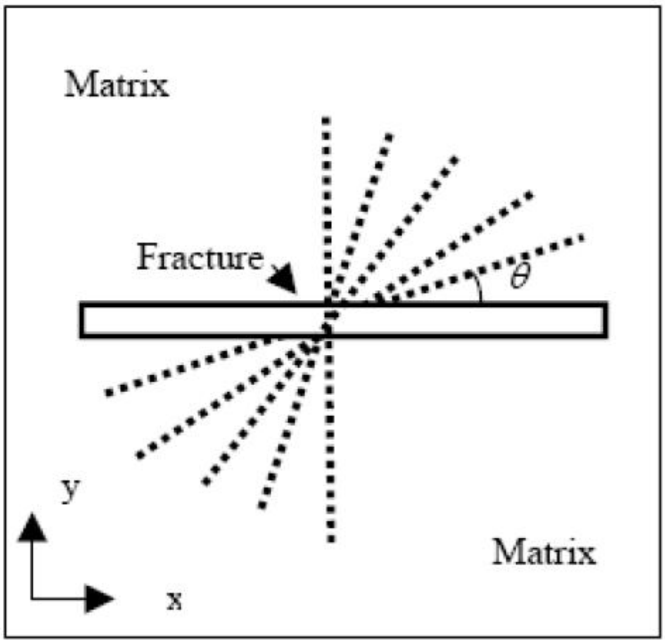

Fig. 3.3: Position of a fracture at different orientations inside a grid block (after Teimoori et al. 2004).

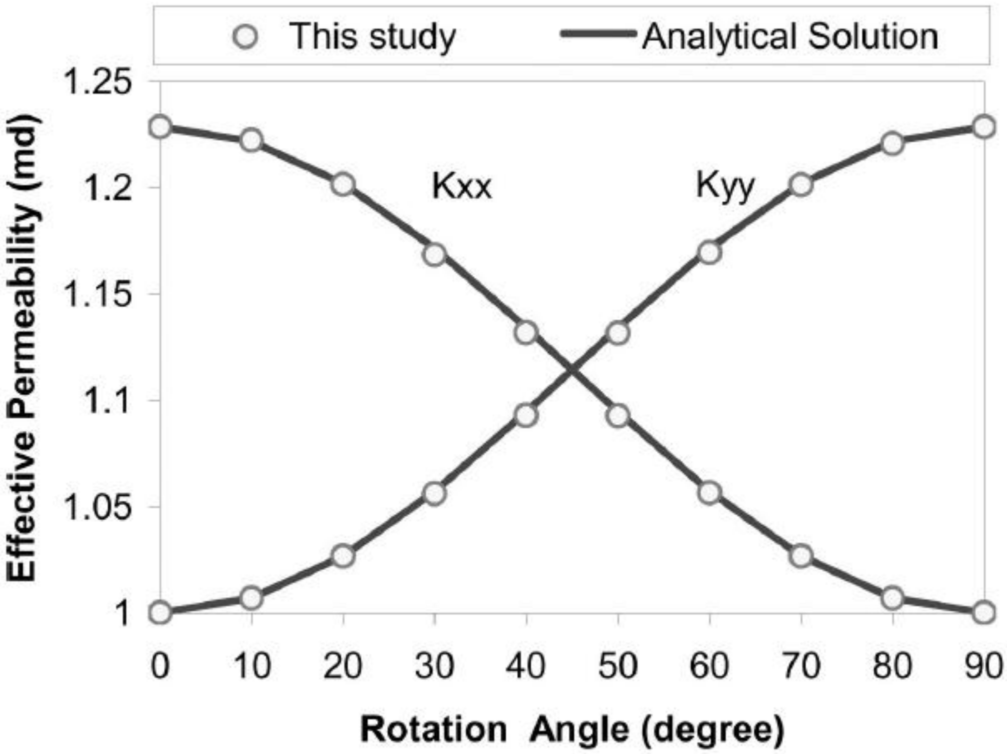

Fig. 3.4: Comparison of analytically and numerically calculated diagonal elements of permeability tensor for a fracture at different orientations in a grid block.

.

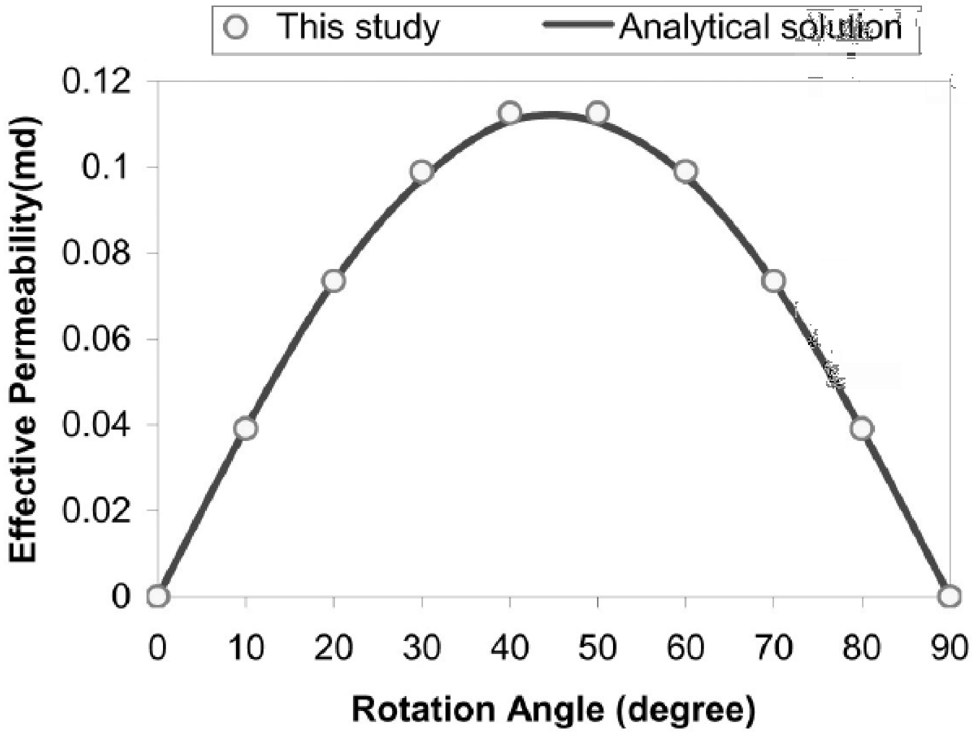

Fig. 3.5: Comparison of analytically and numerically calculated off diagonal elements of the permeability tensor for a fracture at different orientations in a grid block.

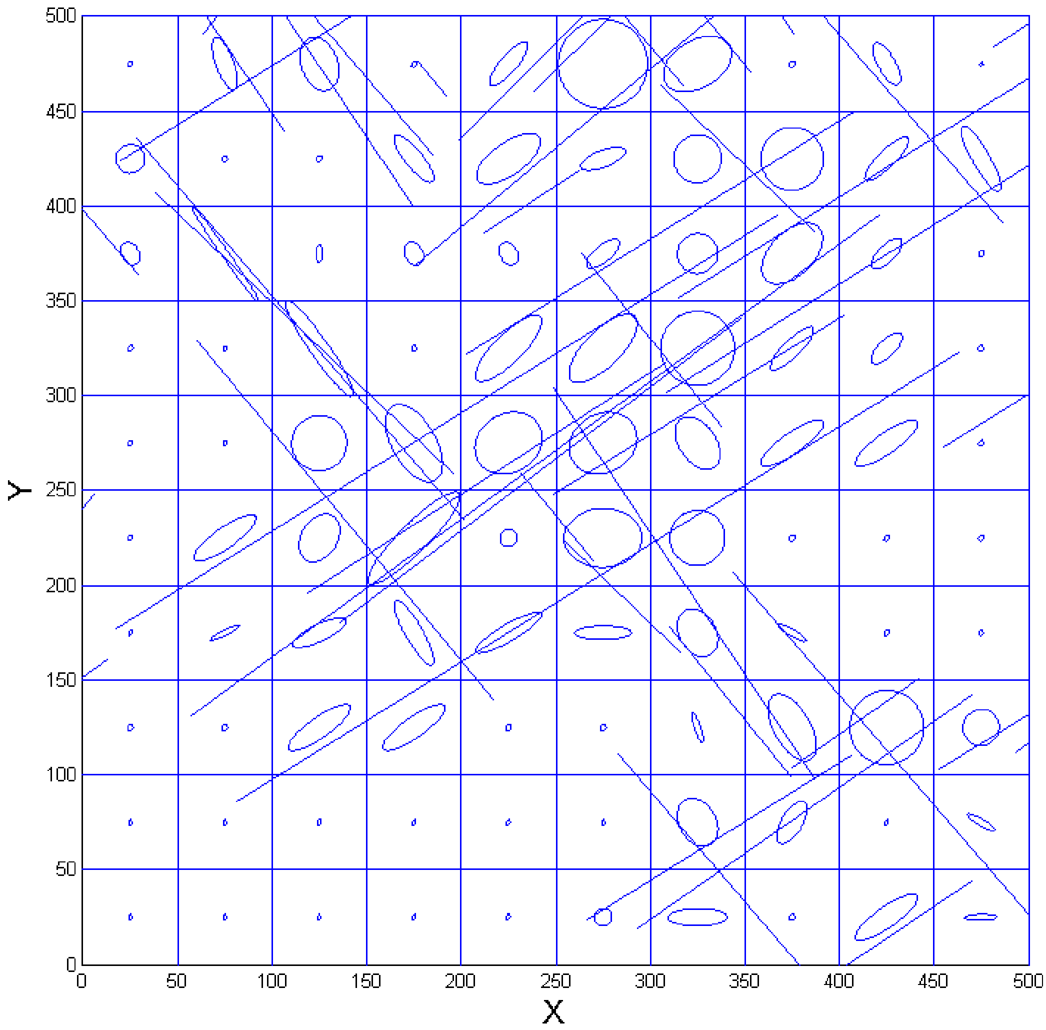

Fig. 3.6: Comparison of numerically calculated permeability tensors for a square reservoir of Soultz geothermal reservoir.

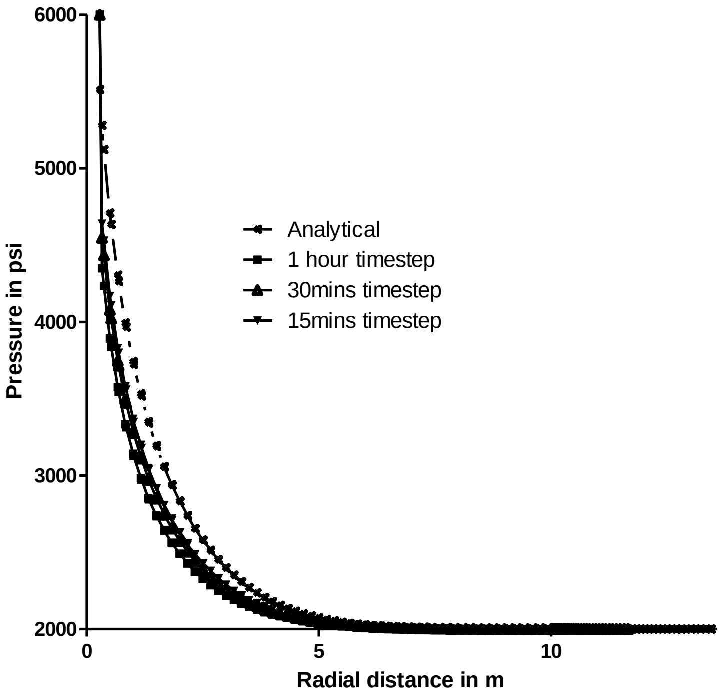

Fig. 3.7: Analytical vs. numerical results of pore pressure. The numerical results are presented in three time steps until the final time is reached.

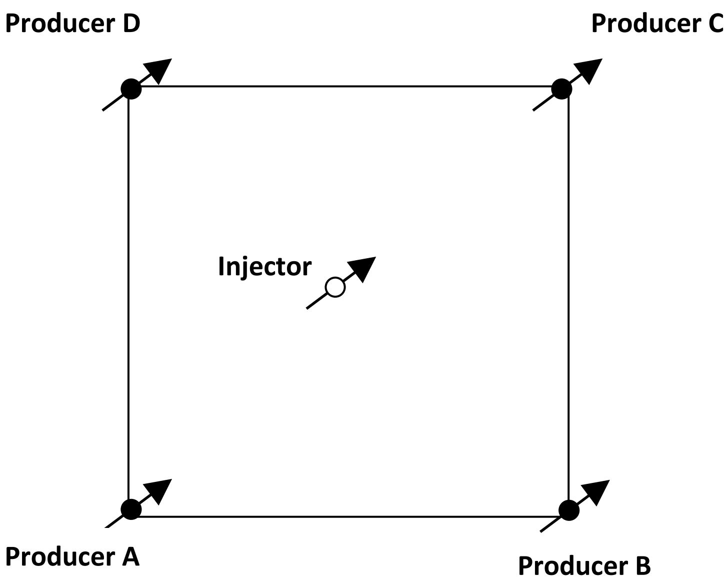

Fig. 3.8: Classic five spot well pattern with one injector and four producers.

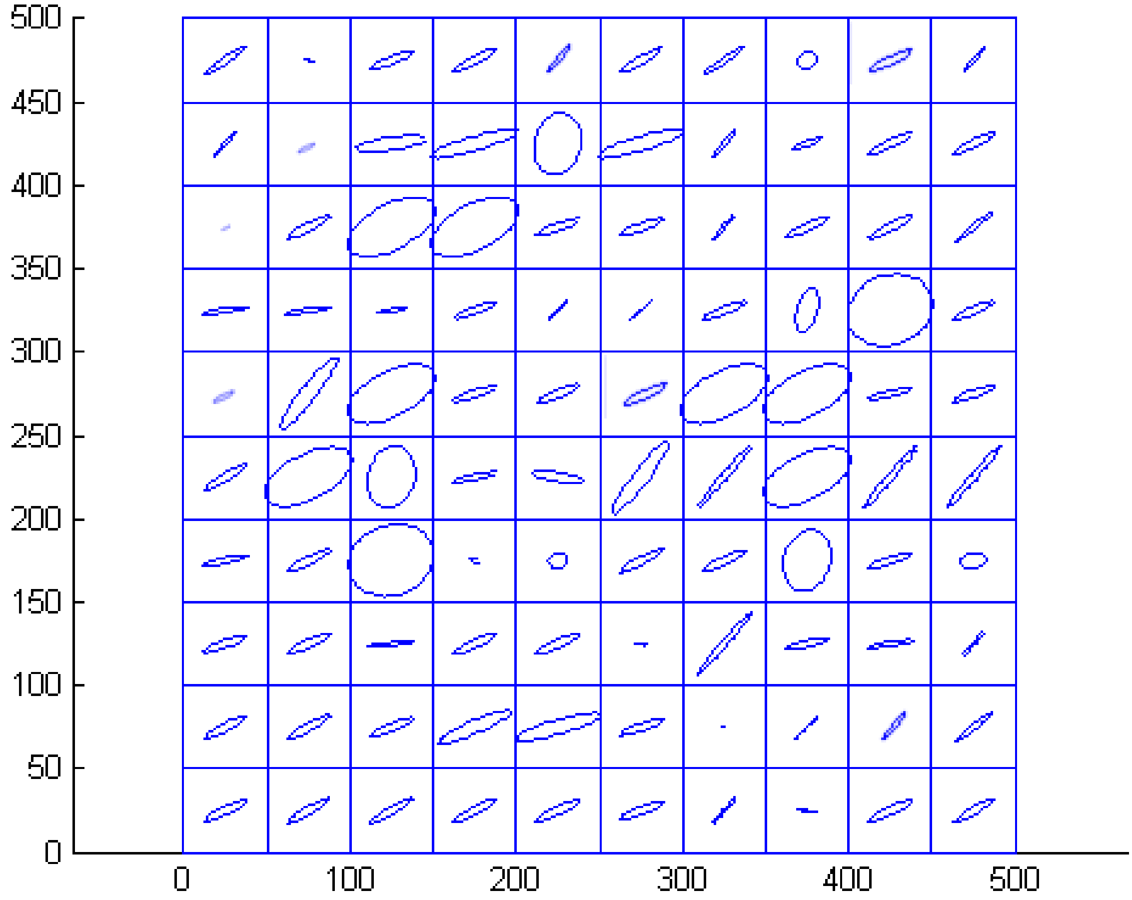

Fig 3.9: Low resolution representation of grid based permeability tensor map at 3150m below surface of discrete fracture map with a fracture density of 0.32 m^{-1} (see Fig 2.12 for the fracture network)

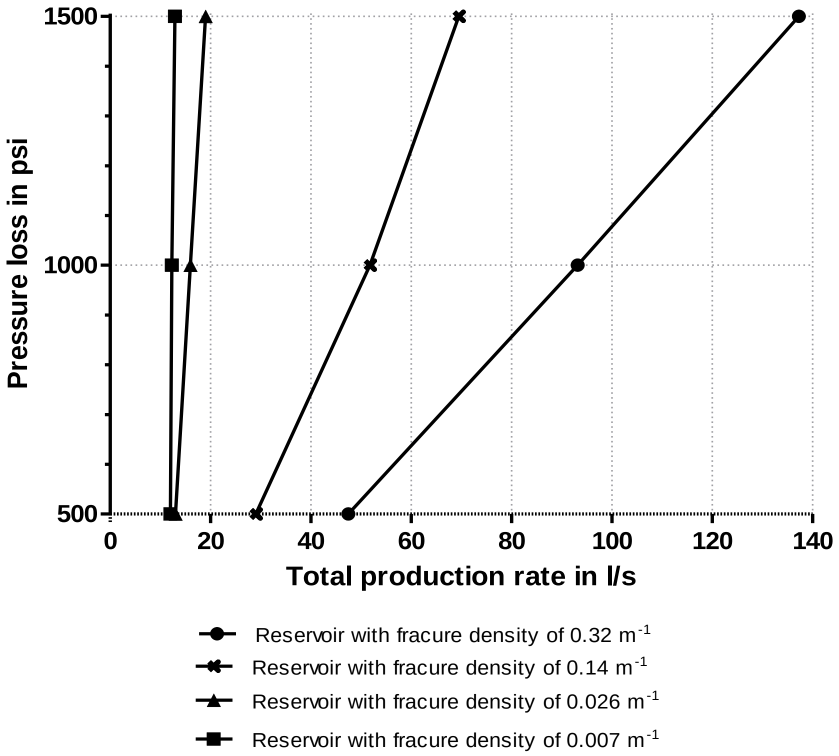

Fig. 3.10: Total production rate from four production wells vs. pressure loss across injector and producers for four different fracture networks with densities 0.007 m^{-1}, 0.026 m^{-1}, 0.14 m^{-1}, 0.32 m^{-1} for a reservoir block of dimensions 1000mx1000mx300m.

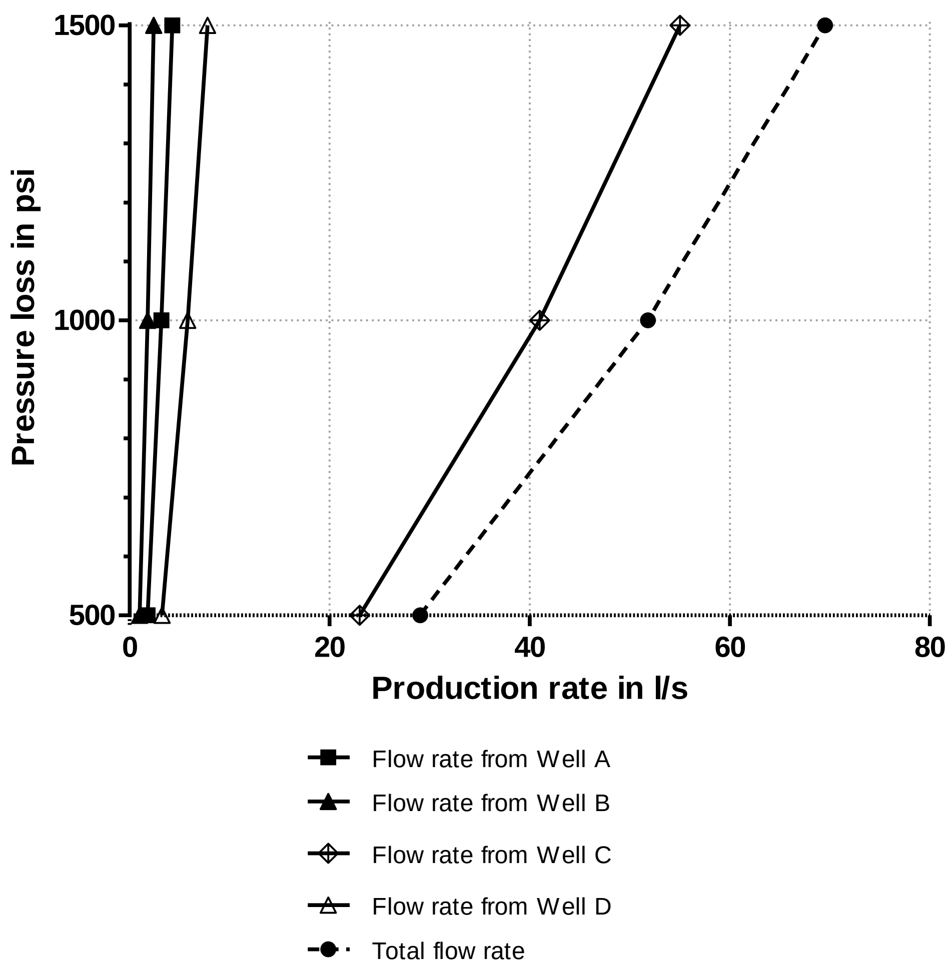

Fig. 3.11: Effect of flow rate on pressure loss across injector and producers A,B,C,D for a reservoir block of dimensions 1000mx1000mx300m with a fracture density of 0.14 m^{-1}.

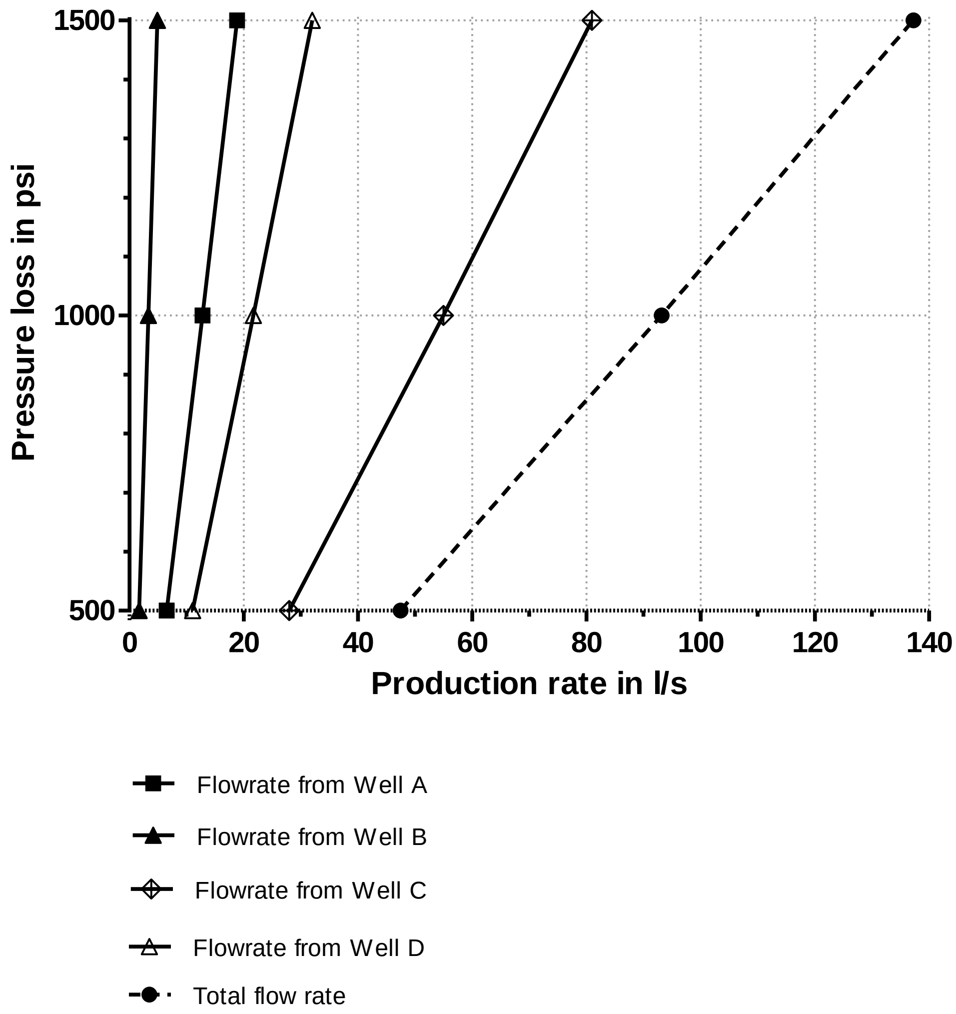

Fig. 3.12: Effect of flow rate on pressure loss across injector and producers A,B,C,D for a reservoir block of dimensions 1000mx1000mx300m with a fracture density of 0.32 m^{-1}.

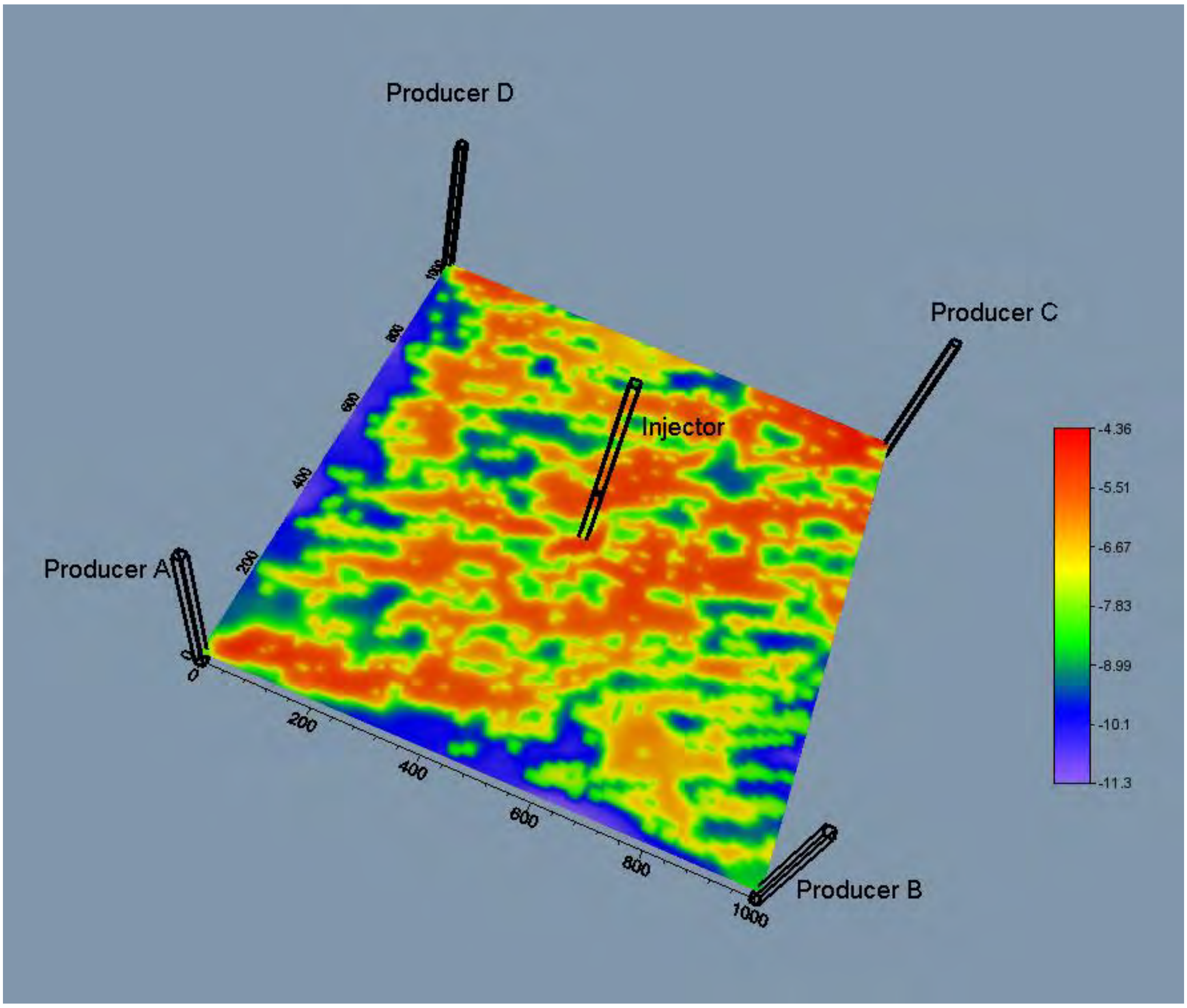

Fig. 3.13: Horizontal cross section of velocity profile (logorithemic RMS format) for the naturally fractured reservoir with fracture density of 0.14 m^{-1}; flowrate : 55 l/s, pressure loss between injector and each producer : 1500psi

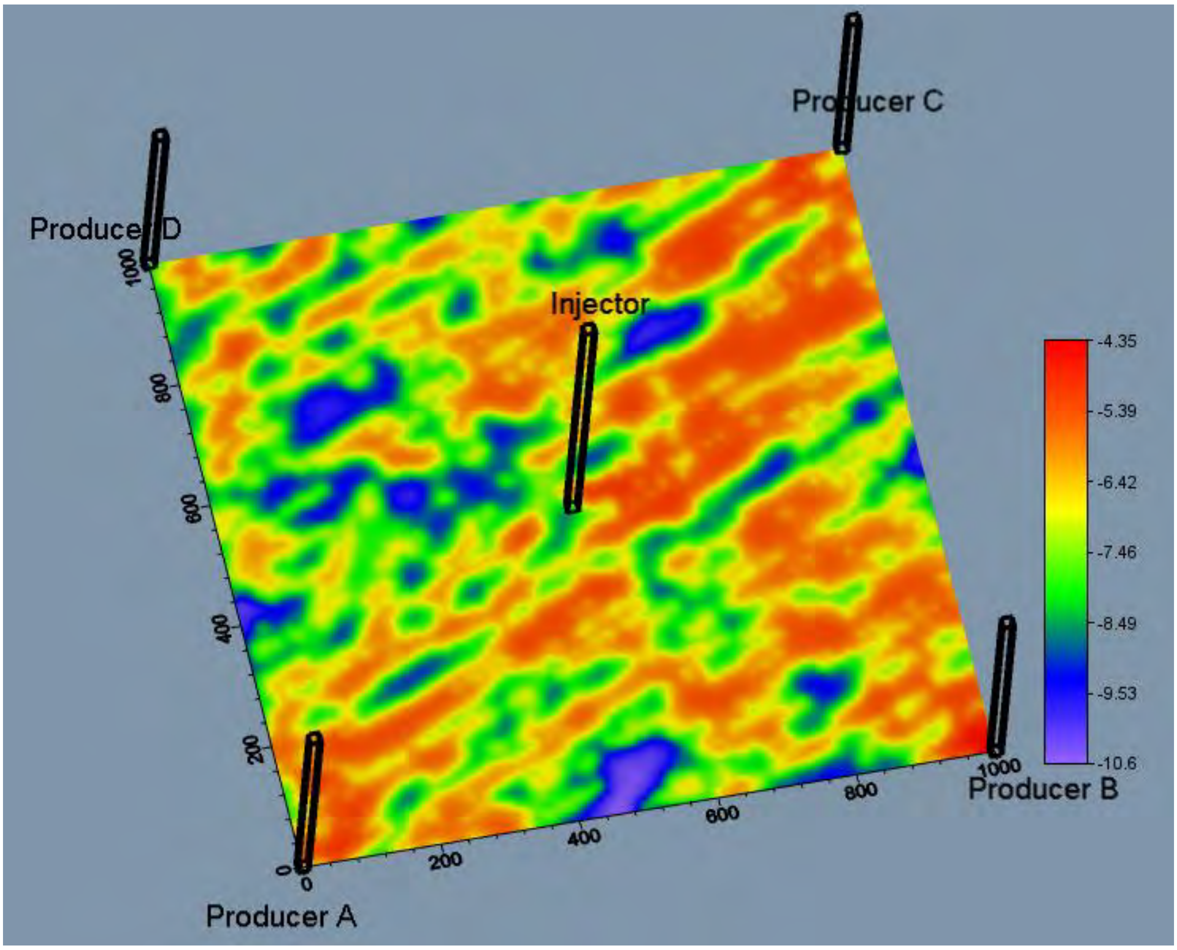

Fig. 3.14: Horizontal cross section of velocity profile (logorithemic RMS format) for the naturally fractured reservoir with fracture density of 0.32 m^{-1}; flowrate : 81 l/s, pressure loss between injector and each producer : 1500psi

Chapter 4

Simulation of Heat Transfer in Fractured Rocks to Estimate Heat Extraction from Naturally Fractured Geothermal Reservoir

In this chapter a numerical model is developed to simulate heat transfer from rock matrix to the circulating fluid in fractured rocks. The heat transfer model is integrated with the fracture generation model and the fluid flow simulation model for naturally-fractured geothermal systems as described in chapters 2 and 3. The integration of these three models allow us to evaluate the geothermal potential of naturally fractured reservoirs. Effects of flow rates, fracture density and heat transfer coefficient on the produced fluid temperature and matrix cooling are investigated. For different fracture sets the effect of flow rate on total thermal energy recovery factor is also studied.

4.1. Introduction

Heat transfer between the matrix and the circulating fluid takes place by conduction and convection. This process is function of rock properties such as thermal conductivity, heat capacity and density, velocity of the circulating fluid and heat transfer coefficient at the rock and fluid interface (Holman 1976; Celli et al. 2010). Factors affecting the fluid velocity in arbitrarily-oriented fractures are discussed in chapters 2 and 3.

Heat transfer in fractured geothermal reservoirs is simulated using three different approaches: equivalent temperature approach (Faust and Mercer 1979), matrix-fracture temperature approach(Ghassemi and Zhou 2011) and rock-fluid temperature approach (Anzelius 1926; Rees et al. 2008). In the equivalent temperature approach a fractured system is represented as a single porous medium and energy balance equation is solved for the single porous medium temperature. This approach is based on the assumption that the fractured medium reaches its local thermal equilibrium instantaneously. This means that the porous medium has a single temperature, therefore matrix, fluid and matrix-fluid interface have the same temperature. This approach is very popular due to its simple numerical formulation (Faust and Mercer 1979). However, the representation of the thermal state of the fractured rock with a single temperature can only be justified if the rock matrix and circulating fluid (fracture edges) remain in thermodynamic equilibrium at all times. The field observations suggests that if the fracture spacing is more than 2-3 meters then instantaneous local thermal equilibrium between matrix and fracture is not a valid assumption (Sanyal et al. 2005). This is due to the fact that heat transfer inside the matrix is controlled only by heat conduction and temperature at fracture surface is controlled by both heat conduction and convection. Once the fracture spacing increases more than 2-3meters matrix and circulating fluid are no longer remains at the same temperature.

In the matrix-fracture temperature approach temperatures at rock matrix and fractures surface are treated individually. Gringarten et.al (1973; 1975) have developed an analytical model for an infinite series of parallel, vertical fractures of uniform thickness, uniformly spaced and separated by blocks of impermeable rock matrix. Rock temperature on the fracture surface is assumed to be equal to the fluid temperature. Fluid is injected into the fracture at a constant flow rate. The results of this study shows that fractured systems provides a more efficient mechanism for heat extraction than a single fracture. When the circulating fluid flows through the fracture system instead of a single fracture (connecting injection and producer) the contact area between rock matrix and circulating fluid increases significantly, this in turn increases the total heat captured by fluid. Later, Bai et al. (1994) derived an analytical solution to study fluid flow and heat transfer in a deformable fractured porous medium. In this model heat transfer between matrix and fracture is taken into consideration through a source/sink term. Only the conductive heat transfer is taken into consideration for both matrix and fracture while the convective heat transfer through the fractures is ignored. In later work the convective heat transfer through deformable fractures is included by Bataille et al. (2006) and Ghassemi and Kumar (2007). With the use of the matrix-fracture temperature approach flow channeling (establishment of major flow paths between wells), which causes the fracture surface to lose temperature rapidly with time, cannot be studied. It is also important to know the rate of cooling of fracture surface which significantly affects the injected fluid to harness heat from the matrix. To incorporate the flow channeling effects on heat recovery the heat transfer between fracture surface and matrix is simulated by introducing a layer of `virtual rock with no thermal mass' lining for each fracture, such a layer of virtual rock mimics the effective heat transfer area near the fracture (Hayashi et al. 1999). Also in the matrix-fracture temperature approach, fluid temperature is always equal to the rock matrix temperature on the fracture surface. In fact, in a typical enhanced geothermal system (EGS) or hot fractured rocks (HFR) system, there exists a high temperature gradient between the host rock and circulating fluid (Sanyal et al. 2005). Moreover, the amount of heat transfer to the circulating fluid from the host rock depends on the heat transfer area, temperature difference between rock and fluid and overall heat transfer coefficient at the rock-fluid interface. Typically the heat transfer coefficient depends on the thermal properties of the rock and circulating fluid and fluid velocity (Holman 1976).

The matrix-fluid temperature approach (also known as the solid-fluid temperature approach) was first introduced by Anzelius (1926) to study the thermal front propagation in the absence of conduction in both solid and fluid phases using the „*method of characteristics*‟. Later, Anzelius‟s approach was extended by Burch, Allen et al. (1976) to study heat transfer in medium packed with beads. In this approach, heat transfer in the fluid phase by conduction is ignored. In a recent study, Rees et al. (2005; 2008) extended the solid-fluid temperature approach to investigate increase in temperature of a cold saturated porous medium due to injection of hot fluid. In this study heat transfer in fluid by both conduction and convection, heat transfer between solid and fluid are taken into account.

The rock-fluid temperature approach is further extended in this thesis to study the heat transfer between rock matrix of fracture geothermal reservoirs and circulating fluid for different scenarios. In the present work the heat transfer between individual fractures to the circulating fluid has taken into account for heat extraction calculations which have been ignored in the previous models. The present model also investigates the temperature drawdown of the fracture surface over time and its effect on the ultimate heat recovery.

4.2. Formulation of 3D heat transfer model

As mentioned earlier heat transfer between matrix and fractures saturated by fluid depends on the heat transfer area, heat transfer coefficient, fluid velocity and temperature difference between the rock and fluid (Holman 1976; Rees et al. 2008). Energy balance equations, which adequately represent matrix and fluid can be expressed as follows:

$$\phi\rho_f c_{pf}\frac{\partial T_f}{\partial t}+\overbrace{\nabla(vT_f)}^{\text{Convection term}}-\overbrace{\kappa_f\nabla^2 T_f}^{\text{Conduction term}}+Q=0$$

(4.1)

$$(1-\phi)\rho_r c_{pr}\frac{\partial T_r}{\partial t}-\kappa_r\nabla^2 T_r-Q=0$$

(4.2)

$$Q=hA(T_f-T_r)$$

(4.3)

Here, T, v, κ, ρ, c_p, Q, h and A represents the temperature, velocity of fluid, thermal conductivity, density, heat capacity and heat transfer rate between rock and fluid, overall heat transfer coefficient and heat transfer area, respectively. Subscripts f, r refer to fluid and rock respectively. Full derivation of the above equation is presented in Appendix-D. The heat transfer coefficient depends primarily on the detailed geometry of the porous medium, the porosity, the flow field and the conductivities and diffusivities of the phases. However, there exists no analytical or numerical model to estimate the heat transfer coefficient for geothermal rock matrix (Holman 1976; Rees et al. 2008). Zhoa (1994) investigated the effect of stress and temperature on hydro-thermo-mechanical properties of Carnmenellis granite using the geothermal rock testing system at Imperial College, London. These experimental data indicates that for low permeable naturally fractured geothermal reservoirs the heat transfer coefficient varies between 0.1 mW/m^2 ^{0}C to 10 mW/m^2 ^{0}C.

The main assumptions of the heat transfer model are as follows:

- Fluid is injected into the reservoir at a constant temperature.

- Thermal conductivity, density and heat capacity of the matrix are constant throughout the fractured reservoir.
- Thermal conductivity, density and heat capacity of the matrix are constant throughout the production life.
- No external heat flow is applied at the top layer and bottom layer. Typically the heat flow coming from top layer and bottom layer has significant effect on initial reservoir temperature. The effect of initial temperature on the heat recovery is not the focus of the present work, hence, the external heat flow assumed to be zero.
- The effect of hydraulic and thermal stress on fracture aperture is ignored. When the cold fluid injected into the hot fractured rock the changes in stresses will cause changes in fracture aperture. However, this is not the focus of the present work, so the effect of hydraulic and thermal stresses on fracture permeability is ignored.
- Typically the heat transfer by radiation has significant effect on initial reservoir temperature. The effect of initial temperature on the heat recovery is not the focus of the present work, There is no heat transfer by radiation inside the reservoir.
- There is no chemical reaction between rock matrix and circulating fluid. Typically, when fluid is injected into the reservoir there exist chemical imbalance and which affect the permeability of the fractured rock.

However, this is not the focus of the present work, hence, the effect of chemical reaction on rock properties is ignored.

- Heat transfer coefficient is assumed to be constant, which means that the analysis presented in this thesis based on the values derived from the laboratory study by Zhoa (1994).
- There is no change of phase for circulating fluid inside the reservoir, i.e. single phase flow.

4.3 Numerical procedure

A flow chart of the overall numerical procedure is presented in **Fig. 4.1**. In order to simulate the heat transfer in fractured geothermal reservoirs constant fluid temperature and constant pressure boundary conditions at the injector and the producer are applied. As shown in Fig. 4.1 at each time step pressures and velocities are evaluated using the fluid flow simulation model, as described in Chapter 3. To solve **Eqns 4.1**–**4.3**, eight-noded isoparametric quadrilateral elements are used for the rock temperature and fluid temperatures. Finite element based standard Galerkin technique is used to solve the matrix temperature (Zienkiewicz and Taylor 2000). Numerical solution of the fluid temperature includes both the convective and diffusive terms (see Eqn. 4.1). A fully implicit Taylor- Galerkin characteristic-based split scheme is developed and used to handle spatial oscillations that occur due to the convective transport term (Lewis et al. 2005). Finite element based numerical discretization of equations 4.1 and 4.2 are shown in Appendix-E.

A multi-frontal technique (Amestoy et al. 2000) is used to solve the equations on parallel computers on a distributed environment using the following libraries: MPICH2 (Gropp 2002), Level II and Level III optimized BLAS library (Dongarra et al. 1990), SCALAPACK library (Blackford 1997), PBLACS library, PORD ordering algorithms (Schulze 2001) and modified form of MUMPS library (Khaitan et al. 2010). First, MPI library routines MPI_INIT, MPI_COMM_SIZE and MPI_COMM_RANK are used to setup a parallel environment. The initial reservoir conditions, rock and fluid properties, reservoir operating conditions and mesh data are given as input through a data file to the host processor. Instead of formulating a FEM based global stiffness matrix and dispense it among the processors individual element stiffness matrixes are evenly distributed among the processors to achieve a good memory balance between the processors. This memory balance procedure is explained in **Fig. 4.2**. This figure shows that a finite element based problem with a four-element domain which can be solved using two processors or four processors in parallel. To solve the equations using two processors the four-element domain with four elements is divided into two sub-domains, each of which has two elements, as shown in **Fig 4.2(b)**. When four processors are available the four-element domain is divided into four sub-domains, each of which has a single element (Raju 2010). Using this approach the total memory requirement of a numerical code can be distributed among all the processors as evenly as possible.

To minimize the memory requirements and decrease the simulation run time only non-zero values of element stiffness matrixes are sent to respective processor which is one of the key features of the present numerical procedure. The memory requirement of each processor must be satisfied by the local memory at a computing node. Once the distribution of the equations are completed then all the processors need to be synchronized to solve the equations efficiently. MPI library command, MPI_Barrier is used for this purpose.

The solution procedure of the set of formulated equations is divided into three stages. computational graph is constructed and the ordering information is passed on from the host to all the other processors. In stage one (analysis stage) the values of matrix are analyzed using PORD algorithm and order of the matrix is calculated. In stage two (factorization stage) based on the ordering information of matrix, the algorithm tries to construct several dense sub matrices that can be processed in parallel. The numerical factorization is carried out in this stage. In stage three (solution stage) the solution vector is computed by using the right hand side vector and the distributed factors. The solution vector is assembled back on the root processor. Finally, MPI_FINALIZE is used to terminate the current MPI threads and cleans up memory.

4.4 Validation of the numerical model

The heat transfer model presented in Section **4.3** is validated in two stages. First an analytical solution for a single fracture imbedded in a matrix is used.

Next, TOUGH2, a commercial software for simulating fluid flow and heat transfer in porous geothermal reservoirs is used (Pruess 1991; Mannington et al. 2004).

In stage 1 an impermeable 2-dimentional rock matrix of size 1m^2 is considered. A fracture is assumed to cut through the block of rock horizontally (see **Fig**. **4.3**). Fluid with a thermal diffusivity coefficient of 10^{-7} m^2/s is injected into the fracture from one end with a velocity of 10^{-5} m/s. The inlet temperature is maintained at 80 ^oC and the initial temperature of matrix and fluid is assumed to be 200 ^oC. Using the Lewis et al. (2005)"s approach dimensionless variables are calculated and the fluid temperature along the fracture length after 15 hours of circulation is shown in **Fig. 4.4**. The results show a general agreement between the exact solution (Fleming and Mansoori 1987) and the numerical solution. The mismatch between numerical results and exact solution is due to the convective nature of the mathematical equation and can be minimized by mesh refinement or decrease in time step.

In stage 2, a homogeneous porous reservoir of size 1kmx 1kmx170m is considered. An injector and a producer are placed 340m apart. The reservoir permeability and temperature are assumed to be 10mD and 215 ^oC respectively. Fluid with initial temperature of 80 ^oC is injected into the reservoir at a flow rate of 10 kg/s. Results of heat extraction rate from both the numerical model developed as part of this thesis and the AuTough2_2 (University of Auckland version of Tough 2_2) are presented in **Fig. 4.5**. Results of the heat extraction rate over time from the current model agree well with that of AuTough2_2. The error in the numerical results is due to fact that AuTough2_2 takes into account the conversion of single phase fluid to two phase inside the wellbore which is not the focus of the present work.

4.5. Numerical experiments

In order to study the rate of heat transfer from matrix to the circulating fluid and its effect on heat extraction a series of numerical experiments have been performed using different heat-transfer coefficients and fluid flow rates for a reservoir with a fracture density of 0.32 m^{-1}. The heat transfer coefficient in a fractured geothermal reservoir typically varies from 0.1 mW/m^2 ^0C to 10 mW/m^2 ^0C (Holman 1976; Zhao 1994). In this study, a quadrant of the reservoir with an injector and a producer C is considered (see **Fig. 4.6)**. The initial reservoir temperature is assumed to be 200 ^0C. The dataset used for the numerical experiments in presented in Table 3.1 (see Chapter 3).

Firstly, flow rate is kept constant at 81 l/s (for which the pressure loss is 1500psi) and heat transfer coefficient is varied from 0.1 mW/m^2 ^0C to 10 mW/m^2 ^0C. Produced fluid temperature of 140 ^0C is considered to be the abandonment temperature (a produced fluid temperature below which the project becomes commercially not viable (Tester et al. 2006)). The results of this study are presented in **Fig. 4.7**. It can be seen from these results that the produced fluid temperature remains constant at 200^0C (which is the initial reservoir temperature) for a heat transfer coefficient of 10 mW/m^2 ^0C over the production period of 15 years. With a decrease in the heat transfer coefficient the produced fluid temperature begins to decrease and the rate of decrease in the fluid temperature depends strongly on heat-transfer coefficient (0.1 mW/m^2 ^{0}C, 1 mW/m^2 ^{0}C and 5 mW/m^2 ^{0}C) than with a high heat-transfer coefficient (10 mW/m^2 ^{0}C). From this figure it can be seen that the reservoir life can be extended to over 40 years for a heat transfer coefficient of 10 mW/m^2 ^{0}C. For a low heat transfer coefficient of 1 mW/m^2 ^{0}C the reservoir life is shortened to 7 years. The numerical results suggest that heat transfer coefficient plays a significant role in determining the production life. Extensive research work is required to understand the how rock and fluid properties effect the heat transfer coefficient for a better prediction of reservoir performance over time.

In **Fig. 4.8**, the temperature of the produced fluid for four different flow rates (28 l/s, 55 l/s, and 81 l/s) for a quadrant of the reservoir with a fracture density of 0.32 m^{-1} and heat transfer coefficient of 5 mW/m^2 ^{0}C is presented. From these results, it can be seen that for low flow rate (28 l/s) the produced fluid temperature remains very high (200^{0}C) for a production period of 25 years. When the flow rate is increased to 55 l/s the produced fluid temperature drops from 200^{0}C to 166^{0}C after 25 years of production. When the flow rate is further increased to 81 l/s, the temperature of the produced fluid falls to 140^{0}C after 20 years of production. The temperature profiles of the rock and the fluid after 5, 10 and 20 years of production are presented in **Figs. 4.9-4.14**. From the Figs. 4.9 and 4.10 it can be seen that after five years of production cooling of the reservoir takes place around the injection well. It can be noted that the cooling of the reservoir is not homogenous around the injection well. This is due to the fact that fractures control the movement of the circulating fluid inside the reservoir and the locations at which fluid flowing with high velocity removes more energy from the rock matrix when compared with the locations fluid flowing with low velocity. It can be seen from **Fig. 4.11** that after 10 years of production the cooling of the reservoir has extended up to 400m from injection well. As the production continues cooling of the reservoir matrix advances towards the production well (see **Fig. 4.14**). The profile of rock matrix temperature along the horizontal section (3100m below surface) for three flow different flow rates: 28 l/s, 55 l/s and 81 l/s after 25 years of production is presented in **Figs. 4.15-4.17**. From these figures it can be seen that for flow rate of 81 l/s it takes around 21 years to cool the rock matrix around the production well. The velocity profile for 81 l/s after 25 years (see fluid flow paths in **Fig. 4.18**) shows that the flow paths connecting the two wellbores are well established. Once high (preferential) flow paths between injector and producer are established the rock matrix along this flow path losses its temperature more rapidly than elsewhere. Similar results were observed by Tester, Anderson et. al (2006) for Soultz Geothermal Field, France. In the GPK3 well, where nine open fractures are observed at the 540 m open-hole section. It was also reported that one fracture at a depth of 4760 m has been contributing to 70% of the total flow. Heat transfer from matrix to fluid is greater in regions which are interconnected by highly conductive fractures than elsewhere. This leads to a rapid cooling of the matrix around the interconnected fractures. Therefore it is essential to strategically control the flow rate through highly conductive fractures as it can affect the total heat recovery.

The heat extraction rate with time for the same flow rates (28 l/s, 55 l/s and 81 l/s) over a period of 25 years are presented in **Fig 4.19**. With an increase in flow rate the heat extraction rate increases and reaches a value of 68MW at a flow rate of 81l/s and remains high for about 7 years. After this production period the heat extraction rate begins to decline for high flow rates in particular for 81 l/s. The heat extraction rate, however, for the low flow rate (28 l/s) remains near constant by over the entire production period of 25 years. It is noteworthy that the commercial viability of a naturally fractured geothermal reservoir is very much a function of injection rate which should be around 70-80 l/s as reported by Tester et. al (2006). Therefore it is crucial to find the economical flow rate which maximizes the total hear recovery as the flow rate significantly effects the production life.

Recovery factor

Recovery factor is defined as the ratio of the total energy extracted over the production life and the total energy stored. Please note that 80^0C is taken as cut-off temperature for calculating total energy storage. It is an important parameter in evaluating the geothermal energy extracting efficiency (Tester et al. 2006). Results of the recovery factor as a function of the injection rates and the heat transfer coefficient for reservoirs with a fracture density of $0.14m^{-1}$ (medium) and 0.32 m^{-1} (high) are presented in **Figs. 4.20** and **4.21**. From the results of this study it can be observed that, for the reservoir with a medium density fracture system ($0.14m^{-1}$) the recovery factor increases with an initial increase in flow rate (from 25 l/s - 50 l/s) and then gradually flattens out at about 51 l/s (see Fig. 4.20). Similarly, for the high density fracture system (with fracture density of $0.32m^{-1}$) initially the recovery factor increased with increase in the flow rate and reached a maximum value of 0.41 for the flow rate of 81 l/s (see Fig. 4.21) and then flattens out. This is due to the fact that thermal recovery depends on the quantity of fluid sweeping the fracture network and the amount of time fluid spent inside the reservoir over a fixed production life. As flow rate increases the amount of fluid enters the reservoir system increases and heat transfer between rock and fluid increases. Once the flow rate exceeds a threshold level the amount of heat extracted from the fracture system stays constant. The results of heat recovery factor are in consistent with typical geothermal reservoirs (Sanyal and Butler 2005).

In order to study the effect of fracture density on the producing fluid temperature and recovery factor two reservoirs with a medium ($0.14m^{-1}$) and high fracture density ($0.32m^{-1}$) are considered. Active fracture volume is used to evaluate the heat recovery factor as it contributes significantly to the fluid flow. Also the placement of well (injector and producer) with respect to the fracture orientation plays an important role in capturing heat. This is due to the fact that both the flow rate and the heat transfer area depends on fracture distribution between the injector and the producer. As shown in Figs 4.17-4.19 that at a fluid velocity of 10^{-5} m/s or greater the rock matrix loses its temperature faster. In this study fractures, in which fluid velocity is greater than

10^{-5} m/s are considered active fractures (fluid conductor) and are used to calculate the active fracture volume. In calculating the active fracture volume two flow rates are considered: 55 l/s and 81 l/s. For the flow rates of 55 l/s and 81 l/s the active fracture volume of reservoir with the medium fracture density is 0.99×10^3 m^3, 1.27×10^3 m^3, respectively and for the high fracture density 1.67×10^3 m^3, 3.19×10^3 m^3, respectively. The produced fluid temperature as a function of time for the two reservoirs with the medium ($0.14 m^{-1}$) and high fracture density ($0.32 m^{-1}$) is shown in **Fig. 4.22**. The numerical results show that for the medium fracture density ($0.14 m^{-1}$) the producing fluid temperature decreases to 140^0C after 13 years of production while for the high fracture density ($0.32 m^{-1}$) the producing fluid temperature decreases to 184^0C after the same production period. This can be explained by the fact that the contact between the rock matrix and the fluid the increases with the increase in active fracture volume which, in turn, increases the heat transfer (the active fracture volume for the medium density is 1.67×10^3 m^3 for the high density is 3.19×10^3 m^3). The result of heat recovery factor with active fracture volume for the flow rates of 55 l/s and 81 l/s are shown in **Fig. 4.23**. These results suggest that, for both flow rates, the recovery factor increases linearly with the increase in active fracture volume. The rate of increase in recovery factor is faster for the low flow rates. This is because the fluid flowing at low flow rate allows more time for the circulating fluid to have contact with the rock matrix and extract more heat.

4.6. Closure

The results of numerical experiments confirm the general belief that heat transfer between rock and fluid has a profound effect on the cooling of the produced fluid. The numerical shows that heat transfer coefficient and the fracture density has profound effect on the produced fluid temperature. From the results of this study and following discussion it can be concluded that the heat recovery factor increases with an increase in the flow rate. However, there exists an optimum flow rate at which the recovery factor reaches it maximum.

The numerical results also suggest that active fracture volume has profound effect on the ultimate heat recovery from naturally fractured geothermal reservoirs. The reservoir and production parameters such as placement of well, fluid production rate must be optimized to achieve a maximum heat extraction from naturally fractured geothermal reservoirs.

4.6. Figures

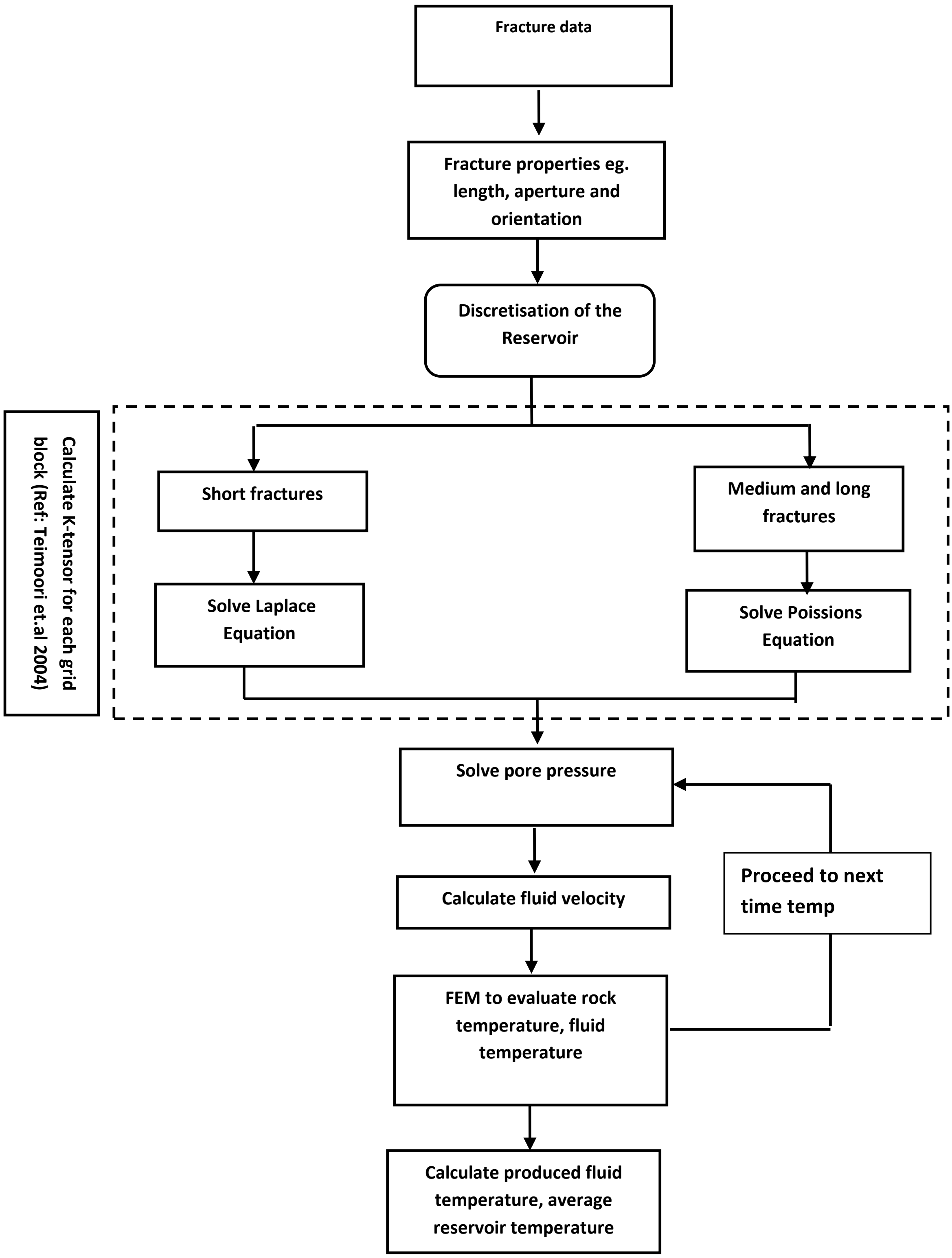

Fig 4.1: Flow chart of the numerical procedure presented in section 4.3.

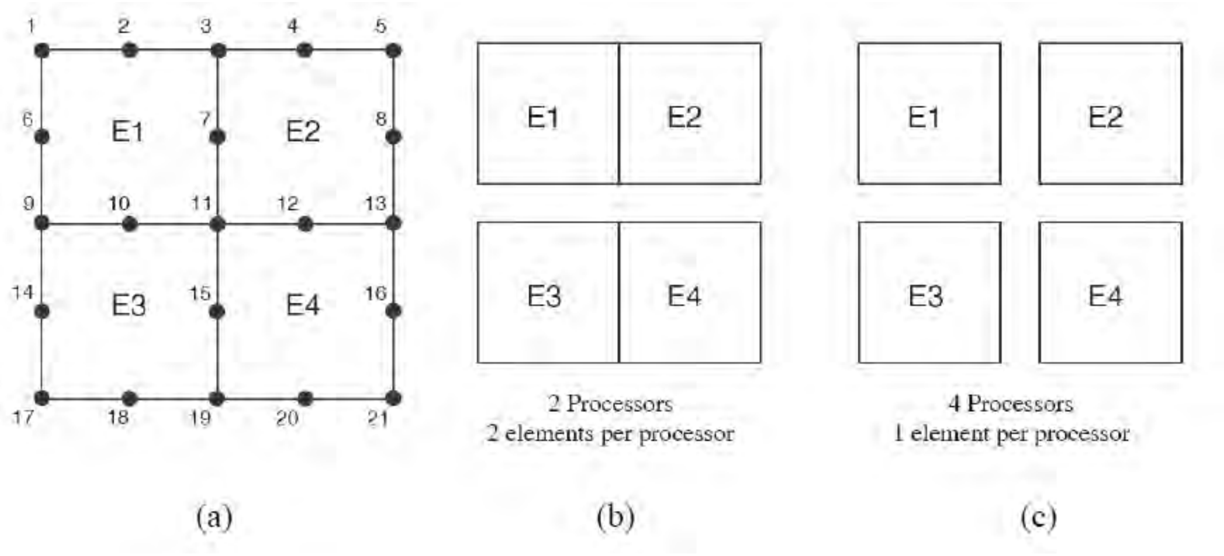

Fig.4.2 : Memory distribution procedure in a parallel programming environment.

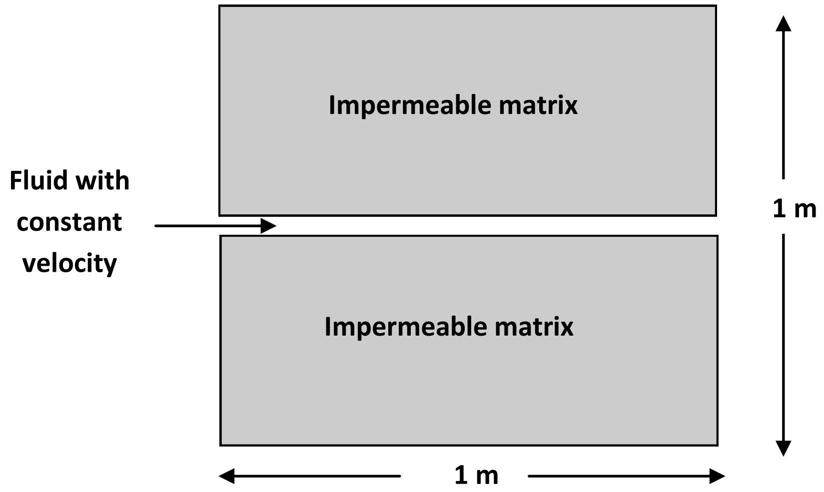

Fig. 4.3: Impermeable rock matrix with a horizontal fracture of length 1m. Fluid velocity: $1x10^{-5}$ m/s, thermal diffusivity of fluid: $1x10^{-7}$ m^2/s.

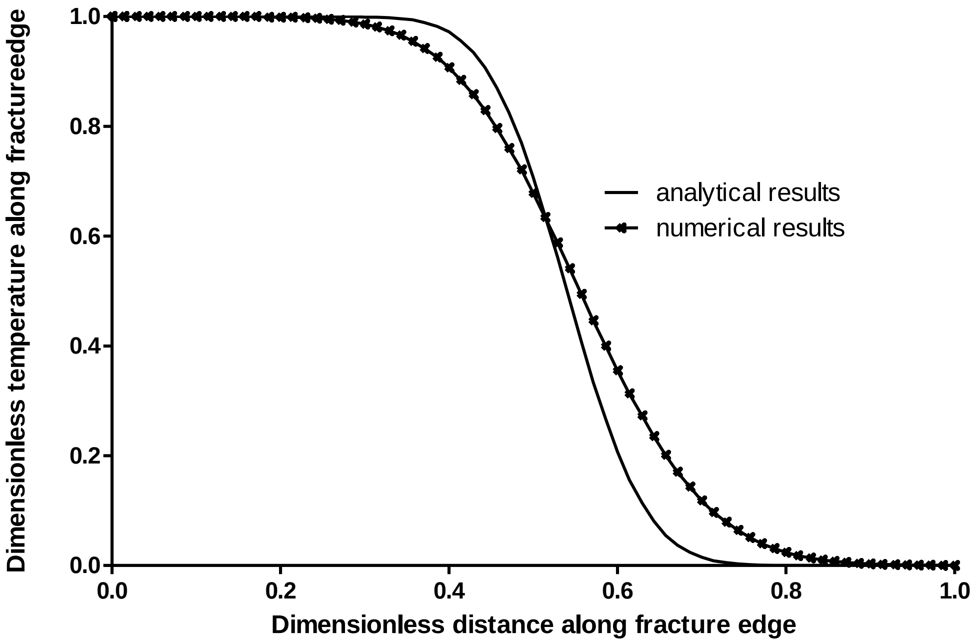

Fig. 4.4: Results of temperature as function of time produced by analytical and numerical solution for fluid velocity: $1x10^{-5}$ m/s, thermal diffusivity of fluid: $1x10^{-7}$ m^2/s.

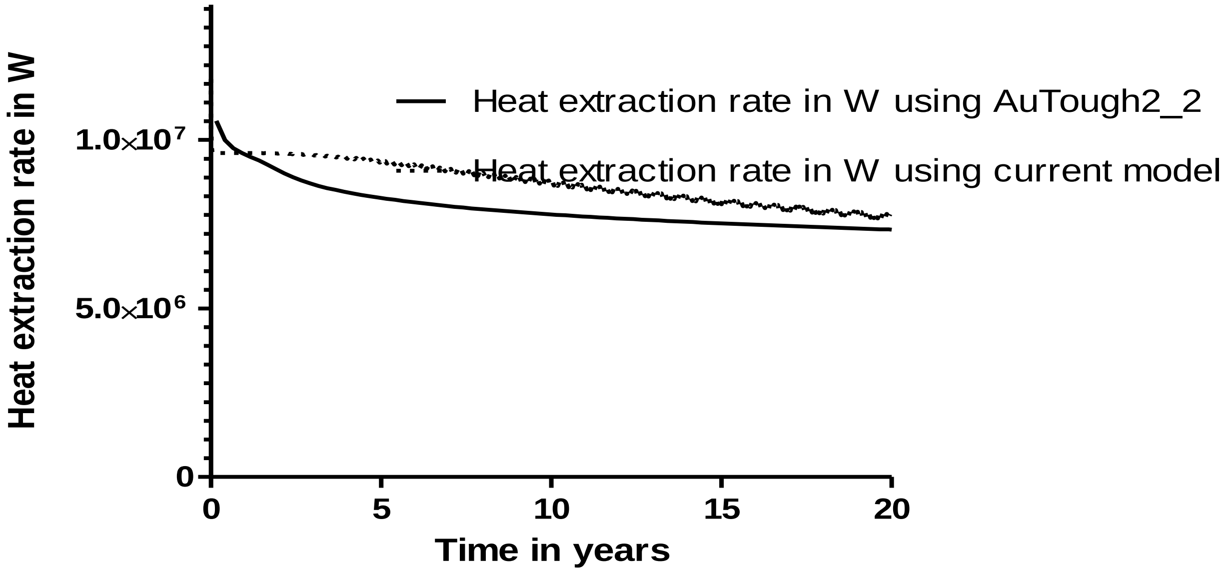

Fig. 4.5: Comparison of produced heat flow for both developed numerical model and AuTough2_2. Reservoir size: 1kmx1kmx170m, reservoir depth 2Km, porosity: 0.1, flow rate 10kg/s, distance between injector and producer: 340m.

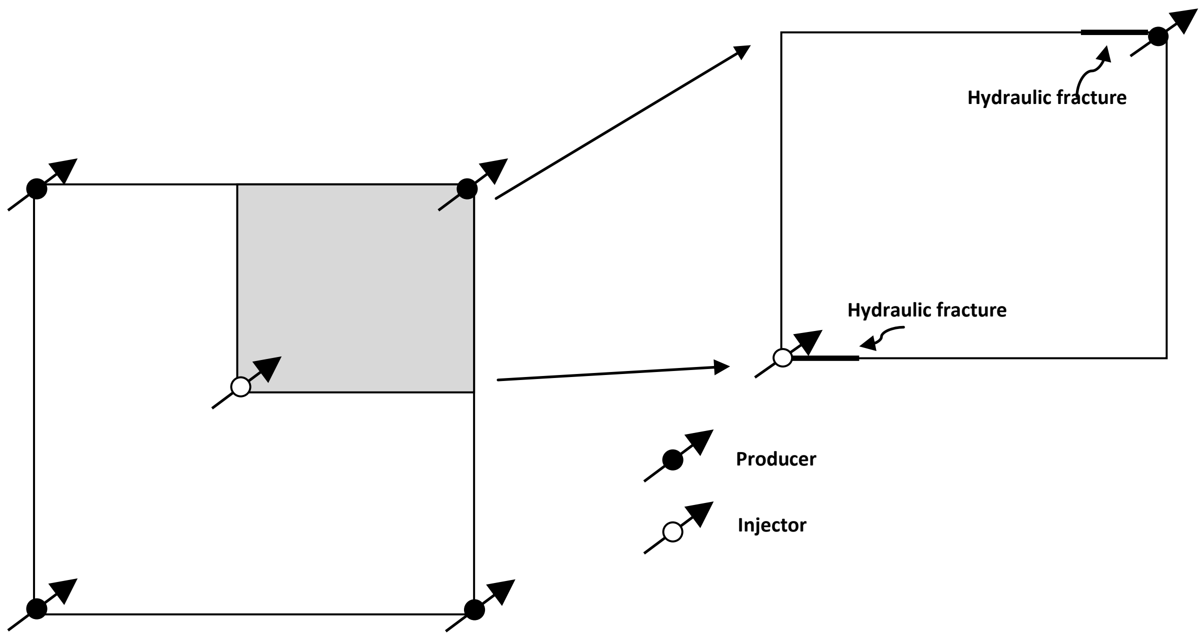

Fig. 4.6: A quadrant of 500x500x300m^3 from a geothermal reservoir with dimensions of 1000x1000x300 m^3.

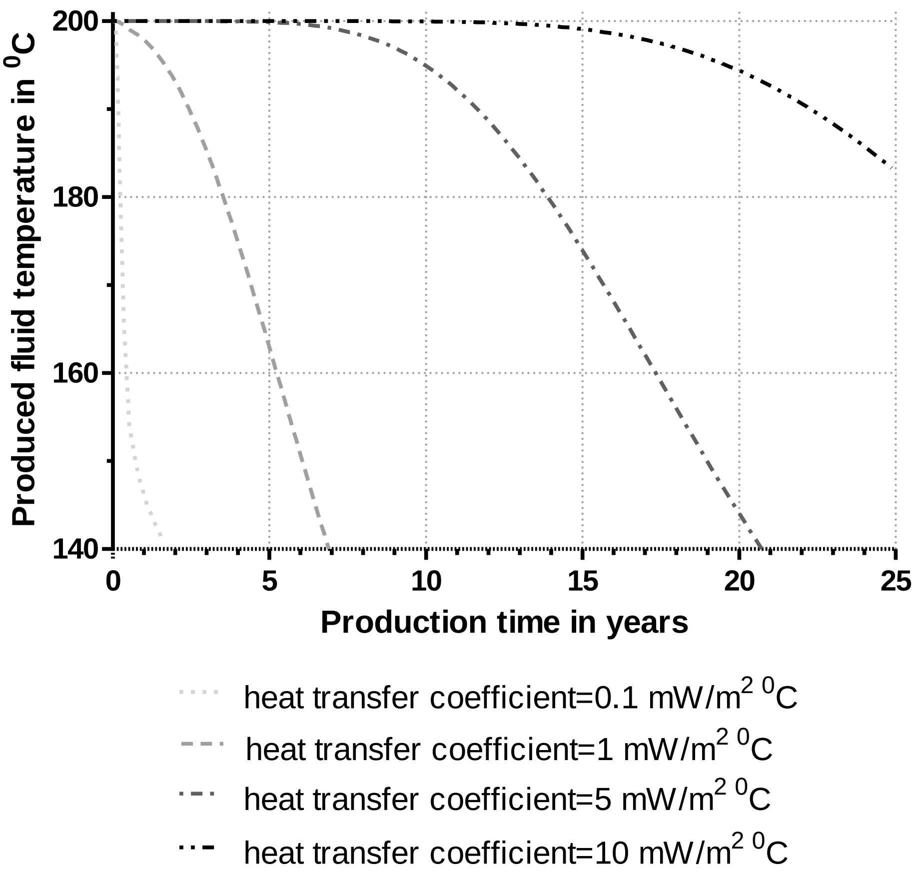

Fig. 4.7: Produced fluid temperature vs. time for different heat transfer coefficient of medium: 0.1 mW/m^2 ^{0}C, 1 mW/m^2 ^{0}C, 2.5 mW/m^2 ^{0}C, 5 mW/m^2 ^{0}C, and 10 mW/m^2 ^{0}C, fracture density: 0.32 m^{-1}, heat transfer area: 2.40x10^7 m^2, pressure loss between injector and producer: 1500psi and production rate: 81 l/s.

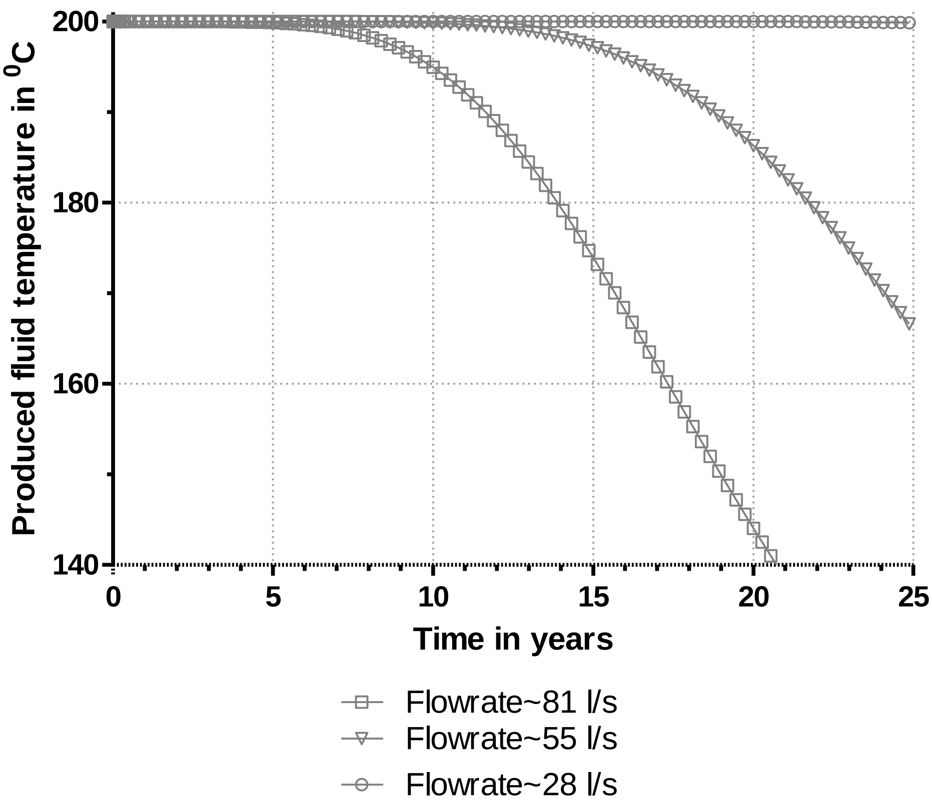

Fig. 4.8: Produced fluid temperature vs. time for three different flow rates: 28 l/s, 55 l/s and 81 l/s, fracture density: 0.32 m^{-1}, heat transfer area: 2.40x10^{7} m^{2} and heat transfer coefficient of medium: 5 mW/m^{2} ^{0}C.

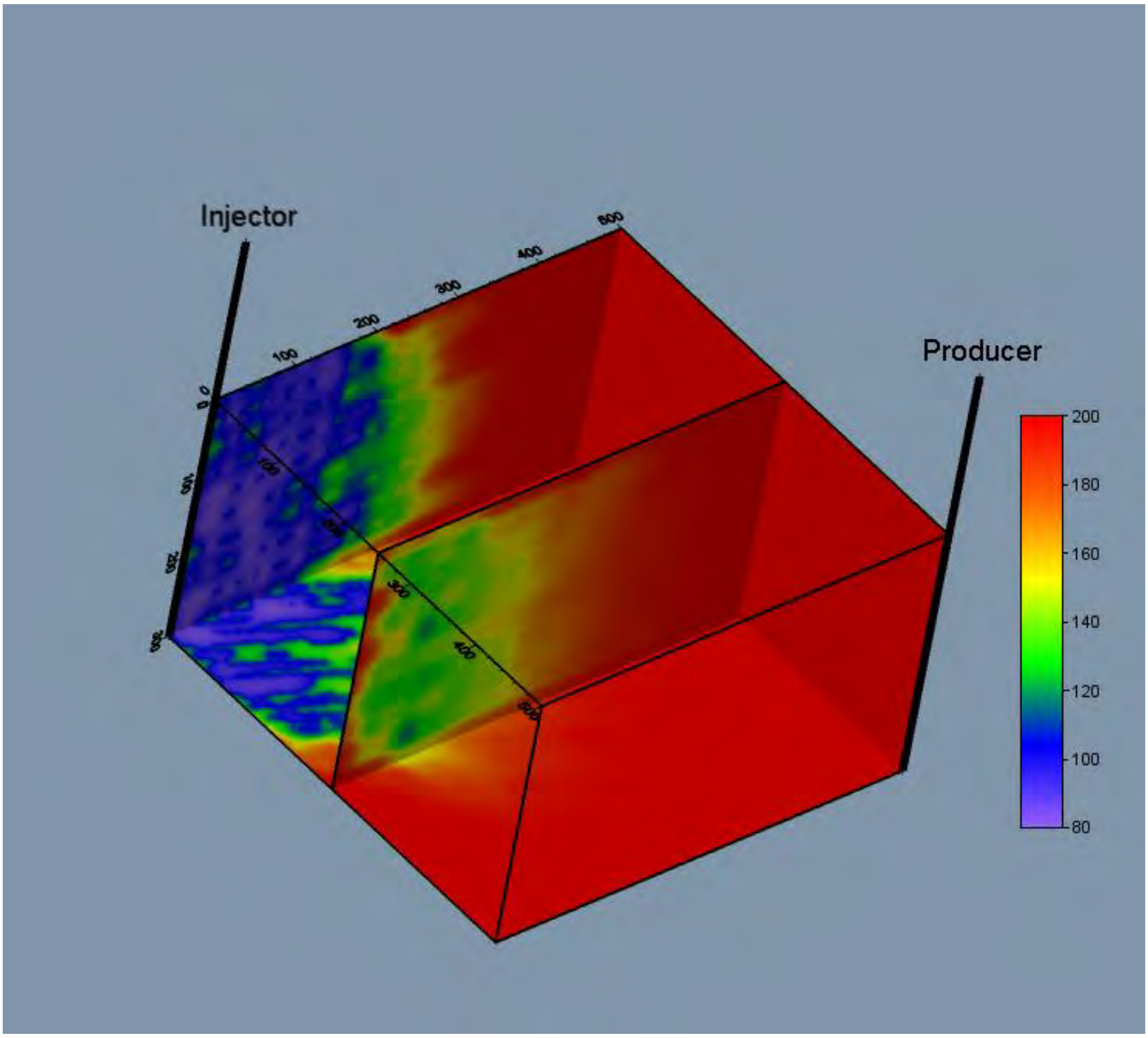

Fig. 4.9: Fluid temperature profile after 5 years of production; heat transfer coefficient of medium: 5 $mW/m^2\ {}^0C$, fracture density: 0.32 m^{-1}, heat transfer area: $2.40x10^7\ m^2$, pressure loss between injector and producer: 1500psi and production rate: 81 l/s.

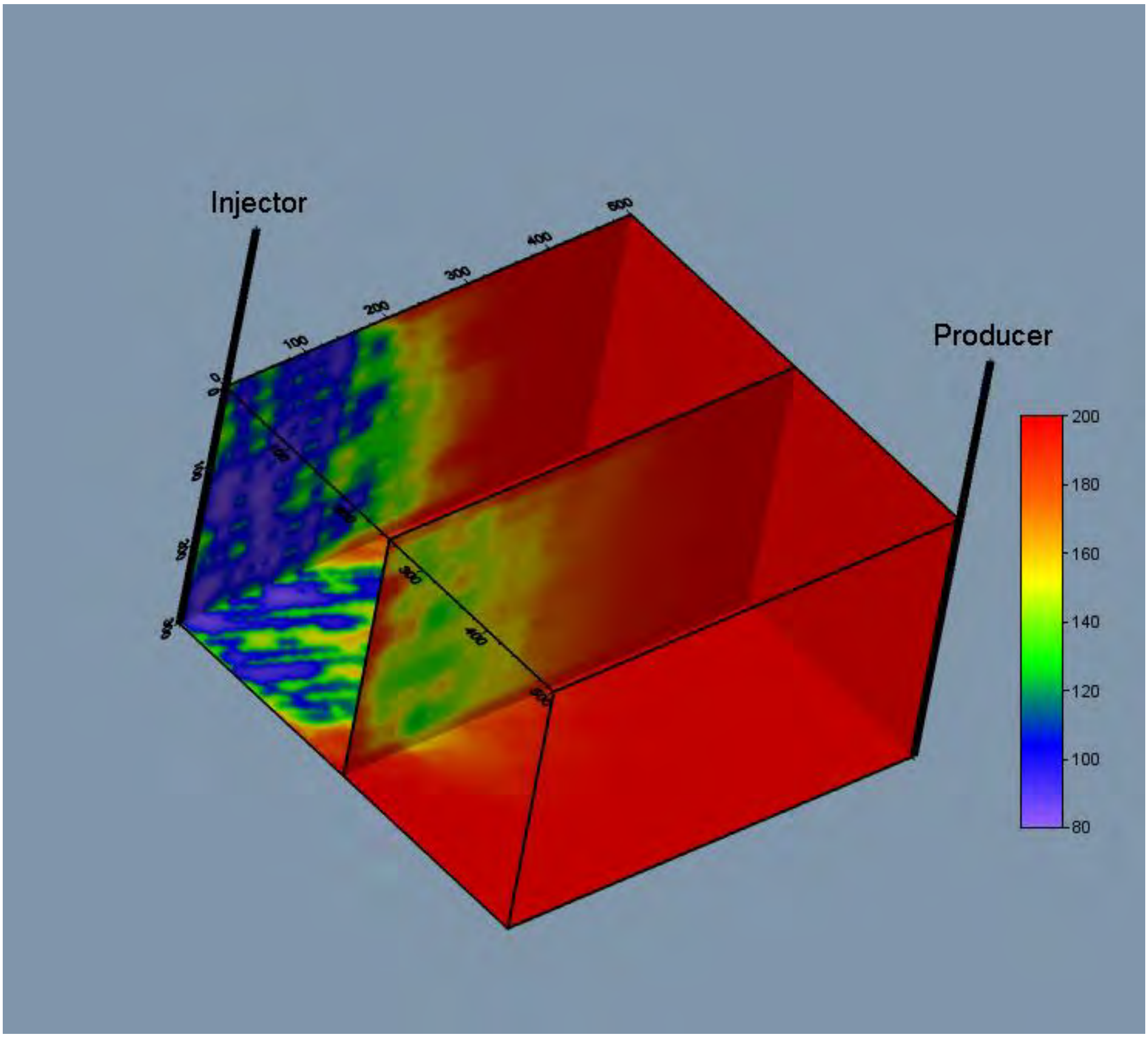

Fig. 4.10: Rock matrix temperature profile after 5 years of production; heat transfer coefficient of medium: 5 mW/m^2 ^{0}C, fracture density: 0.32 m^{-1}, heat transfer area: 2.40x10^7 m^2, pressure loss between injector and producer: 1500psi and production rate: 81 l/s.

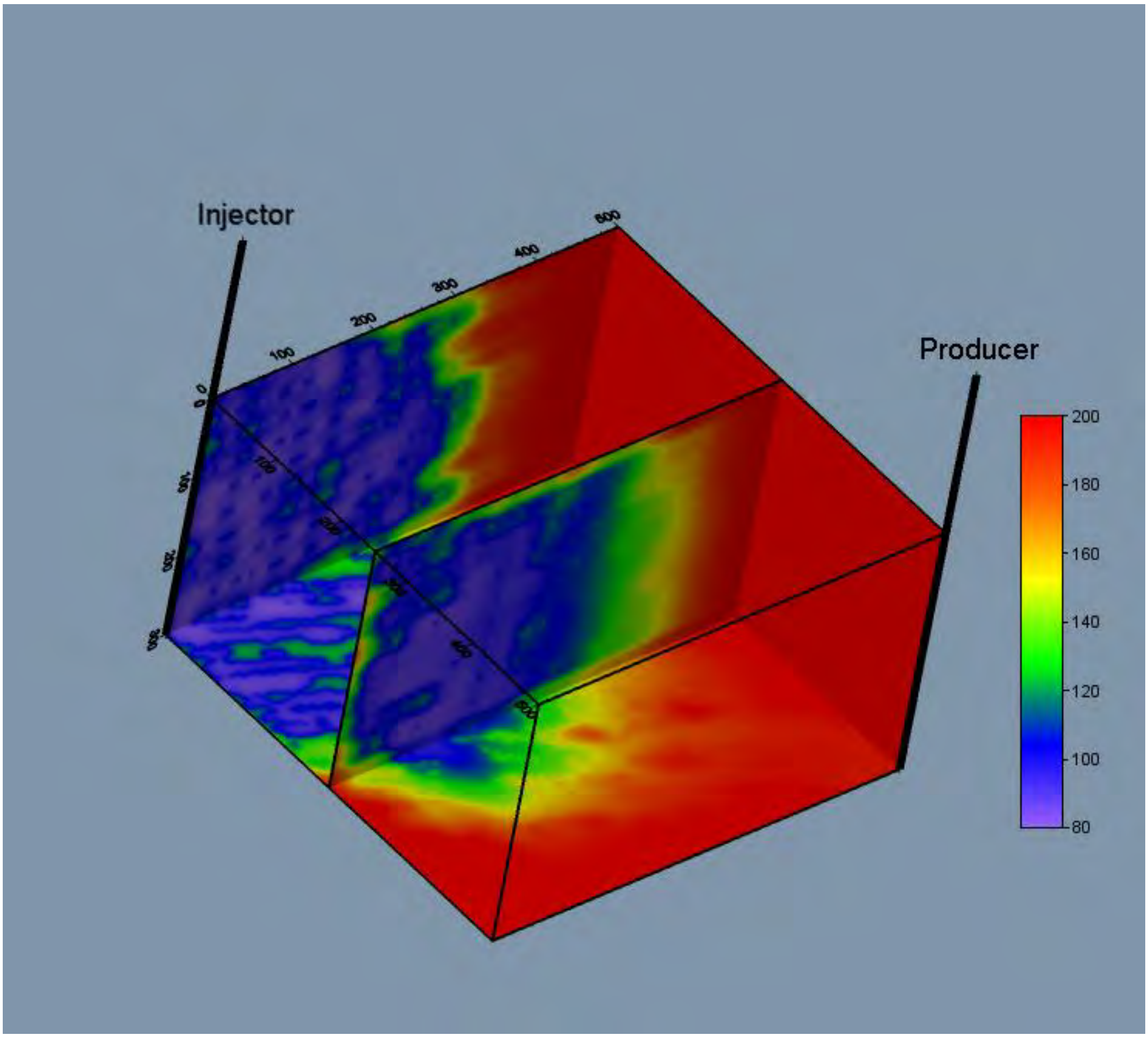

Fig. 4.11: Fluid temperature profile after 10 years of production; heat transfer coefficient of medium: 5 mW/m^2 ^0C, fracture density: 0.32 m^{-1}, heat transfer area: $2.40x10^7$ m^2, pressure loss between injector and producer: 1500psi and production rate: 81 l/s.

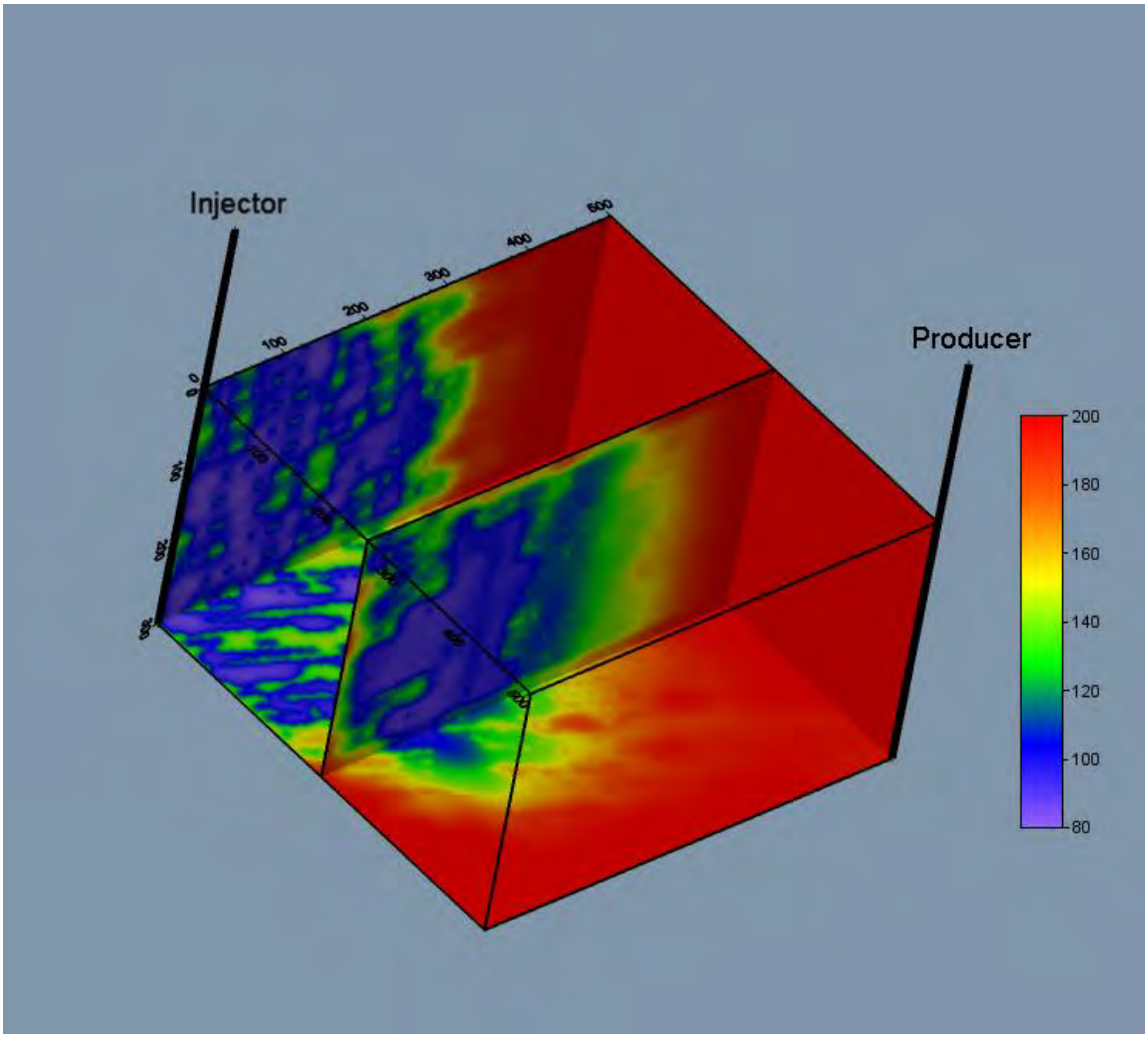

Fig. 4.12: Rock matrix temperature profile after 10 years of production; heat transfer coefficient of medium: 5 $mW/m^2\ {}^0C$, fracture density: 0.32 m^{-1}, heat transfer area: $2.40x10^7\ m^2$, pressure loss between injector and producer: 1500psi and production rate: 81 l/s.

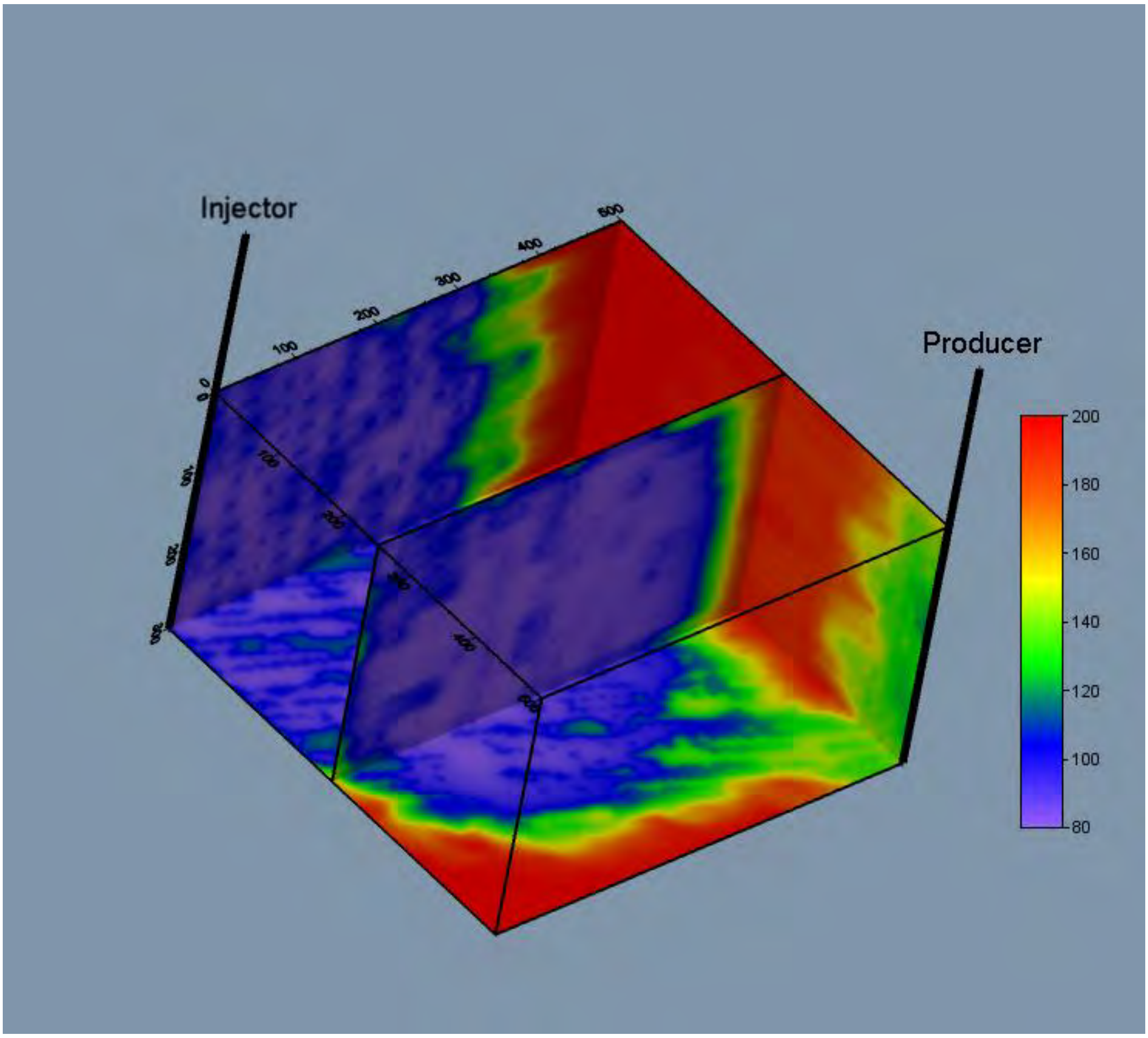

Fig. 4.13: Fluid temperature profile after 25 years of production; heat transfer coefficient of medium: 5 mW/m^2 ^{0}C, fracture density: 0.32 m^{-1}, heat transfer area: 2.40x10^7 m^2, pressure loss between injector and producer: 1500psi and production rate: 81 l/s.

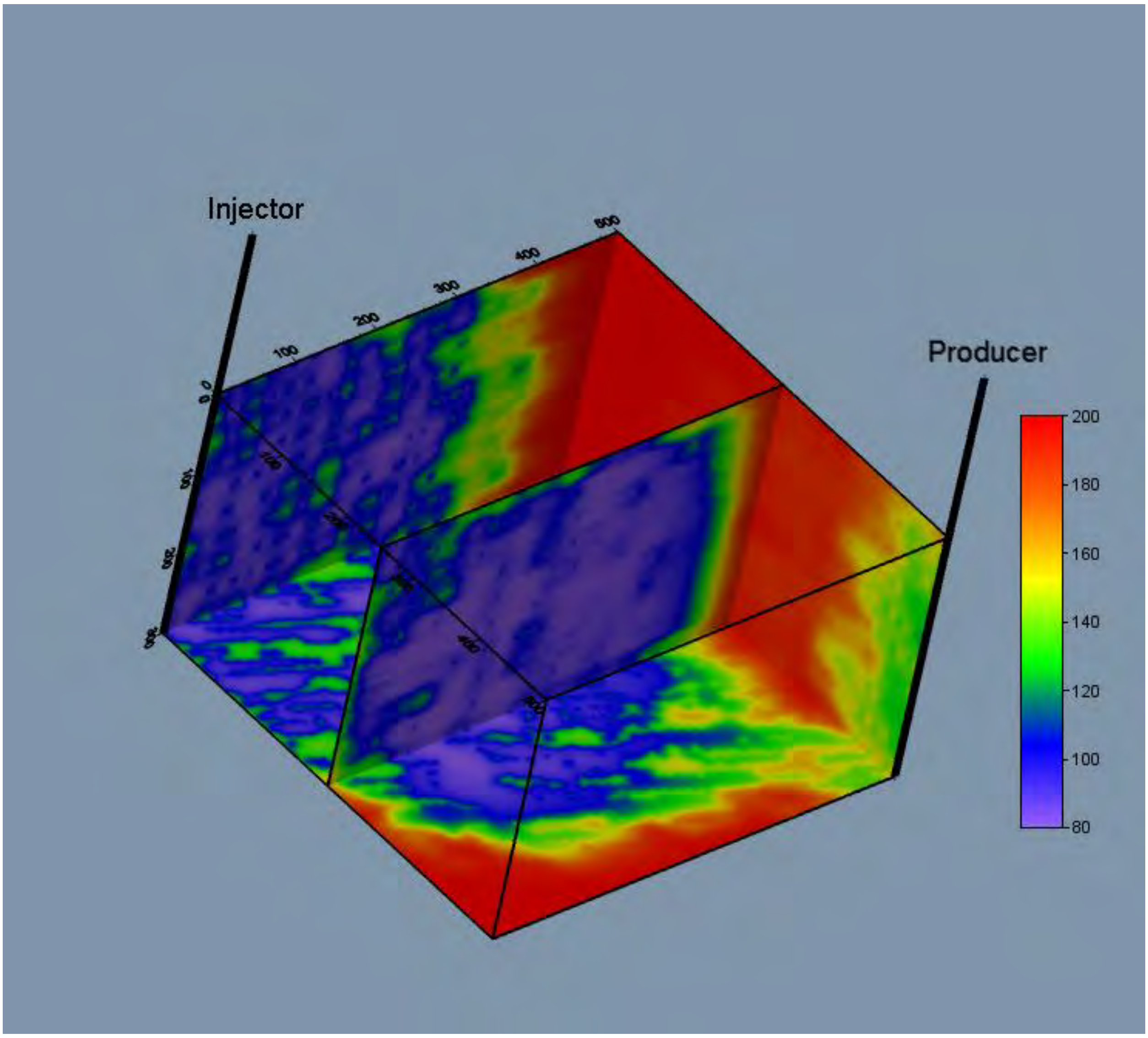

Fig. 4.14: Rock matrix temperature profile after 25 years of production; heat transfer coefficient of medium: 5 $mW/m^2\ ^0C$, fracture density: 0.32 m^{-1}, heat transfer area: $2.40x10^7\ m^2$, pressure loss between injector and producer: 1500psi and production rate: 81 l/s.

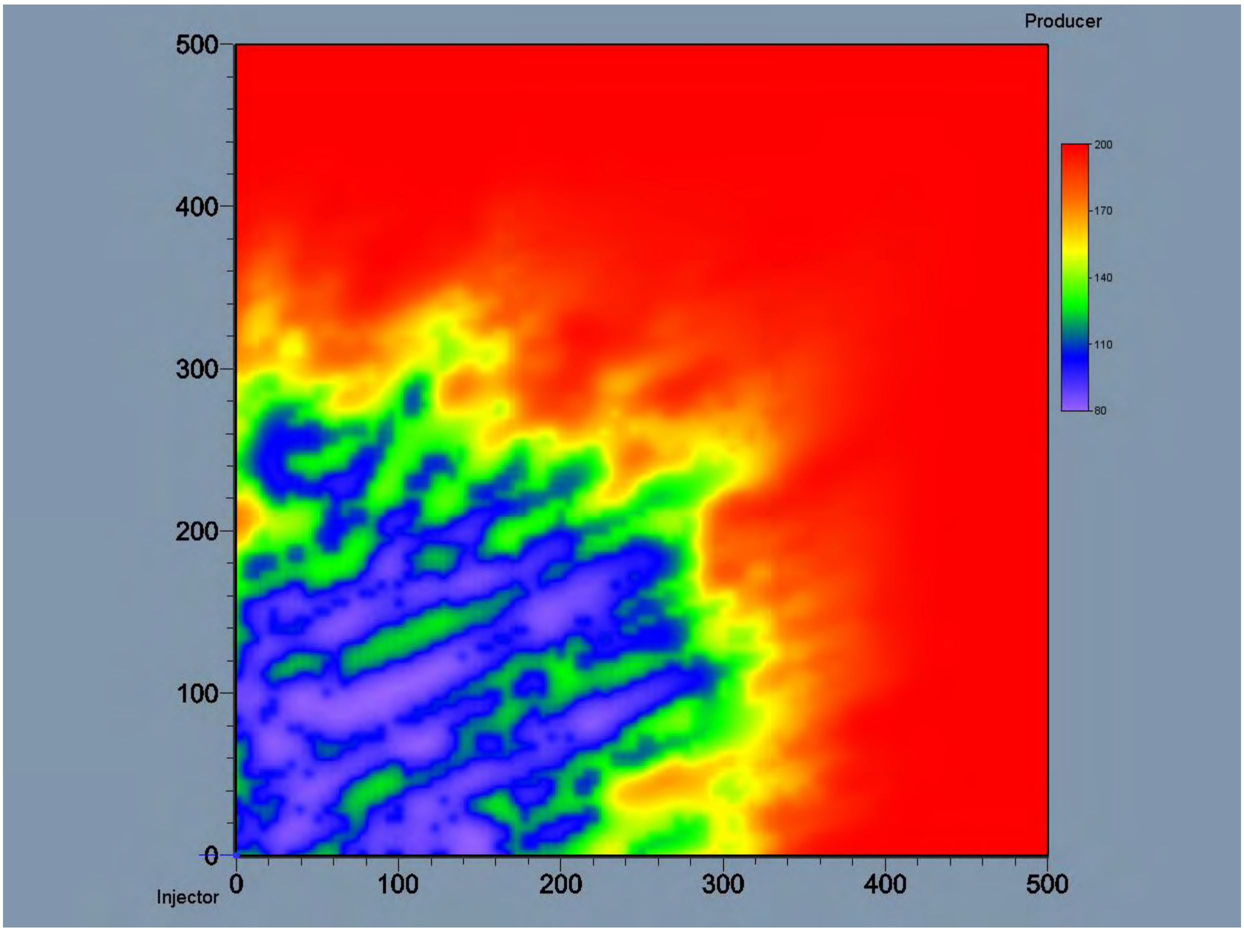

Fig. 4.15: The rock matrix temperature profile after 25 years of production along the horizontal section at 3100m for heat transfer coefficient of medium: 5 $mW/m^2\ {}^0C$, fracture density: 0.32 m^{-1}, heat transfer area: 2.40E+07 m^2 and production rate: 28 l/s.

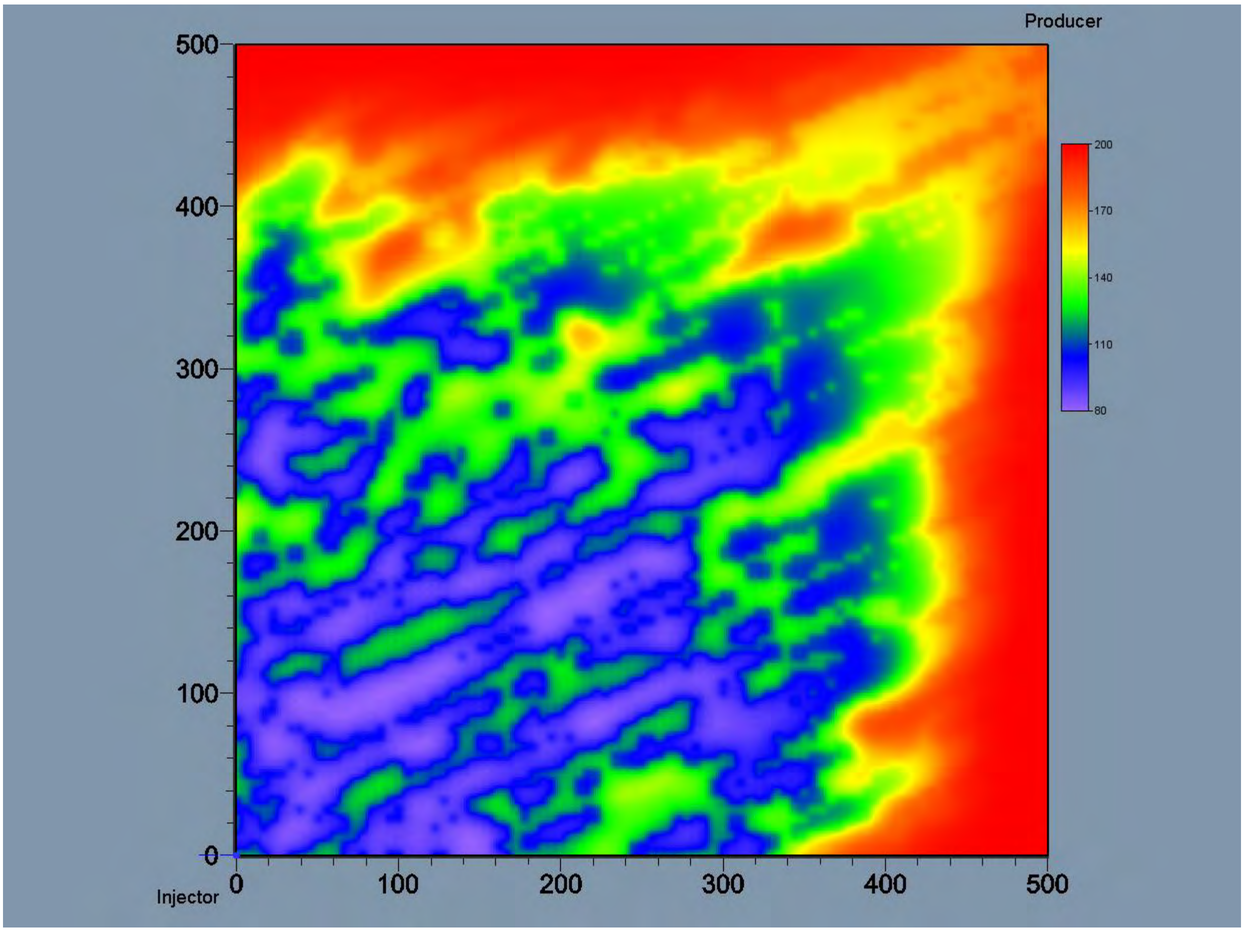

Fig. 4.16: The rock matrix temperature profile after 25 years of production along the horizontal section at 3100m for heat transfer coefficient of medium: 5 $mW/m^2\ ^0C$, fracture density: 0.32 m^{-1}, heat transfer area: $2.40x10^7\ m^2$ and production rate: 55 l/s.

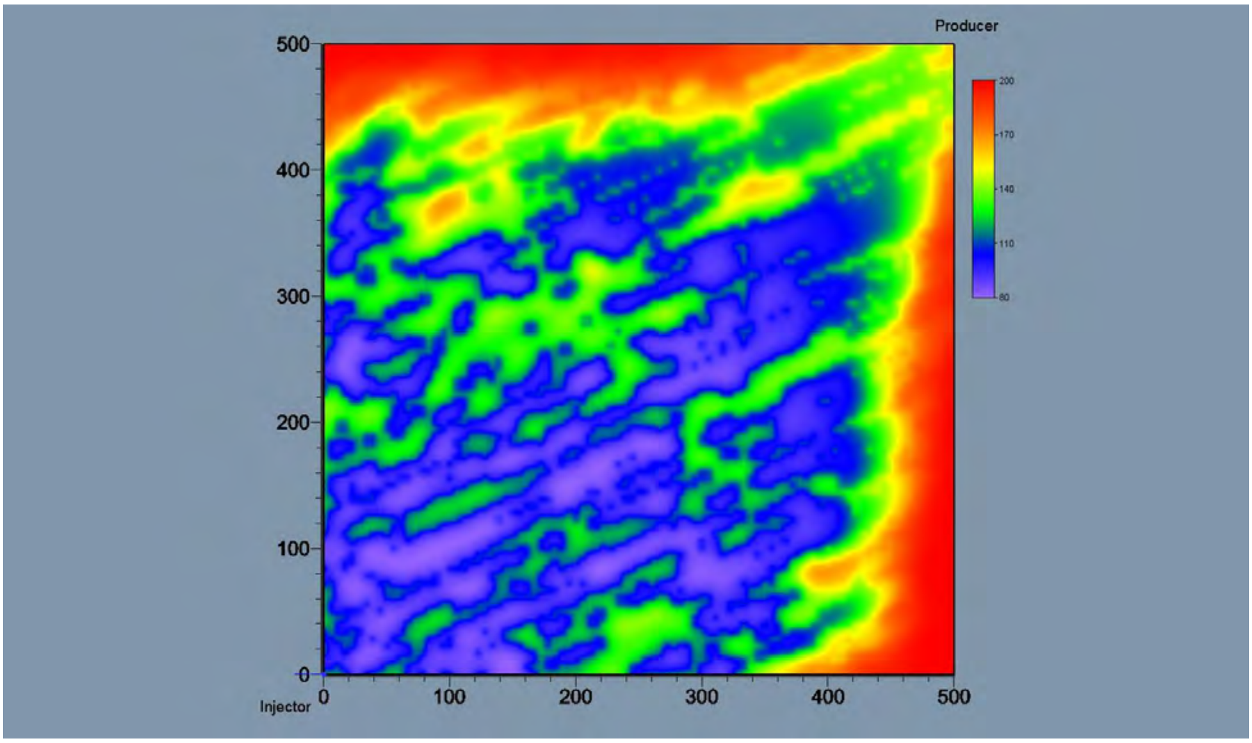

Fig. 4.17: The rock matrix temperature profile after 25 years of production along the horizontal section at 3100m for heat transfer coefficient of medium: 5 $mW/m^2\ {}^0C$, fracture density: 0.32 m^{-1}, heat transfer area: $2.40x10^7\ m^2$ and production rate: 81 l/s.

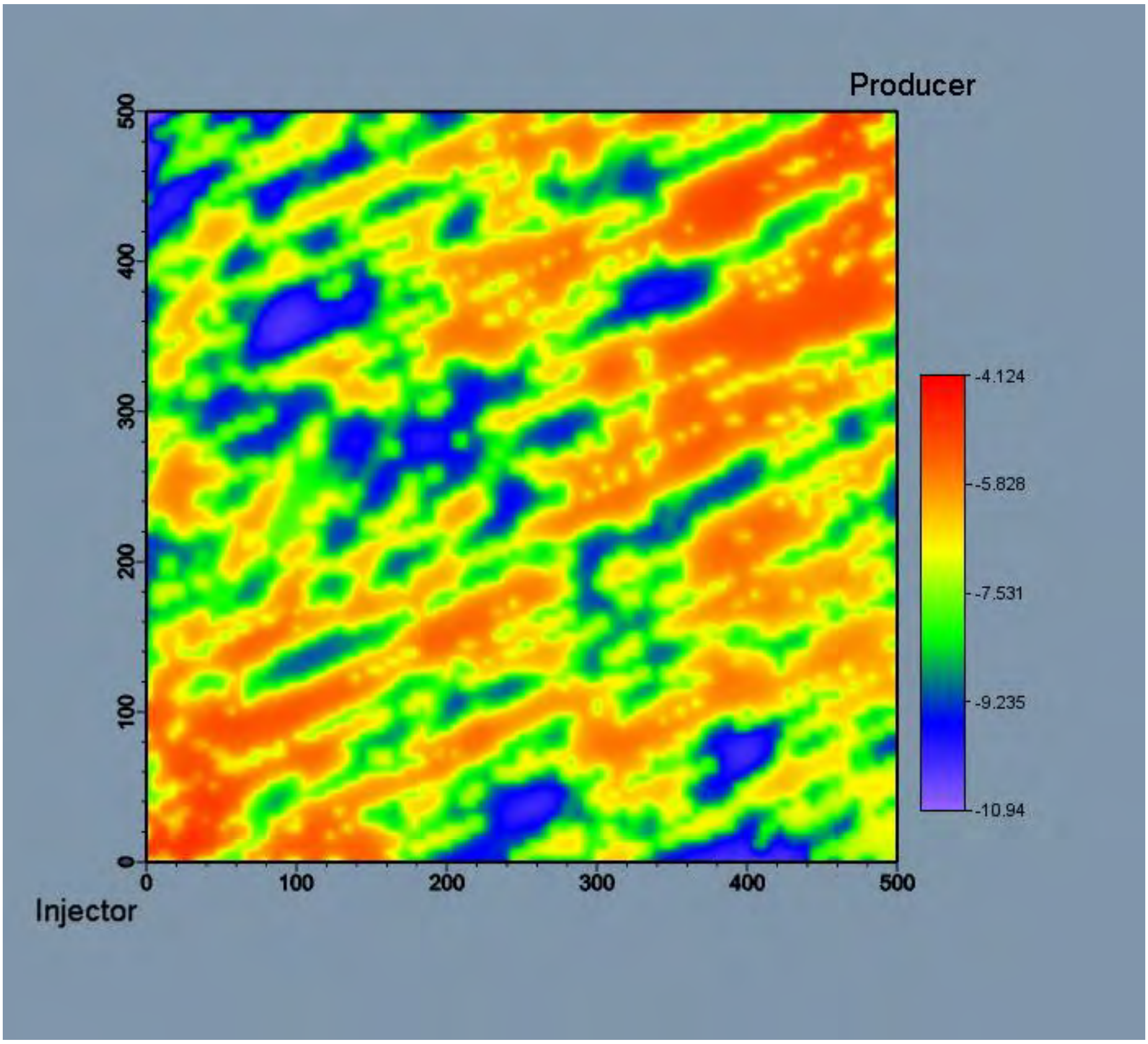

Fig. 4.18: The fluid velocity (rms) profile after 25 years of production along the horizontal section at 3100m for heat transfer coefficient of medium: 5 mW/m^2 ^{0}C, fracture density: 0.32 m^{-1}, heat transfer area: 2.40x10^7 m^2 and production rate: 81 l/s.

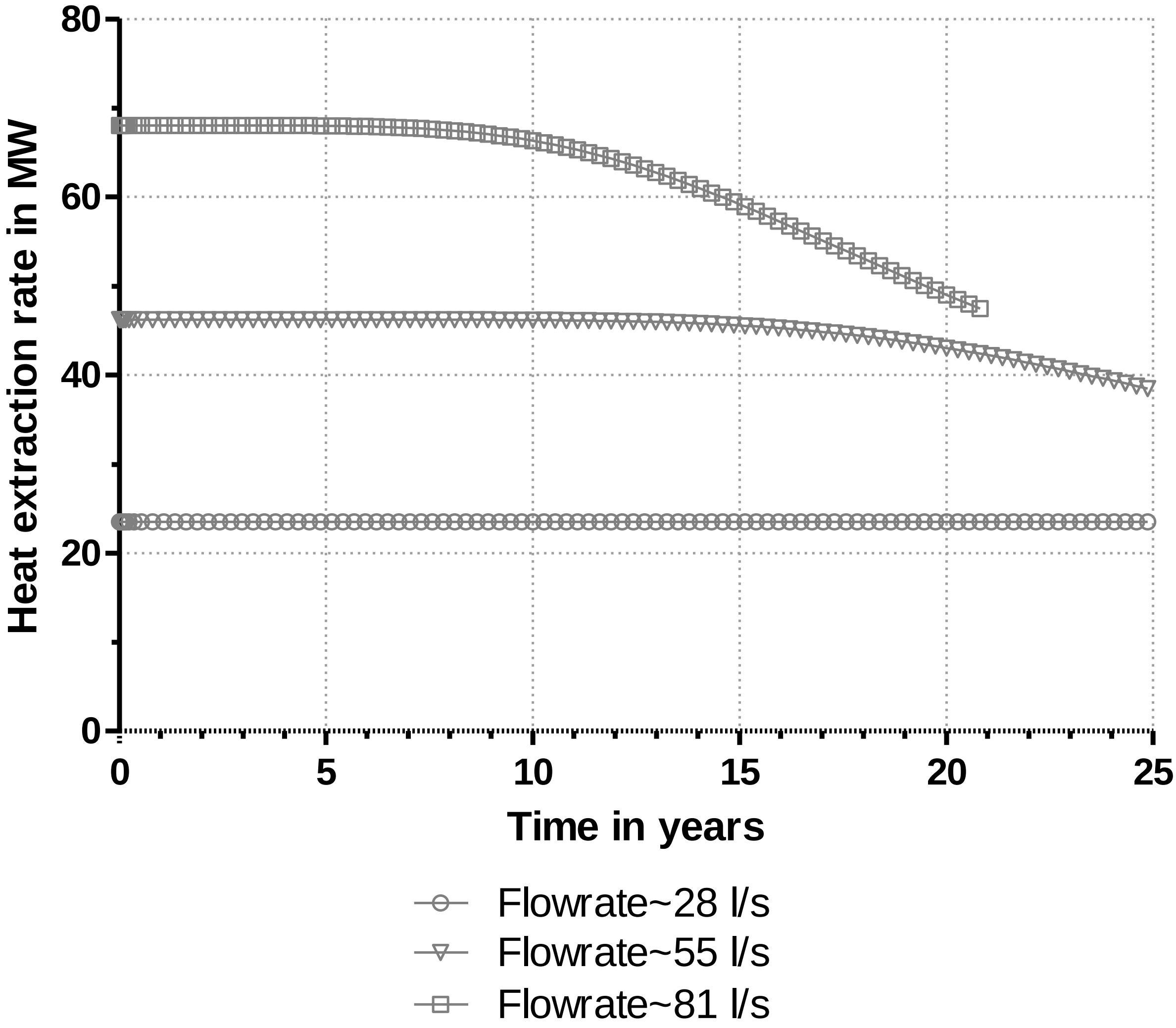

Fig. 4.19: Heat extraction rate vs. time for three different flow rates: 28 l/s, 55 l/s and 81 l/s, heat transfer area: 2.40×10^7 m^2 and heat transfer coefficient of medium: 2.5 mW/m^2 ^0C.

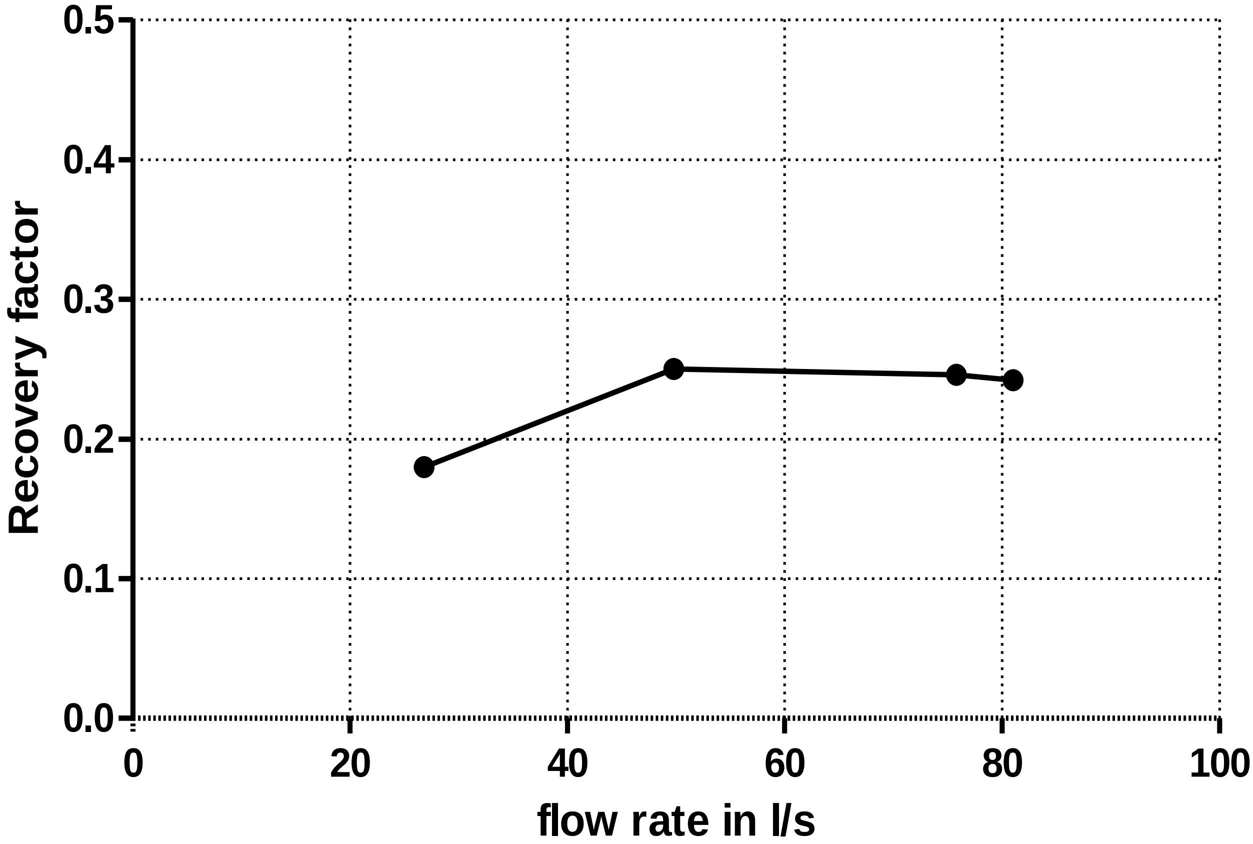

Fig. 4.20: Recovery factor vs. flow rate; fracture density: 0.14 m^{-1}, reservoir abandonment temperature 140^0C and heat transfer coefficient of medium: 5 mW/m^2 ^0C.

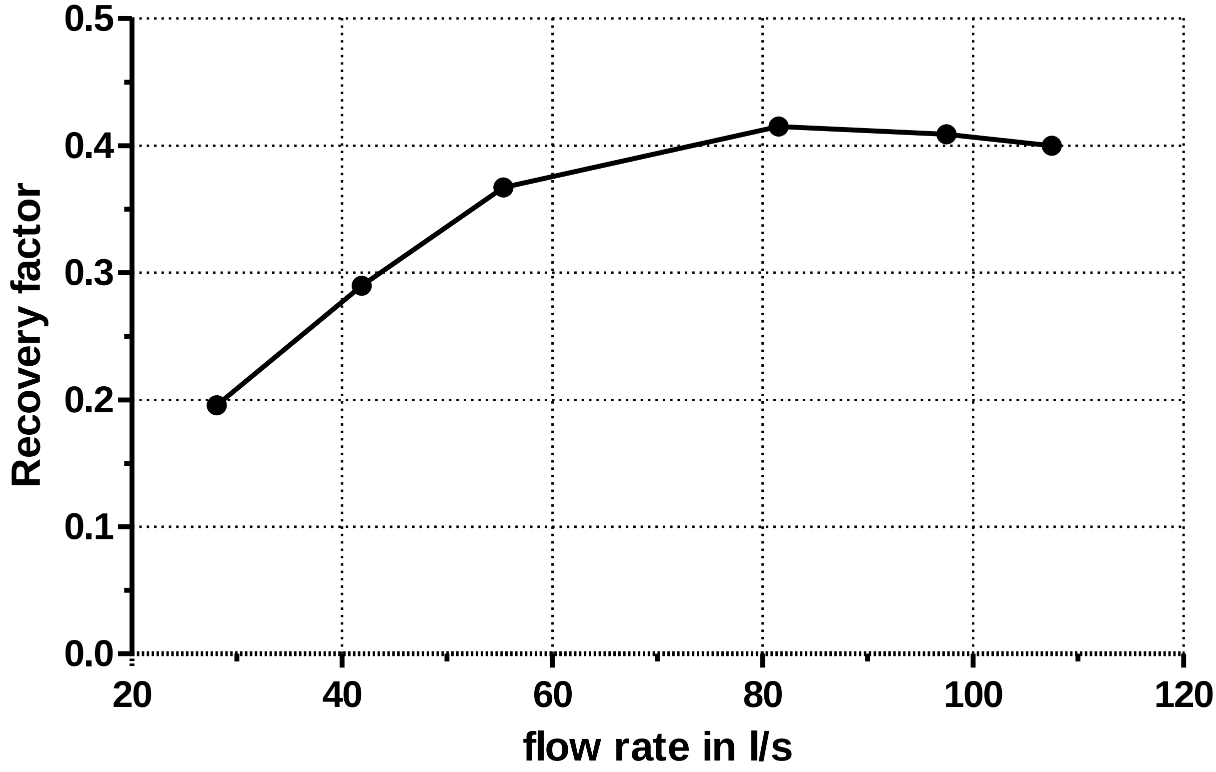

Fig. 4.21: Recovery factor vs. flow rate; fracture density: 0.32 m^{-1}, heat transfer area: $2.40x10^7$ m^2 , reservoir abandonment temperature 140^0C and heat transfer coefficient of medium: 5 $mW/m^{2}\,{}^0C$.

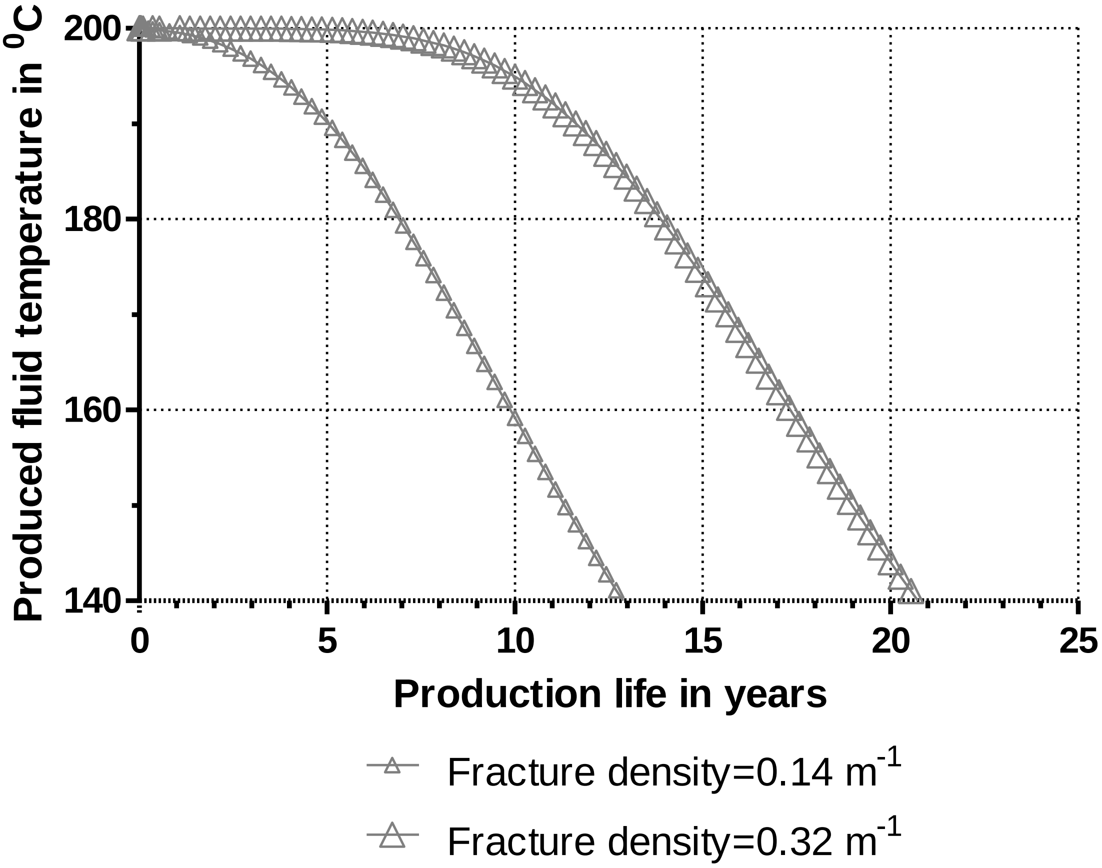

Fig. 4.22: Produced fluid temperature vs. time for two reservoirs with fracture density of 0.32 m^{-1} and 0.14 m^{-1}, flow rate: 81 l/s, reservoir abandon temperature: 140^{0}C and heat transfer coefficient of medium: 5E-3 W/m^2 ^{0}C.

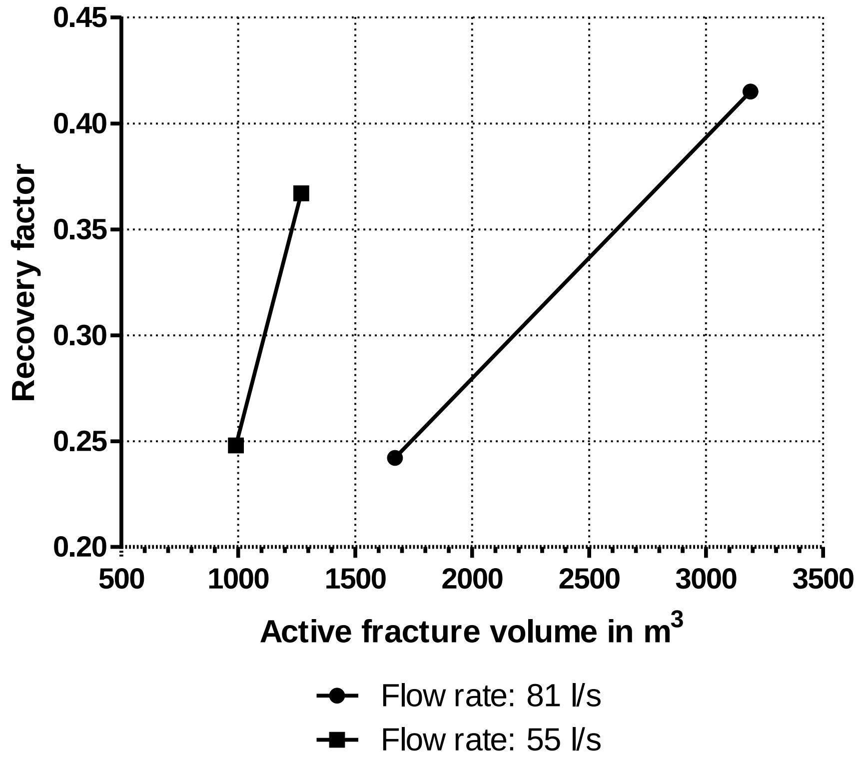

Fig. 4.23: Recovery factor vs. flow rate for two reservoirs with a fracture density of 0.32 m^{-1} and 0.14 m^{-1}, flow rates: 55 l/s, 81 l/s, production period: 25 years, reservoir abandon temperature: 140^{0}C and heat transfer coefficient of medium: 5x10^{-3} W/m^2 ^{0}C.

Chapter 5

Conclusion and Recommendations

Typically, geothermal reservoirs are tectonically stressed and fractured. Due to secondary-mineralisation processes, however, these fractures have healed over time resulting in low permeability. Estimating heat extraction from such a complicated fracture system is a challenging task. Several attempts are made in the past to simulate fluid flow and heat transfer through naturally-fractured geothermal reservoirs. Most of the previous models have one of more of the following limitations in their models.

i. Applicable to uniform fracture network only
ii. Ignored the effect of fracture interconnectivity
iii. Applicable to the homogenous reservoirs only
iv. Only a single fracture connecting injector and producer is considered
v. Ignored the dynamic heat transfer between rock matrix and circulating fluid
vi. Unable to present a optimum flowrate where the ultimate heat recovery is maximum

vii. Unable to study the effect of active fracture volume on the ultimate heat recovery

viii. Unable to study the effect of fracture density on the active fracture volume

This thesis presents a methodology that involves simulation of fluid flow and heat transfer in naturally-fractured reservoirs to predict heat extraction, thermal breakthrough and economic production life. A boundary element based numerical model is adapted to generate grid based effective permeability tensor map representing local directional permeability of the fractured rock. A finite element based flow model is coupled with the grid based effective permeability tensor model to study the fluid flow through the arbitrary oriented fractured network. A finite element based heat transfer model is developed and integrated with the flow model to estimate produced water temperature, thermal drawdown of matrix, and heat recovery under different conditions. The numerical models used in this study as well as the mesh generator were coded as part of the work using the programming language FORTRAN.

The effects of the following reservoir parameters and operating conditions were studied in this thesis:

ix. Effect of the fracture density on the pressure loss between injector and producer.

x. Effect of the well placement on the production rate.
xi. Effect of the injection rate on the produced water temperature
xii. Effect of the injection rate on the matrix temperature drawdown
xiii. Effect of the injection rate on the recovery factor
xiv. Effect of the fracture density on the active fracture volume
xv. Effect of the fracture density on the produced fluid temperature
xvi. Effect of the active fracture volume on the heat recovery factor.

Based on the results of this study the following conclusions can be drawn:

i. For a given flow rate the pressure loss between injector and production is mainly controlled by characteristic properties of fractures such as orientation and their interconnectivity. It has been observed that for a reservoir with a fracture density of 0.32 m^{-1} the pressure loss between an injector and a producer reaches a value of 1500 psi for a total flow rate of 138 l/s (0.29 $MPa.l^{-1}$ s). However, when the fracture density of the reservoir decreases to 0.027 m^{-1} the total flow rate decreases to 14 l/s for the same pressure loss of 1500psi.

ii. Temperature draw down is also significantly affected by facture density due to change in active fracture volume between matrix and circulating fluid. For example, for a low fracture density reservoir (0.14 m^{-1}) the produced fluid temperature drops to 140^{o}C for a flow rate of 81 l/s and a pressure drop of 2200 psi over a production period of 16 years. When the fracture density is increased to 0.32 m^{-1} the active fracture volume increases which in turn increases the productive life to 21 years for the same flow rate.

iii. Fracture orientation and their connectivity play dominant role in conducting fluid flow through fractured porous medium. From the study of five-spot well pattern it was found that the well, which is primarily oriented along the major fracture direction and is well connected, provides maximum production while the well, which is off the major fracture direction, provides least production (see chapter three).

iv. Flow rate has a significant impact on the produced fluid temperature and the heat recovery. In this study the produced fluid temperature of 140 ^{o}C (abandoned produced fluid temperature) is assumed to be the temperature below which the hot water production becomes commercially not viable. At low flow rates the change in produced fluid temperature is really small when compared to the same at high flow rates. This is due to the fact that low flow rates allows more time for the circulating fluid to have in contact with the rock matrix and extract more heat.

v. The heat recovery factor increases with increase in the flow rate till it reaches its maximum threshold value. A heat recovery factor of

0.19 (ratio of total heat recovered to total heat stored) can be obtained from a reservoir with a high fracture density (0.32 m^{-1}) for a flow rate of 28 l/s. When the flow rate is increased to 55 l/s the recovery factor is increase to 0.41. With further increase in the flow rate does not increase the heat recovery factor. This is due to the fact that once the heat recovery reaches its threshold any further increase in flow rate will have little impact on the heat recovery factor.

vi. It has been observed that with increase in the fracture density the recovery factor increases. This is due to the fact that when the fracture density increases the circulating fluid sweeping efficiency increases which in turn increases the thermal draw down and therefore the heat recovery.

5.1 Further Work

In the present work a 3D numerical model is developed to evaluate potential for heat recovery from naturally fractured geothermal reservoirs. The numerical procedure presented in this thesis comprises of a discrete fracture model, a fluid flow simulation model and a heat transfer model. The discrete fracture model is based on the stochastic analysis of field data and doesn't consider regional tectonic history. The fluid flow model used in this study simulation of single phase only and effective permeability tensor is used to represent the directional hydraulic properties of fractures. The heat transfer model is based on the rock-fluid temperature approach. In order to improve accuracy of the results following recommendations are made.

In the discrete fracture model, the regional tectonic history along with field data can be used to generate fracture network. A global optimization technique, such as the simulated annealing technique can be used to the minimize gap between the existing fracture network in the reservoir and the generated one, thereby improving the predictive capability of the model. It is recommended to treat long fractures (fractures that are longer than the grid blocks) discretely in the simulation of fluid flow. Finite element method has been proven to be inefficient in discretising large number of fractures. It is recommended to use extended finite element method or an mesh less numerical methods which does not require a extensive mesh generation. The fluid flow model can be extended from single phase to multiphase flow to investigate the phase transfer between phases due to changes in the reservoir conditions, such as pressure and temperature. It can also be extended to incorporate open flow boundary conditions to investigate the fluid loss from the reservoir. The heat flow model can be extended to include the heat flux coming from the layers below the reservoir. Further use of advanced stabilization techniques, such as the multi-step Taylor

Galerkin scheme and minimization of data transfer between parallel processors can improve the efficiency of numerical modeling.

References:

Aghighi M. A. (2007). Fully coupled fluid flow and geomechanics in the study of hydraulic fracturing and post-fractuer production. School of Petroleum Engineering. Sydney, University of New South Wales. Phd Thesis.

Ahmed T. (2006). Reservoir engineering handbook, Gulf Professional Publishing.

Amestoy P. R., Duff, I. S. and L'Excellent, J. Y. (2000). "Multifrontal parallel distributed symmetric and unsymmetric solvers." Computer Methods in Applied Mechanics and Engineering 184(2-4): 501-520.10.1016/s0045-7825(99)00242-x

Anzelius A. (1926). "Uber erwarmung vermittels durchstromender medien." Z. Angew. Math. Mech 6: 291–294

Auradou H., Drazer, G., Boschan, A., Hulin, J.-P. and Koplik, J. (2006). "Flow channeling in a single fracture induced by shear displacement." Geothermics 35(5-6): 576-588

Bagheri M. A. and Settari, A. (2006). "Effects of fractures on reservoir deformation and flow modeling." Canadian Geotechnical Journal 43(6): 574-586

Bai M., Ma, Q. and Roegiers, J. C. (1994). "Dual-porosity behaviour of naturally fractured reservoirs." International Journal for Numerical and Analytical Methods in Geomechanics 18(6): 359-376.10.1002/nag.1610180602

Barenblatt G. I., Entov, V. M. and Ryzhik, V. M. (1990). Theory of fluid flows through natural rocks. Dordrecht ; Boston, Kluwer Academic Publishers.

Bataillé A., Genthon, P., Rabinowicz, M. and Fritz, B. (2006). "Modeling the coupling between free and forced convection in a vertical permeable slot: Implications for the heat production of an Enhanced Geothermal System." Geothermics 35(5-6): 654-682.10.1016/j.geothermics.2006.11.008

Blackford L. (1997). "ScaLAPACK Users' Guide."

Blum P., Mackay, R. and Riley, M. S. (2009). "Stochastic simulations of regional scale advective transport in fractured rock masses using block upscaled hydro-mechanical rock property data." Journal of Hydrology 369(3-4): 318-325.DOI 10.1016/j.jhydrol.2009.02.009

Bourbiaux B., Cacas, M., C., Sarda, S. and Sabathier, J., C. (1998). "Méthodologie rapide et efficace pour convertir les images de réservoir fracturé en modèle à double porosité." Oil & Gas Science and Technology - Rev. IFP 53(6): 785-799

Burch D. M., Allen, R. W. and Peavy, B. A. (1976). "Transient Temperature Distributions Within Porous Slabs Subjected to Sudden Transpiration Heating." Journal of Heat Transfer 98(2): 221-225

Carslaw H. S. and Jaeger, J. C. (1959). "Conduction of heat in solids." Oxford: Clarendon Press, 1959, 2nd ed. 1

Castaing C., Genter, A., Bourgine, B., Chilès, J. P., Wendling, J. and Siegel, P. (2002). "Taking into account the complexity of natural fracture systems in reservoir single-phase flow modelling." Journal of Hydrology 266(1-2): 83-98

Celli M., Rees, D. A. S. and Barletta, A. (2010). "The effect of local thermal non-equilibrium on forced convection boundary layer flow from a heated surface in porous media." International Journal of Heat and Mass Transfer 53(17-18): 3533-3539

Chin L. Y. and Nagel, N. B. (2004). "Modeling of Subsidence and Reservoir Compaction under Waterflood Operations." International Journal of Geomechanics 4(1): 28-34

Deo M., Huang, C.-K. and Wang, H. (2008). Parallel, Multigrid Finite Element Simulator for Fractured/Faulted and Other Complex Reservoirs based on Common Component Architecture (CCA), Project report, DOI 10.2172/949977.

Dongarra J. J., Croz, J. D., Hammarling, S. and Duff, I. S. (1990). "A set of level 3 basic linear algebra subprograms." ACM Trans. Math. Softw. 16(1): 1-17.10.1145/77626.79170
El-Zein A. H., Carter, J. P. and Airey, D. W. (2005). "Multiple-Porosity Contaminant Transport by Finite-Element Method." International Journal of Geomechanics 5(1): 24-34
Fahad M., Rahman, S. S. and Cinar, Y. (2011). A Numerical and Experimental Procedure to Estimate Grid Based Effective Permeability Tensorfor for Geothermal Reservoirs. The GRC Annual Meeting 2011. San Diego, California,October 23-26.
Faust C. R. and Mercer, J. W. (1979). "Geothermal reservoir simulation: 2. Numerical solution techniques for liquid- and vapor-dominated hydrothermal systems." Water Resour. Res. 15(1): 31-46.10.1029/WR015i001p00031
Fleming P. D. and Mansoori, J. (1987). "An Accurate Numerical Technique for Solution of Convection-Diffusion Equations Without Numerical Dispersion " SPE Reservoir Engineering Volume 2, Number 3: 373-386
Geiger-Boschung S., Huangfu, Q., Reid, F., Matthai, S., Coumou, D., Belayneh, M., Fricke, C. and Schmid, K. (2009). Massively Parallel Sector Scale Discrete Fracture and Matrix Simulations. SPE Reservoir Simulation Symposium Proceedings 1, pp. 344-358
Ghassemi A., Nygren, A. and Cheng, A. (2008). "Effects of heat extraction on fracture aperture: A poro-thermoelastic analysis." Geothermics 37(5): 525-539.DOI 10.1016/j.geothermics.2008.06.001
Ghassemi A. and Suresh Kumar, G. (2007). "Changes in fracture aperture and fluid pressure due to thermal stress and silica dissolution/precipitation induced by heat extraction from subsurface rocks." Geothermics 36(2): 115-140.10.1016/j.geothermics.2006.10.001
Ghassemi A., Tarasovs, S. and Cheng, A. H. D. (2007). "A 3-D study of the effects of thermomechanical loads on fracture slip in enhanced geothermal reservoirs." International Journal of Rock Mechanics and Mining Sciences 44(8): 1132-1148.10.1016/j.ijrmms.2007.07.016
Ghassemi A. and Zhou, X. (2011). "A three-dimensional thermo-poroelastic model for fracture response to injection/extraction in enhanced geothermal systems." Geothermics In Press, Corrected Proof.DOI: 10.1016/j.geothermics.2010.12.001
Gong, Karimi-Fard and Durlofsky, L. J. (2006). An Upscaling Procedure for Constructing Generalized Dual-Porosity/Dual-Permeability Models From Discrete Fracture Characterizations. SPE Annual Technical Conference and Exhibition. San Antonio, Texas, U.S.A.
Gringarten A., Witherspoon, P. and Ohnishi, Y. (1975). "Theory of heat extraction from fractured hot dry rock." Journal of Geophysical Research 80(8): 1120-1124
Gringarten A. C. and Witherspoon, P. A. (1973). "Extraction of heat from multiple-fractured dry hot rock." Geothermics 2(3-4): 119-122.10.1016/0375-6505(73)90018-7
Gropp W. (2002). MPICH2: A New Start for MPI Implementations. Recent Advances in Parallel Virtual Machine and Message Passing Interface. D. Kranzlmüller, J. Volkert, P. Kacsuk and J. Dongarra, Springer Berlin / Heidelberg. 2474: 37-42.
Hayashi K., Willis-Richards, J., Hopkirk, R. J. and Niibori, Y. (1999). "Numerical models of HDR geothermal reservoirs--a review of current thinking and progress." Geothermics 28(4-5): 507-518
He L.-W. and Jin, Z.-H. (2010). "A Local Thermal Nonequilibrium Poroelastic Theory for Fluid Saturated Porous Media." Journal of Thermal Stresses 33(8): 799 - 813
Hirata T. (1989). "Fractal dimension of fault systems in Japan: Fractal structure in rock fracture geometry at various scales." Pure and Applied Geophysics 131(1): 157-170.10.1007/bf00874485
Holman J. (1976). Heat Transfer.(4th edn. ed.), McGraw-Hill, New York.

Hossain M. M., Rahman, M. and Rahman, S. (2002). "A shear dilation stimulation model for production enhancement from naturally fractured reservoirs." Spe Journal 7(2): 183-195

Hoteit H. and Firoozabadi, A. (2008). "An efficient numerical model for incompressible two-phase flow in fractured media." Advances in Water Resources 31(6): 891-905.10.1016/j.advwatres.2008.02.004

Jafari A. and Babadagli, T. (2011). "Effective fracture network permeability of geothermal reservoirs." Geothermics 40(1): 25-38.10.1016/j.geothermics.2010.10.003

Jensen C., Lee, S., Milliken, W., Kamath, J., Narr, W., Wu, H. and Davies, J. (1998). Field simulation of naturally fractured reservoirs using effective permeabilities derived from realistic fracture characterization. SPE Annual Technical Conference and Exhibition, 27-30 September New Orleans, Louisiana,

Juliusson E. and Horne, R. N. (2010). Study and simulation of tracer and thermal transport in fractured reservoirs. PROCEEDINGS, Thirty-Fifth Workshop on Geothermal Reservoir Engineering. Stanford University, Stanford, California, February 1-3.

Kapel A. (1972). "The geology of the Patchawarra area, Cooper Basin." APEA Journal 12(1): 53-57

Kazemi H., Merril, L. S., Porterfield, K. L. and Zeman, P. R. (1976). Numerical Simulation of Water-Oil Flow in Naturally Fractured Reservoirs. SPE Journal. 317.

Kemmler D., Adamidis, P., Wang, W., Bauer, S. and Kolditz, O. (2005). Solving Coupled Geoscience Problems on High Performance Computing Platforms. Computational Science – ICCS 2005: 1064-1071.

Khaitan S., McCalley, J. and Raju, M. (2010). "Numerical methods for on-line power system load flow analysis." Energy Systems 1(3): 273-289.10.1007/s12667-010-0013-6

Koh J., N., G.-D., Shaik, A. R., Rahman, S. S. and Mortimer, L. (2010). Reservoir characterisation and numerical modelling to reduce project risk and maximise the chance of success. An example of how to design a stimulation program and assess fluid production from the Soultz geothermal field, France. Australian geothermal energy conference, 10–13 November.179-202

Koh J., Roshan, H. and Rahman, S. S. (2011). "A numerical study on the long term thermo-poroelastic effects of cold water injection into naturally fractured geothermal reservoirs." Computers and Geotechnics 38(5): 669-682.10.1016/j.compgeo.2011.03.007

Lee S. H., Lough, M. F. and Jensen, C. L. (2001). "Hierarchical modeling of flow in naturally fractured formations with multiple length scales." Water Resour. Res. 37(3): 443-455.10.1029/2000wr900340

Lewis R. W., Nithiarasu, P. and Seetharamu, K. N. (2005). Fundamentals of the Finite Element Method for Heat and Fluid Flow, John Wiley & Sons, Ltd.

Lough M. F., Lee, S. H. and Kamath, J. (1998). "An Efficient Boundary Integral Formulation for Flow Through Fractured Porous Media." JOURNAL OF COMPUTATIONAL PHYSICS 143(2): 462-483

Mannington W., O'Sullivan, M. and Bullivant, D. (2004). "Computer modelling of the Wairakei–Tauhara geothermal system, New Zealand." Geothermics 33(4): 401-419.10.1016/j.geothermics.2003.09.009

Mildren S., Burgess, J. and Meyer, J. (2005). Multiple Application of Image Log Data to EOR Operations in the Cooper Basin, Australia. SPE International Improved Oil Recovery Conference in Asia Pacific. 5-6 December, Kuala Lumpur, Malaysia.

Min K.-B., Jing, L. and Stephansson, O. (2004). "Determining the equivalent permeability tensor for fractured rock masses using a stochastic REV approach: Method and application to the field data from Sellafield, UK." Hydrogeology Journal 12(5): 497-510.10.1007/s10040-004-0331-7

N. G.-D. S. S. R. (2011). "3D Hybrid Tectono-Stochastic Modeling of Naturally Fractured Reservoirs: Application of Finite Element Method and Stochastic Simulation Technique." Journal of Geophysical Research Revision submitted

Nelson R. A. (2001). Geologic analysis of naturally fractured reservoirs, Gulf Professional Publishing.

Niessner J., Helmig, R., Jakobs, H. and Roberts, J. E. (2005). "Interface condition and linearization schemes in the Newton iterations for two-phase flow in heterogeneous porous media." Advances in Water Resources 28(7): 671-687

Novakowski K., Bickerton, G., Lapcevic, P., Voralek, J. and Ross, N. (2006). "Measurements of groundwater velocity in discrete rock fractures." Journal of Contaminant Hydrology 82(1-2): 44-60

Oda M. (1985). "Permeability tensor for discontinuous rock masses." Geotechnique 35(4): 483-495

Pruess K. (1991). TOUGH2: A general-purpose numerical simulator for multiphase fluid and heat flow.

Pruess K. and Narasimhan, T. (1985). "A practical method for modeling fluid and heat flow in fractured porous media." Society of Petroleum Engineers journal 25(1): 14-26

Rahman M. K., Hossain, M. M. and Rahman, S. S. (2002). "A shear-dilation-based model for evaluation of hydraulically stimulated naturally fractured reservoirs." International Journal for Numerical and Analytical Methods in Geomechanics 26(5): 469-497.10.1002/nag.208

Raju M. P. (2010). "Parallelization of Finite Element Navier-Stokes codes using MUMPS Solver." Innovations and Advances in Computer Sciences and Engineering: 515-518.10.1007/978-90-481-3658-2_90

Rees D., Bassom, A. and Siddheshwar, P. (2008). "Local thermal non-equilibrium effects arising from the injection of a hot fluid into a porous medium." Journal of Fluid Mechanics 594: 379-398

Rees D. A. S., Pop, I., Ingham, D. B. and Pop, I. (2005). Local thermal non-equilibrium in porous medium convection. Transport Phenomena in Porous Media III. Oxford, Pergamon: 147-173.

Rijken M. C. M. (2005). Modeling naturally fractured reservoirs : from experimental rock mechanics to flow simulation, The University of Texas at Austin. Doctoral dissertation.

Sanyal S. K. and Butler, S. J. (2005). An Analysis of Power Generation Prospects from Enhanced Geothermal Systems. Geothermal Resources Council Transactions, Vol:29,

Sanyal S. K., Granados, E. E., Butler, S. J. and Horne, R. N. (2005). An Alternative and Modular Approach to Enhanced Geothermal Systems. World Geothermal Congress 2005, Antalya, Turkey, April 2005.24-29

Schulze J. (2001). "Towards a Tighter Coupling of Bottom-Up and Top-Down Sparse Matrix Ordering Methods." BIT Numerical Mathematics 41(4): 800-841.10.1023/a:1021908421589

Teimoori A., Chen, Z., Rahman, S. S. and Tran, T. (2005). "Effective Permeability Calculation Using Boundary Element Method in Naturally Fractured Reservoirs." Petroleum Science and Technology 23(5): 693 - 709

Tester J., Anderson, B., Batchelor, A., Blackwell, D., DiPippo, R., Drake, E., Garnish, J., Livesay, B., Moore, M. and Nichols, K. (2006). "The future of geothermal energy: impact of Enhanced Geothermal Systems (EGS) on the United States in the 21st Century." Final Report to the US Department of Energy Geothermal Technologies Program. Cambridge, MA.: Massachusetts Institute of Technology

Tran N. H. (2007). "Simulated annealing technique in discrete fracture network inversion: optimizing the optimization." Computational Geosciences 11(3): 249-260.DOI 10.1007/s10596-007-9049-7

Tran N. H., Chen, Z. and Rahman, S. S. (2007). "Characterizing and modelling of fractured reservoirs with object-oriented global optimization." Journal of Canadian Petroleum Technology 46(3): 39-45

Warren J. and Root, P. J. (1963). "The behavior of naturally fractured reservoirs." SPE Journal 3(3): 245-255

Watanabe K. and Takahashi, H. (1995a). "Fractal Geometry Characterization of Geothermal Reservoir Fracture Networks." Journal of Geophysical Research-Solid Earth 100(B1): 521-528

Watanabe K. and Takahashi, H. (1995b). "Parametric Study of the Energy Extraction from Hot Dry Rock Based on Fractal Fracture Network Model." Geothermics 24(2): 223-236

Watanabe N., Wang, W. Q., McDermott, C. I., Taniguchi, T. and Kolditz, O. (2010). "Uncertainty analysis of thermo-hydro-mechanical coupled processes in heterogeneous porous media." Computational Mechanics 45(4): 263-280.DOI 10.1007/s00466-009-0445-9

Xing H. (2008). "Progress Report: Supercomputer Simulation of Hot Fractured Rock Geothermal Reservoir Systems." ESSCC/ACcESS Technical Repor: 1-48

Zhao J. (1994). "Geothermal testing and measurements of rock and rock fractures." Geothermics 23(3): 215-231.10.1016/0375-6505(94)90001-9

Zienkiewicz O. C. and Taylor, R. L. (2000). Finite Element Method (5th Edition) Volume 1 - The Basis, Elsevier.

Appendix A

Derivation of governing equation for slightly compressible fluid when the fluid is flowing through porous medium

Consider a flow element as shown in **Fig. 1**. The element has a width of dr and is located at a distance of r from the centre of the well. The porous element has a differential volume of dV. According to the concept of the material-balance equation the rate of mass flow into an element minus the rate of mass flow out of the element during a differential time Δt must be equal to the mass rate of accumulation during that time interval:

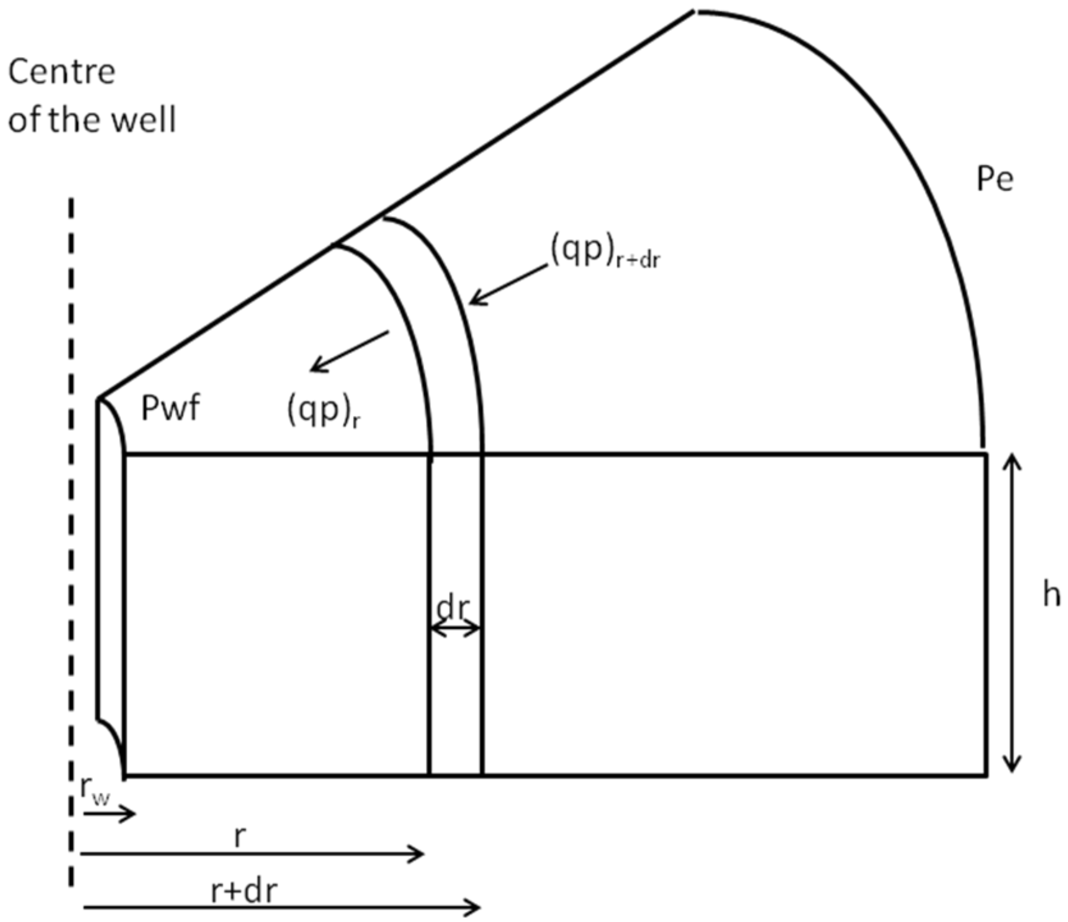

Fig.1 : Illustration of radial flow(Ahmed 2006)

[mass entering volume element during interval Δt] - [mass leaving volume element during interval Δt]

$$= \text{[rate of mass accumulation during interval } \Delta t\text{]} \quad \text{(A.1)}$$

Mass entering the volume element during time interval Δt :

$$(\text{Mass})_{\text{in}} = \Delta t[Av\rho]_{r+dr} \tag{A.2}$$

where v, A, Δt and ρ are velocity of flowing fluid, area at (r+dr), time interval and fluid density at (r+dr).

The area of the element at the entering side is:

$$A_{r+dr} = 2\pi(r+dr)h \tag{A.3}$$

Combining Eqns. (A.2) and (A.3) gives:

$$[\text{Mass}]_{\text{in}} = 2\pi\Delta t(r+dr)h(v\rho)_{r+dr} \tag{A.4}$$

Mass leaving the volume element during time interval Δt :

$$[\text{Mass}]_{\text{out}} = 2\pi rh\Delta t(v\rho)_r \tag{A.5}$$

Total Accumulation of Mass:

The volume of some element with a radius of r is given by:

$$V = \pi r^2 h$$

Differentiating the above equation with respect to r gives:

$$\frac{dV}{dr} = 2\pi rh$$

which means $dV = 2\pi rhdr$ (A.6)

Total mass accumulation during Δt $= dV[\ \phi\rho\ _{t+dt} - \ \phi\rho\ _{t}]$

where ϕ represents porosity.

Substituting for dV gives:

Total mass accumulation during Δt $= 2\pi rhdr[\ \phi\rho\ _{t+dt} - \ \phi\rho\ _{t}]$ (A.7)

Replacing terms of Eqn.A.1 with those of calculated relationship gives:

$$2\pi h(r+dr)\Delta t(\phi\rho)_{r+dr} - 2\pi hr\Delta t(\phi\rho)_{r} = (2\pi hr)dr[(\phi\rho)_{t+\Delta t} - (\phi\rho)_{t}]$$

Simplifying the above equation gives:

$$\frac{1}{r(dr)}[(r+dr)(v\rho)_{r+dr} - r(v\rho)_{r}] = \frac{1}{\Delta t}[(\phi\rho)_{t+\Delta t} - (\phi\rho)_{t}]$$

which in turn change to:

$$\frac{1}{r}\frac{\partial}{\partial r}[r(v\rho)] = \frac{\partial}{\partial t}(\phi\rho) \quad \text{(A.8)}$$

The above equation is called the continuity equation and it provides the principle of conservation of mass in radical coordinates.

By applying Darcy"s law the Eqn.8 becomes as:

$$\frac{1}{r}\frac{\partial}{\partial r}\left[\frac{k}{\mu}(r\rho)\frac{\partial p}{\partial r}\right] = \frac{\partial}{\partial t}(\phi\rho)$$

Expanding the right-hand side by taking the indicated derivatives eliminates the porosity from the partial derivative term on the right-hand side and applying chain rule:

$$\frac{\partial}{\partial t}(\phi\rho) = \phi\frac{\partial\rho}{\partial t} + \rho\frac{\partial\phi}{\partial\rho}\frac{\partial\rho}{\partial t} \tag{A.9}$$

As per the definition of the formation compressibility

$$c_f = \frac{1}{\phi}\frac{\partial\phi}{\partial\rho} \tag{A.10}$$

Combining Eqns. A.9 and A.10 gives:

$$\frac{1}{r}\frac{\partial}{\partial r}\left[\frac{k}{\mu}(r\rho)\frac{\partial p}{\partial r}\right] = \rho\phi c_f\frac{\partial p}{\partial t} + \phi\frac{\partial\rho}{\partial t}$$

Simplifying and expanding the above equation gives:

$$\frac{k}{\mu}\left[\frac{\rho}{r}\frac{\partial p}{\partial r} + \rho\frac{\partial^2 p}{\partial r^2} + \frac{\partial p}{\partial r}\frac{\partial\rho}{\partial t}\right] = \rho\phi c_f\frac{\partial p}{\partial t} + \phi\frac{\partial\rho}{\partial t}$$

Using the chain rule and diving by ρ gives:

$$\frac{k}{\mu}\left[\frac{1}{r}\frac{\partial p}{\partial r} + \frac{\partial^2 p}{\partial r^2} + \left(\frac{\partial p}{\partial r}\right)^2\left(\frac{1}{\rho}\frac{\partial\rho}{\partial\rho}\right)\right] = \phi c_f\frac{\partial p}{\partial t} + \phi\frac{\partial p}{\partial t}\left(\frac{1}{\rho}\frac{\partial\rho}{\partial p}\right)$$

Recalling that the compressibility of any fluid is related to its density by:

$$c = \frac{1}{\rho}\frac{\partial\rho}{\partial\rho}$$

Combining the above two equations gives:

$$\frac{k}{\mu}\left[\frac{1}{r}\frac{\partial p}{\partial r}+\frac{\partial^2 p}{\partial r^2}+c\left(\frac{\partial p}{\partial r}\right)^2\right]=\phi c_f\frac{\partial p}{\partial t}+\phi c\frac{\partial p}{\partial t}$$

The term $c\left(\frac{\partial p}{\partial r}\right)^2$ is considered very small and may be ignored then the above equation becomes:

$$\frac{k}{\mu}\left[\frac{\partial^2 p}{\partial r^2}+\frac{1}{r}\frac{\partial p}{\partial r}\right]=\phi c_t\frac{\partial p}{\partial t} \qquad \text{(A.11)}$$

Here $c_t = c_f + c$, which is total system compressibility. This equation is called diffusivity equation. Representing Eqn. A.11 in cartesian form in the presence of anisotropic permeability:

$$\phi c_t\frac{\partial p}{\partial t}=\frac{\partial}{\partial x}\left(\frac{k_{xx}}{\mu}\frac{\partial p}{\partial x}\right)+\frac{\partial}{\partial x}\left(\frac{k_{xy}}{\mu}\frac{\partial p}{\partial x}\right)+\frac{\partial}{\partial y}\left(\frac{k_{yx}}{\mu}\frac{\partial p}{\partial x}\right)+\frac{\partial}{\partial y}\left(\frac{k_{yy}}{\mu}\frac{\partial p}{\partial x}\right)$$

Appendix B

Finite element discretization of slightly compressible fluid when the fluid is flowing through fractured medium

A linear diffusivity equation is discretized via finite element method and applied. For a slightly compressible fluid, the diffusivity equation in expanded can be written as follows,

$$\phi c_t \frac{\partial p}{\partial t} = \frac{\partial}{\partial x}\left(\frac{k_{xx}}{\mu}\frac{\partial p}{\partial x}\right) + \frac{\partial}{\partial x}\left(\frac{k_{xy}}{\mu}\frac{\partial p}{\partial x}\right) + \frac{\partial}{\partial y}\left(\frac{k_{yx}}{\mu}\frac{\partial p}{\partial x}\right) + \frac{\partial}{\partial y}\left(\frac{k_{yy}}{\mu}\frac{\partial p}{\partial x}\right) \tag{B.1}$$

Multiplying both sides by a trail function w and integrating over the domain Ω yields:

$$\int_{\Omega} w\phi c_t \frac{\partial p}{\partial t} d\Omega = \int_{\Omega} w\left(\frac{\partial}{\partial x}\left(\frac{k_{xx}}{\mu}\frac{\partial p}{\partial x}\right) + \frac{\partial}{\partial x}\left(\frac{k_{xy}}{\mu}\frac{\partial p}{\partial x}\right) + \frac{\partial}{\partial y}\left(\frac{k_{yx}}{\mu}\frac{\partial p}{\partial x}\right) + \frac{\partial}{\partial y}\left(\frac{k_{yy}}{\mu}\frac{\partial p}{\partial x}\right)\right) d\Omega \tag{B.2}$$

Using the green formulae, the above equation becomes:

$$\begin{aligned}
&\int_{\Omega} w\phi c_t \frac{\partial p}{\partial t} d\Omega + \int_{\Omega} \frac{\partial w}{\partial x}\left(\frac{k_{xx}}{\mu}\frac{\partial p}{\partial x}\right) d\Omega + \int_{\Omega} \frac{\partial w}{\partial x}\left(\frac{k_{xy}}{\mu}\frac{\partial p}{\partial x}\right) d\Omega \\
&+ \int_{\Omega} \frac{\partial w}{\partial y}\left(\frac{k_{yx}}{\mu}\frac{\partial p}{\partial y}\right) d\Omega + \int_{\Omega} \frac{\partial w}{\partial y}\left(\frac{k_{yy}}{\mu}\frac{\partial p}{\partial y}\right) d\Omega = \\
&\oint_{\tau} w\left(\frac{k_{xx}}{\mu}\frac{\partial p}{\partial x} n_x + \frac{k_{xy}}{\mu}\frac{\partial p}{\partial x} n_x + \frac{k_{yx}}{\mu}\frac{\partial p}{\partial y} n_y + \frac{k_{yy}}{\mu}\frac{\partial p}{\partial y} n_y\right) d\tau
\end{aligned} \tag{B.3}$$

Where τ is the boundary and n is the outward normal to the boundary.

The boundary integral can be eliminated from the formulation for no flow boundaries and boundaries with constant pressure. Finite difference method is then used to discretize the terms including derivatives with respect to time. As its uncoupled fluid flow formulation, porosity, permeability total system compressibility, fluid compressibility, viscosity and quadratic pressure gradient term have no considerable change over each time step. After the rearrangement, on can obtain:

$$\int_{\Omega} w\phi^{i-1} c_t^{\,i-1} \frac{p^i - p^{i-1}}{\Delta t^i} d\Omega + \int_{\Omega} \frac{\partial w}{\partial x}\left(\frac{k_{xx}^{\;\;i-1}}{\mu}\frac{\partial p^i}{\partial x}\right) d\Omega + \int_{\Omega} \frac{\partial w}{\partial x}\left(\frac{k_{xy}^{\;\;i-1}}{\mu}\frac{\partial p^i}{\partial x}\right) d\Omega + \int_{\Omega} \frac{\partial w}{\partial y}\left(\frac{k_{yx}^{\;\;i-1}}{\mu}\frac{\partial p^i}{\partial x}\right) d\Omega + \int_{\Omega} \frac{\partial w}{\partial y}\left(\frac{k_{yy}^{\;\;i-1}}{\mu}\frac{\partial p^i}{\partial x}\right) d\Omega = 0 \tag{B.4}$$

in which superscripts i and i-1 are current and previous time steps respectively

Using Galerkin method (Zienkiewicz and Taylor, 2000) the above equation becomes

$$\left[\int_{\Omega} c_t \phi^i \overline{N}^T{}_p \overline{N}_p\right] \frac{\overline{P}^i - \overline{P}^{i-1}}{\Delta t^i} + \left[\int_{\Omega} \begin{pmatrix} \dfrac{k_{xx}^{\;\;i-1}}{\mu^{i-1}} \dfrac{\partial \overline{N}^T{}_p}{\partial x} \dfrac{\partial \overline{N}_p}{\partial x} + \dfrac{k_{xy}^{\;\;i-1}}{\mu^{i-1}} \dfrac{\partial \overline{N}^T{}_p}{\partial x} \dfrac{\partial \overline{N}_p}{\partial x} + \\ \dfrac{k_{yx}^{\;\;i-1}}{\mu^{i-1}} \dfrac{\partial \overline{N}^T{}_p}{\partial y} \dfrac{\partial \overline{N}_p}{\partial y} + \dfrac{k_{yyx}^{\;\;i-1}}{\mu^{i-1}} \dfrac{\partial \overline{N}^T{}_p}{\partial y} \dfrac{\partial \overline{N}_p}{\partial y} \end{pmatrix} d\Omega\right] \overline{P}^i = 0$$

(B.5)

where:

$$\vec{P}^T = (\text{p1 p2 ..... } p_n)$$

$$\overrightarrow{N_p}^T = (\text{N1 N2 ..... } N_n)$$

and n is the number of nodes. After rearranging above equation, one can obtain

$$\overline{\overline{M1}}(\overline{P}^i - \overline{P}^{i-1}) + \Delta t^i \overline{\overline{M2}}\,\overline{P}^i = 0 \tag{B.6}$$

where:

$$\overline{\overline{M1}} = \sum_{e=1}^{ne} \overline{\overline{M1^e}}$$

in which ne is the number of elements and

$$\overrightarrow{\overline{M1^e}} = \int_{\Omega} \begin{pmatrix} \frac{k_{xx}{}^{i-1}}{\mu^{i-1}} \frac{\partial \overline{N}^T{}_p}{\partial x} \frac{\partial \overline{N}_p}{\partial x} + \frac{k_{xy}{}^{i-1}}{\mu^{i-1}} \frac{\partial \overline{N}^T{}_p}{\partial x} \frac{\partial \overline{N}_p}{\partial x} + \\ \frac{k_{yx}{}^{i-1}}{\mu^{i-1}} \frac{\partial \overline{N}^T{}_p}{\partial y} \frac{\partial \overline{N}_p}{\partial y} + \frac{k_{yyx}{}^{i-1}}{\mu^{i-1}} \frac{\partial \overline{N}^T{}_p}{\partial y} \frac{\partial \overline{N}_p}{\partial y} \end{pmatrix} d\Omega$$

Equation (B.6) in an incremental form can be written as:

$$\overrightarrow{\overline{M}} + \Delta t^i \overrightarrow{\overline{M2}} \;(\overline{P}^i - \overline{P}^{i-1}) = \overrightarrow{\overline{f_1}} \qquad \text{(B.7)}$$

where

$$\overrightarrow{\overline{f_1}} = -\Delta t^i \overrightarrow{\overline{M2}}\overline{P}^{i-1}$$

All the integrations can be calculated numerically using the Gauss-Lagrandre integration technique. The above equation is valid where constant BHP is maintained. Where BHP is not constant, the Eqn B.1 will be changed as follows:

$$\overrightarrow{\overline{M}} + \Delta t^i \overrightarrow{\overline{M2}} \;(\overline{P}^i - \overline{P}^{i-1}) = \overrightarrow{\overline{f_1}} + q \qquad \text{(B.8)}$$

where q represents flow rate at the well bore

Appendix C

An analytical solution for slightly compressible fluid when the flowing through porous medium

For a slightly compressible fluid, the diffusivity equation can be written as

$$\nabla\left(\frac{\vec{\vec{k}}}{\mu}\nabla^2 p\right) = c_t \phi \frac{\partial p}{\partial t} + q \tag{C.1}$$

here ϕ, c_t, k, μ represents porosity, compressibility, permeability and viscosity. Charlez (1997) used Eqn. C.1 and solved it analytically. If p_R is initial rock pressure, p_w is well bore pressure then the solutions are:

$$p = p_R + (p_w - p_R) g(r,t) \tag{C.2}$$

$$g(r,t) = 1 - \frac{2}{\pi}\int_0^\infty e^{-t_d x^2} \frac{J_0(x)Y_0(xr_d) - J_0(xr_d)Y_0(x)}{J_0(x)^2 + Y_0(x)^2} \frac{dx}{x} \tag{C.3}$$

where J_0 and Y_0 are zero order Bessel function of the first and second kind, respectively and:

$$r_d = \frac{r}{r_w} \tag{C.4}$$

$$t_d = \frac{kt}{\mu \phi c_T r_w^{\ 2}} \tag{C.5}$$

Detournay (1998) also solved a similar problem and by comparison we can write:

$$\tilde{g}(r,s) = \frac{K_0(\xi)}{sK_0(\beta)} \tag{C.6}$$

where $\tilde{g}$ is the Laplace transform of g and:

$$\xi = r\sqrt{\frac{s}{c}} \tag{C.7}$$

$$\beta = r\sqrt{\frac{s}{c}} \tag{C.8}$$

The Laplace transform can be inverted using:

$$f(r,t) \approx \frac{\ln 2}{t}\sum_{n=1}^{N} C_n \tilde{f}(r, n\frac{\ln 2}{t}) \tag{C.9}$$

where ln is the natural algorithm and:

$$C_n = (-1)^{n+N/2}\sum_{k=\left\lfloor \frac{n+1}{2} \right\rfloor}^{\min(n,N/2)} \frac{k^{N/2}(2k)!}{(N/2-k)!k!(k-1)!(n-k)!(2k-n)!} \tag{C.10}$$

where $\lfloor \; \rfloor$ is the floor function and min() is the minimum. A good value to use for N is 10.

Appendix D

Full derivation of Energy balance equation for slightly compressible fluid and matrix when the fluid is flowing through fractured medium

A slightly compressible fluid is entering the infinitesimal control volume with the velocity of $V(v_x, v_y)$ of the energy balance equation for the control volume can be obtained as:

Heat entering the control volume by convection + Heat entering the control volume by diffusion = Exiting the control volume by convection + Heat exiting the control volume by diffusion + Rate of change of energy within the control volume

Heat entering the control volume by convection through x-direction can be expressed as:

$$\rho_f c_{pf} v_x T_f \Delta y \qquad \text{(D-1)}$$

here $\rho_f, c_{pf}, v, T_f, \Delta y$ are the density of the fluid, heat capacity of fluid, velocity of fluid, temperature of fluid and size of the control volume in y-direction respectively. Heat entering the control volume by convection through y-direction can be expressed as:

$$\rho_f c_{pf} v_y T_f \Delta x \qquad \text{(D-2)}$$

here Δx is the size of control volume in x-direction. When Taylor series expansion is used to express the energy convected out of the control volume in both x and y direction can be obtained as:

$$\rho_f c_{pf} v_x T_f \Delta y + \rho_f c_{pf} \frac{\partial v_x T_f}{\partial x} \Delta x \Delta y \qquad \text{(D-3)}$$

and

$$\rho_f c_{pf} v_y T_f \Delta x + \rho_f c_{pf} \frac{\partial v_y T_f}{\partial y} \Delta x \Delta y \qquad \text{(D-4)}$$

According to Fourier's law of heat conduction the heat diffusing into the control volume through x and y-direction is:

$$\Delta y q_x = -k_f \frac{\partial T_f}{\partial x} \Delta y \tag{D-5}$$

and

$$\Delta x q_y = -k_f \frac{\partial T_f}{\partial y} \Delta x \tag{D-6}$$

Here k_f is the thermal conductivity of the fluid entering the medium. When the Taylor series expansion is used the heat diffusing out of the control volume in the x- direction is

$$-k_f \frac{\partial T_f}{\partial x} \Delta y + \frac{\partial(-k_f \frac{\partial T_f}{\partial x})}{\partial x} \Delta y \Delta x \tag{D-7}$$

and in the y-direction is

$$-k_f \frac{\partial T_f}{\partial y} \Delta x + \frac{\partial(-k_f \frac{\partial T_f}{\partial y})}{\partial y} \Delta x \Delta y \tag{D-8}$$

The rate of change in energy within the control volume is:

$$\Delta x \Delta y \rho_f c_{pf} \frac{\partial T_f}{\partial t} \tag{D-9}$$

Finally, based on the Eqns D1-D9 the energy balance equation for the control volume after rearranging will be:

$$\frac{\partial T_f}{\partial t} + \frac{\partial v_x T_f}{\partial x} + \frac{\partial v_y T_f}{\partial y} = \frac{1}{\rho_f c_{pf}} \left[\frac{\partial(k_f \frac{\partial T_f}{\partial x})}{\partial x} + \frac{\partial(k_f \frac{\partial T_f}{\partial y})}{\partial y} \right] \tag{D-10}$$

The continuity equation in two dimensions can be expressed as:

$$\frac{\partial \rho_f v_x}{\partial x} + \frac{\partial \rho_f v_y}{\partial y} + \frac{\partial \rho_f}{\partial t} = 0 \tag{D-11}$$

If density is assumed to be constant then the continuity equation will be converted to

$$\frac{\partial v_x}{\partial x} + \frac{\partial v_y}{\partial y} = 0 \qquad \text{(D-12)}$$

Differentiating the convection terms in Eqn. D-10 by parts and substituting Eqn. D-12 and substituting in Eqn.D-10 then the simplified form of the energy balance equation will be

$$\frac{\partial T_f}{\partial t} + v_x \frac{\partial T_f}{\partial x} + v_y \frac{\partial T_f}{\partial y} = \frac{k_f}{\rho_f c_{pf}} \left[\frac{\partial^2 T_f}{\partial x^2} + \frac{\partial^2 T_f}{\partial y^2} \right] \qquad \text{(D-13)}$$

The above equation represents energy balance equation for fluid when its flowing through a infinitesimal control volume in two dimension. In three dimensions the energy balance equation will be expressed as:

$$\frac{\partial T_f}{\partial t} + v_x \frac{\partial T_f}{\partial x} + v_y \frac{\partial T_f}{\partial y} + v_z \frac{\partial T_f}{\partial z} = \frac{k_f}{\rho_f c_{pf}} \left[\frac{\partial^2 T_f}{\partial x^2} + \frac{\partial^2 T_f}{\partial y^2} + \frac{\partial^2 T_f}{\partial z^2} \right] + Q \qquad \text{(D-14)}$$

Here Q represent source or sink attached to the control volume. In our case Q represents the heat transfer between matrix and fluid.

Similarly the energy balance equation for the matrix can be expressed as:

$$\frac{\partial T_r}{\partial t} = \frac{k_r}{\rho_r c_{pr}} \left[\frac{\partial^2 T_r}{\partial x^2} + \frac{\partial^2 T_r}{\partial y^2} + \frac{\partial^2 T_r}{\partial z^2} \right] + Q \qquad \text{(D-14)}$$

here ρ_r, c_{pr}, T_r, k_r are the density of the matrix, heat capacity of matrix , temperature of matrix and thermal conductivity of the matrix respectively.

Appendix E

Finite element discretization of Energy balance equation for slightly compressible fluid when the fluid is flowing through fractured medium

An energy balance equation for slightly compressible fluid moving through fractured medium in one dimension is:

$$\frac{\partial T_f}{\partial t} + v\frac{\partial T_f}{\partial x} - \frac{\partial}{\partial x}\left(k_f \frac{\partial T_f}{\partial x}\right) = 0 \tag{E.1}$$

Let us consider a characteristic of the flow as shown in **Fig. 2** in the time-space domain. The incremental time period covered by the flow is Δt from the nth time level to the n+1th time level and the incremental distance covered during this time period is Δx_1, that is, from

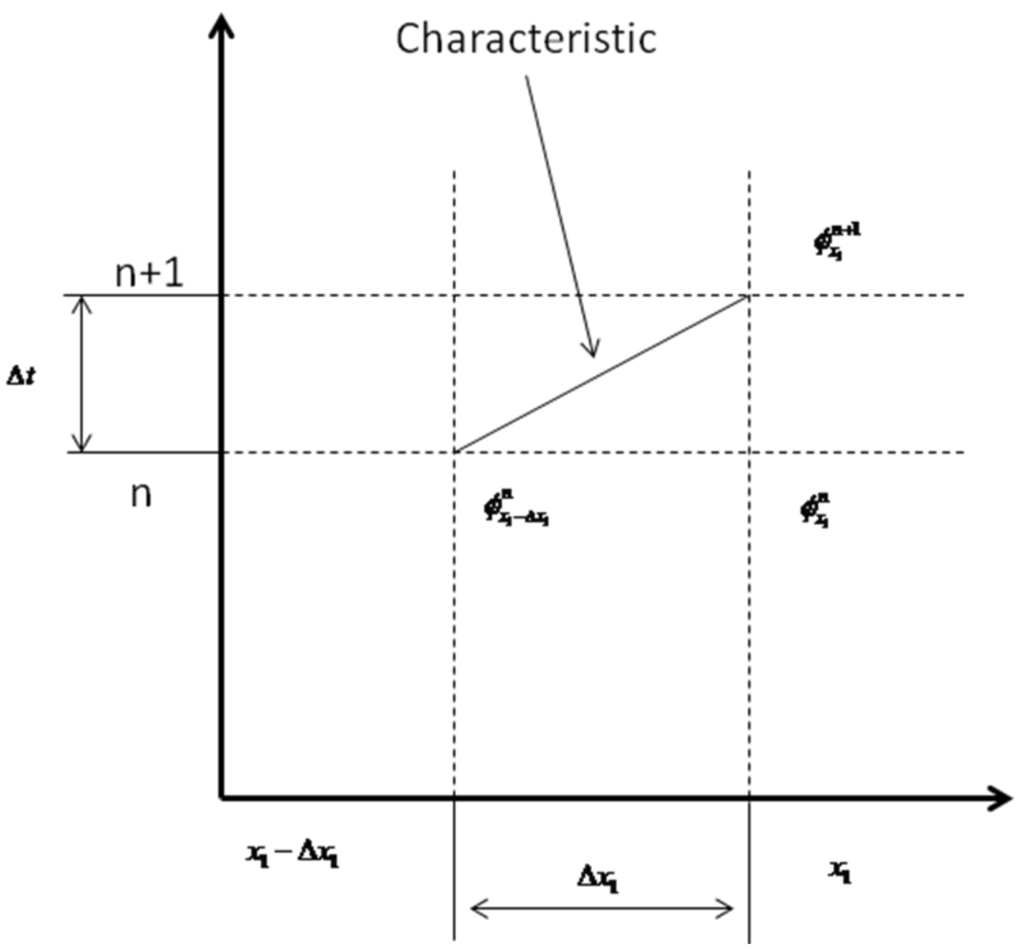

Fig 2: Characteristic in space-time domain (ref: ht book)

$x_1 - \Delta x_1$ to x_1. If a moving coordinate is assumed along the path of the characteristic wave with a speed of v, the convection terms of Eqn.2 disappear (as in a Lagarangian fluid dynamics approach). Although this approach eliminates the convection term responsible for spatial oscillation when discretized in space, the compilation of a moving coordinate system x_1' is introduced, then the Eqn. A.1 converts to:

$$\frac{\partial T_f}{\partial t}(x_1', t) - \frac{\partial}{\partial x_1'}\left(k_f \frac{\partial T_f}{\partial x_1'}\right) = 0 \qquad \text{(E.2)}$$

The semi-discrete form of the above equation can be written as:

$$\frac{T_f^{n+1}\Big|_{x_1} - T_f^n\Big|_{x_1-\Delta x_1}}{\Delta t} - \frac{\partial}{\partial x_1'}\left(k_f \frac{\partial T_f}{\partial x_1'}\right)^n\Bigg|_{x_1-\Delta x_1} = 0 \qquad \text{(E.3)}$$

Note that the diffusion term is treated explicitly. Now, it is possible to solve the above equation by adapting a moving co-ordinate strategy. However, a simple spatial Taylor series expansion in space avoids such a moving coordinate approach. With reference to Fig. 2 we can write using Taylor series expansion as follows:

$$T_f^{n+1}\Big|_{x_1-\Delta x_1} = T_f^n\Big|_{x_1} - \frac{\partial T_f^n}{\partial x_1}\frac{\Delta x_1}{1!} - \frac{\partial^2 T_f^n}{\partial x_1^2}\frac{\Delta x_1^2}{1!} + ... \qquad \text{(E.4)}$$

Similarly the diffusion term is expanded as:

$$\frac{\partial}{\partial x_1'}\left(k_f \frac{\partial T_f}{\partial x_1'}\right)^n\Bigg|_{x_1-\Delta x_1} = \frac{\partial}{\partial x_1}\left(k_f \frac{\partial T_f}{\partial x_1}\right)^n\Bigg|_{x_1} - \frac{\partial}{\partial x_1}\left[\frac{\partial}{\partial x_1}\left(k_f \frac{\partial T_f}{\partial x_1}\right)^n\right]\Delta x \qquad \text{(E.5)}$$

On substituting Eqns. E.4, E.5 in E.3 and neglecting the higher-order terms then:

$$\frac{T_f^{n+1} - T_f^n}{\Delta t} = -\frac{\Delta x}{\Delta t}\frac{\partial T_f^n}{\partial x_1} + \frac{\Delta x^2}{2\Delta t}\frac{\partial^2 T_f^n}{\partial x_1^2} + \frac{\partial}{\partial x_1}\left(k_f \frac{\partial T_f}{\partial x_1}\right)^n \qquad \text{(E.6)}$$

If the flow velocity is u_1 then $\Delta x = u_1 \Delta t$. Substituting into Eqn. E5, we can obtain the semi-discrete form as:

$$\frac{T_f^{n+1}-T_f^n}{\Delta t}=-u_1\frac{\partial T_f^n}{\partial x_1}+u_1^2\frac{\Delta t}{2}\frac{\partial^2 T_f^n}{\partial x_1^2}+\frac{\partial}{\partial x_1}\left(k_f\frac{\partial T_f}{\partial x_1}\right)^n \qquad \text{(E.7)}$$

If Galerking weighing is applied to Eqn. E.7 then:

$$\int_\Omega N^T\frac{T_f^{n+1}-T_f^n}{\Delta t}d\Omega+\int_\Omega N^T\left(u_1\frac{\partial T_f}{\partial x_1}\right)^{n+1}d\Omega-\frac{\Delta t}{2}\int_\Omega N^T\left(u_1^2\frac{\partial^2 T_f}{\partial x_1^2}\right)^{n+1}d\Omega-\int_\Omega N^T\frac{\partial}{\partial x_1}\left(k_f\frac{\partial T_f}{\partial x_1}\right)^{n+1}d\Omega=0$$

where N is the shape function. When linear approximation for the variable T_f

Applying linear spatial approximation in conjunction with greens lemma the above equation is converted as:

$$N^T N\frac{T_f^{n+1}-T_f^n}{\Delta t}=-u_1 N^T\left(\frac{\partial N_f}{\partial x_1}\right)T_f^{n+1}-\frac{\Delta t}{2}u_1^2\left(\frac{\partial N_f}{\partial x_1}\right)^T\left(\frac{\partial N_f}{\partial x_1}\right)T_f^{n+1}$$
$$-D\left(\frac{\partial N_f}{\partial x_1}\right)^T\left(\frac{\partial N_f}{\partial x_1}\right)T_f^{n+1}+N^T Q$$

Simplifying the above equation we get:

$$\{[S1]+[M1]\Delta t+B\Delta t[S1]\}(T_f^{n+1}-T_f^n)=-[M1]\Delta t T_f^n+B[S1]T_r^n\Delta t-B[S1]T_f^n\Delta t$$

Here

$$[S1]=N^T N$$

$$[S2]=\left(\frac{\partial N_f}{\partial x_1}\right)^T\left(\frac{\partial N_f}{\partial x_1}\right)$$

$$[M1]=u_1[SVx]+\frac{\Delta t}{2}u_1^2[S2]+D[S2]T_f^n$$

$$[SVx]=N^T\left(\frac{\partial N_f}{\partial x_1}\right)$$

Similarly, the Finite element discretization of Energy balance equation for matrix can be derived as:

$$\{[S1]+[M1]\Delta t+B\Delta t[S1]\}(T_r^{n+1}-T_r^n)=-[M2]\Delta t T_r^n+B[S1]T_f^n\Delta t-B[S1]T_r^n\Delta t$$

Here

$$[S1]=\ N^{\ T}\ \ N$$

$$[S2]=\left(\frac{\partial\ \ N_{\ \ f}}{\partial x_1}\right)^T\left(\frac{\partial\ \ N_{\ \ f}}{\partial x_1}\right)$$

$$[M2]=D[S2]T_f^n$$